TRIBHUVAN UNIVERSITY
INSTITUTE OF ENGINEERING
PULCHOWK CAMPUS

THESIS NO: PUL078MSGtE002

Numerical Study of Bearing Capacity under Strip footing having underground void : A case of Lamachaur Pokhara

by

Bibek Nepal

A THESIS
SUBMITTED TO THE DEPARTMENT OF CIVIL ENGINEERING
IN PARTIAL FULFILLMENT OF THE REQUIREMENTS FOR THE DEGREE OF MASTER OF SCIENCE IN
GEOTECHNICAL ENGINEERING

DEPARTMENT OF CIVIL ENGINEERING
LALITPUR, NEPAL

DECEMBER, 2023

COPYRIGHT

TRIBHUVAN UNIVERSITY

INSTITUTE OF ENGINEERING

PULCHOWK CAMPUS

DEPARTMENT OF CIVIL ENGINEERING

PULCHOWK, LALITPUR

APPROVAL PAGE

The undersigned certify that they have read, and recommended to the Institute of Engineering for acceptance, a thesis entitled, " **Numerical Study of Bearing Capacity under Strip footing having underground void: A case of Lamachaur Pokhara**" submitted by Mr. Bibek Nepal (078/MSGtE/002) in partial fulfillment of the requirement for the degree of Master of Science in Geotechnical Engineering.

……

Supervisor,

Dr. Santosh Kumar Yadav

Department of Civil Engineering

Institute of Engineering, Pulchowk Campus

……

External Examiner,

Name: Bharat Bahadur Dhakal

Institute of Engineering, Pulchowk Campus

……

Program Coordinator,

Dr. Santosh Kumar Yadav

Department of Civil Engineering

Institute of Engineering, Pulchowk Campus

December,2023

ABSTRACT

This thesis' major objective is to conduct a detailed examination of strip footing behavior—those with an infinite length to width ratio—on Pokhara soil with voids in different location with respect to the foundation. The results are laid up in a way that will make the impact of the presence of a void with different sizes and shapes in the soil layer clear. To develop a series of models for this assignment while considering many factors, commercially available finite element analysis has been employed. The outputs of these models will subsequently be used to produce quality foundation problem solutions in the Pokhara Valley. First, the foundation model over Homogenous layered soil will be examined. Secondly, identical models with void at different depth and size will be analyzed. This dissertation, a comprehensive investigation aiming at examining the effects of voids on the behavior of shallow foundations, describes the findings as well as their implications.

The study's findings show that there is a critical zone of influence under the foundation. The presence of a void in the soil layer will only have a major impact on the foundation's performance if it is situated in this area. This zone of influence's dimensions are determined by a number of variables, including the location and magnitude of voids as well as the soil's properties. The bearing capacity of the foundation varies significantly depending on the location of the void when it is situated within the critical zone.

ACKNOWLEDGEMENT

Foremost, I want to extend my heartfelt appreciation to Dr. Santosh Kumar Yadav, the program coordinator, and my esteemed thesis supervisor, for his great guidance, advice, understanding, support, and willingness to let me perform a study on Numerical Study of Bearing Capacity under Strip footing having underground void: A case of Lamachaur Pokhara. His help has been instrumental in shaping the direction of my research and providing invaluable feedback.

I extend my thanks to the faculty members of the Department of civil Engineering, IOE, Pulchowk Campus for their encouragement, valuable discussions, and for creating an enriching academic environment.

I'm also grateful to my MSGtE/078 batch pals for their suggestions and assistance. Notably, Mr. Ritesh Baral for providing necessary borehole data and Bharat Aryal for supporting in this study. My deepest gratitude also goes out to everyone who provided crucial assistance, scathing criticism, recommendations, and guidance at various points during my research.

Ultimately, I express my gratitude to my friends and family for their constant support, comprehension, and motivation during this demanding journey. Their belief in me kept me motivated even in the face of difficulties.

Bibek Nepal
078/MSGtE/002
December 2023

TABLE OF CONTENT

LIST OF FIGURES

LIST OF TABLES

ABBREVIATION AND SYMBOLS

b, B	Width of foundation
c, c_u	Cohesion
D_f	Depth of foundation
D_d	Depth of soil domain
E	Modulus of elasticity of soil
FE	Finite Element
FEA	Finite Element Analysis
FEM	Finite Element Method
h	height of void
N_c, N_q, N_γ	Bearing capacity factors
W_d	Width of soil domain
W, w, D	Width of void
x, X	horizontal offset of the void.
y, Y	Depth of crest of void from the base of foundation
2D	Two Dimensional
3D	Three Dimensional
φ, ϕ	Angle of internal friction
ψ	Dilatancy angle
σ_z	Overburden stress
μ	Poisson's ratio
γ_{sat}	Saturated unit weight of soil
σ_t	Tensile Strength of soil
γ	Unsaturated unit weight of soil

q_u, q_{ult}	Ultimate bearing capacity
σ_u	Ultimate Bearing Capacity

1. INTRODUCTION

1.1 Background information

In nature, Natural soil deposits are frequently stratified and have strength characteristics that are either irregular or uniformly vary. It is typical in such soil deposits to discover a thin soil layer underlying a large layer of another soil or vice versa. Moreover, there are presences of heterogeneity in the Soil strata. The foundation design of conventional methods is uniformity, which assumes that the soil in each layer is uniform and homogeneous(Karl Terzaghi, 1943). However, due to the process through which soil is formed, it has an anisotropic nature. Although horizontal soil layers are common, neither their characteristics nor their distribution are random or distinct. However, the focus of the current study is on how the existence of subsurface voids affects the functionality of the foundation, including the bearing capacity and deformation behavior of the footing over voids of various sizes, shapes, and locations.

1.2 Statement of Problem

Several natural and artificial processes can lead to void in the natural world. Natural processes like the dissolving of dolomites and gypsum can result in voids. By artificially excavating mines, pipe galleries, tunnels, etc. Looking at the history of formation of soil in Pokhara region. The basin is filled with the quaternary deposits of gravel silt and clay which is brought by the series of debris flows(R.M. Pokhrel, 2015). The Analysis based on this situation was discovered to be important since there are many different implications that the presence of such an underground void can have on the behavior of the foundation. The presence of voids may have a detrimental effect on the stability of construction, increasing the risk of unequal settlement of superstructures and structural collapse. Soil strata can have voids with widely disparate characteristics formed by natural or manmade causes. Such voids may result in undesirable and erratic performance from the buildings constructed atop them. In that case, such voids should be studied thoroughly before construction over or near its vicinity.

Numerous studies have been conducted worldwide over the course of a century to predict the behavior of foundation using a variety of theories, tests, and models. The approximate solutions for the shallow foundation's bearing capacity on layered soil are intended for a number of frequently occurring non-homogeneous soil profiles. In the past few decades, Numerous studies have been conducted on the impact of underground voids on the stability

of foundations. But the study of performance of shallow foundation in Nepal, particularly in Pokhara soil is scare or it is non in existence. Since there are various effects that the presence of such underground void can result in the behavior of foundation, analysis based on this circumstance was found to be necessary for the assessment of the bearing capacity.

1.3 Objective of study

1.3.1 General objective

The inherent regional variability of the soil properties has a major influence on the performance of foundations. The objective of the research is the " **Numerical Study of Bearing Capacity under Strip footing having underground void: A case of Lamachaur Pokhara**.

1.3.2 Specific objective

This study has the following specific objectives:

- To Generate FE model representing the problem using commercially available finite element software.
- Studying the bearing capacity patterns of strip foundations parametrically.
- To explore deformation behaviors of foundation and void parametrically.
- To evaluate the effect of water table in the bearing capacity of foundation and void

1.4 Scope and Limitation of study

Due to increased urbanization, building and other structure development may necessitate establishing footing over soil having subterranean voids. Since this thesis encompass the effect of underground voids with consideration of various parameters like shape, size and position of voids in the form of the graph which provide the meaningful estimation of bearing capacity and deformation pattern for the design of structures.

The research is limited to Pokhara valley only, which is not favorable for wide range of soil type present in nature. Below is a list of some additional limitations.:

- Only a single soil layer is considered, which limits the effect of multilayer soil.
- When examining the model, only the plain strain condition is utilized. Which limits the effect of the extend of the void.

- Only a single void effect has been considered but in nature there may be presence of more than one void and their interaction may be complex one.

In addition to these, the study is constrained to a small set of parameters, which may not account for real-world issues.

1.5 Location of Study Area

The city of Pokhara is located at the foot of the Annapurna Massif in the Seti khola valley. Precambrian metamorphic sandstone, shales, and dolomites dominate Pokhara's geology. The other rocks are lower Himalayan range schists and Paleozoic phyllites. The Annapurna Massif's partially glaciated, and debris filled Sabache Cirque is drained by the upper Seti khola, which created the sizable sediment fan that Pokhara is situated on (Schwanghart et al., 2016). Pokhara is covered in a significant amount of Quaternary-aged layered clastic deposits. The Seti River and its tributaries create magnificent river terraces and steep gorges because the clastic sediments contain easily soluble calcareous material (25–65% by volume). Both below and above ground, karst structures—such as underground flow channels, solution cavities, sinkholes, pinnacles, and solution chimneys—are extensively formed. Ghachok, Pokhara, and Phewa formations are three of the seven formations in Pokhara that are important lithologies that are susceptible to the development of karstic features. An exceptionally hard represents the Ghachok Formation. Conglomerate bed made of subrounded to subangular gravels of sandstone, limestone, and shale, cemented by calcareous material. The Pokhara Formation consists of river gravels with lacustrine sediment intercalations; the gravels are composed of limestone and calcareous shale cobbles that are sub-angular to sub-rounded and show weak cementation, ill-sorting, and partial stratification. The Phewa Formation is made up of deposits with a composition ranging from calcarenite to calcisiltite that are porous, well-layered, and somewhat weak.(Gautam et al., 2000)

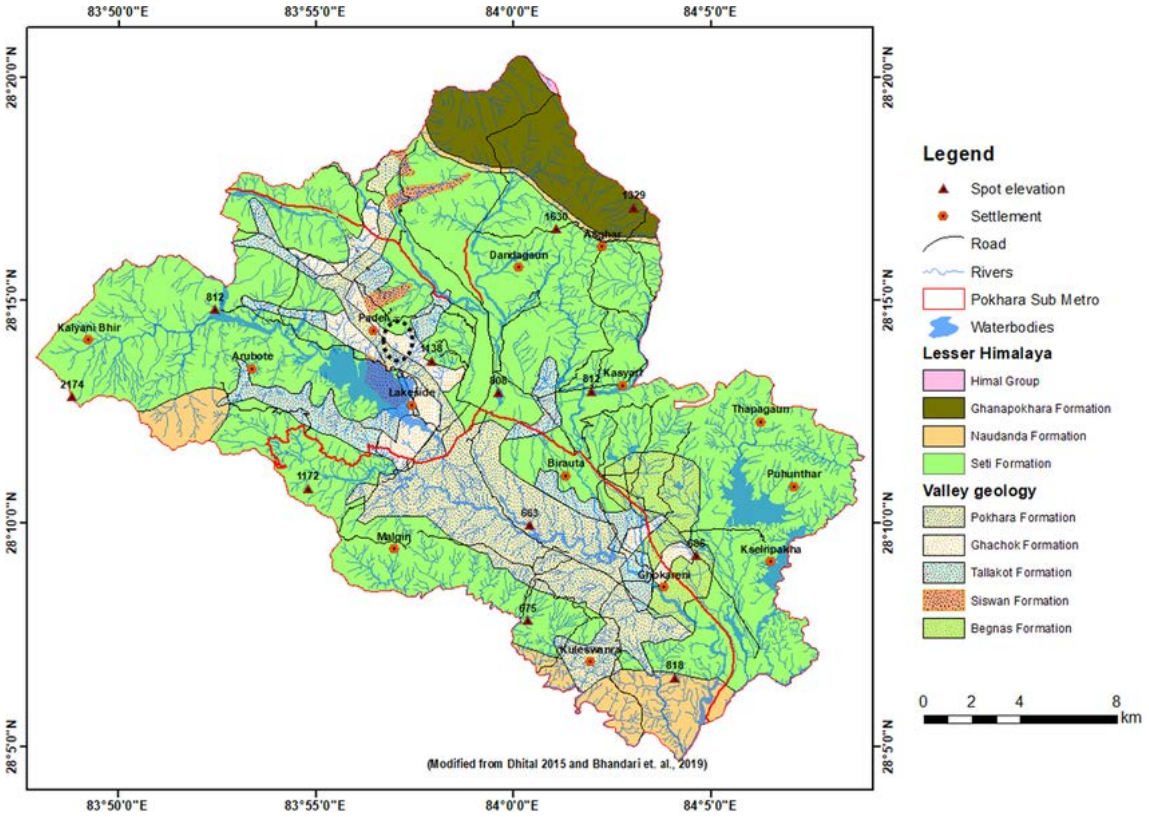

Figure 1.1: Geology of Pokhara valley (modified from Dhital 2015 and Bhandari et al. 2021)(Jain et al., 2023)

1.6 Organization of Dissertation

The dissertation is provided in six chapters to describe the details of prior related study, work done, and the key findings of this research. This is done considering the scope of work and purpose of this research. The dissertation's detailed structure is as follows:

- **Chapter 1** is an overview of this Research. To show the research curriculum, the typical geotechnical issues, goals, and objectives are outlined, along with the range of work and constraints.
- **Chapter 2** presents a brief overview of the many features of shallow foundation bearing capacity. The failure mechanism of soil in the presence of the underground voids and without one is presented in this chapter. Literature reviews on the bearing capacity and deformation of foundation with underground are briefed. Last but not least, a brief overview of the finite element method software has been made.
- **Chapter 3** gives details of the tools and procedures employed to accomplish the goals and objectives of this research. It contains information about the materials, the geometrical model, and the numerical model utilized to end the dissertation.

- **Chapter 4** comprises the analysis's findings and conclusions, presented in an effective, organized manner. The investigation and analysis that were done are used to help generate conclusions in this chapter.
- **Chapter 5** includes the conclusion of the study and suggestions.

2. LITERATURE REVIEW

This section provides a brief overview of earlier research and published literature that is necessary to comprehend the study's fundamental premises. The literature review focuses on current developments in the field of foundation behavior across heterogeneous soil. The basic concepts and hypotheses pertaining to the study are included in the first half of this section, and a review of prior research projects is included in the second.

2.1 Introduction

A foundation is a structure that acts as an interface for transferring loads from superstructures to the ground. Soil, being a weak substance cannot withstand the concentrated load coming from the superstructure hence the load has to be divided into larger areas for safe dissipation of the load. When building a foundation, it's important to calculate a reasonable factor of safety to prevent the structure from settling and to have enough permissible bearing capacity. According to the depth to the width ratio of the footing, it is categorized as shallow and deep foundation. But it this dissertation this only shallow foundations will be explored. According to (K. Terzaghi, 1943),shallow foundation are those foundation whose Df/B ratio is less than or equal to 1.Hence such foundations are near to the surface and construction is fully visible. Strip footings, mat footings, combination footings, and isolated spread footings are the four main varieties of shallow footings. Among these four isolated footing is more extensive in use. The three main design objectives for the foundations are ultimate bearing capacity (also known as strength), total and differential settlements (also known as serviceability), and economic viability (i.e. economic feasibility). Hence shallow foundations are economically viability for small structures.

2.2 Bearing capacity of footing

The term "bearing capacity" describes a soil's capacity to sustain the load from structure, such as a building, bridge, or foundation, without experiencing significant deformation or failure. "The maximum load per unit area which the soil or rock can carry without yielding or displacement."(K. Terzaghi, 1943)

Consider a footing that rests on the soil's surface. As the foundation load increases, the foundation settles. The soil fails quickly when the weight per unit area reaches the footing's bearing capacity. and the failure surface may extend to the ground surface according to

failure mode of the soil, and it typically coincides with a considerable rise in footing settlement.

2.3 Bearing capacity failure theories

Shear failure of a soil mass supporting a foundation will typically occur in one of three modes: general shear, local shear, or punched shear(Vesić, 1973).

2.3.1 General shear failure

General shear failure is defined as a downward movement of the side edges of the footing into the soil structure, followed by an upward movement to the ground surface, generated by a well-defined wedge beneath a foundation moving diagonally on its slip surface. Figure 2.1(a) depicts general shear failure. According to Das and Sivakugan (2018), failure typically happens on just one side of the footing, resulting in some tilting, even though at stress levels below failure, bulging of the ground surface on either side of the footing may be observed. A structure that prevents a footing from rotating can raise structural moments, perhaps leading to collapse or excessive settlement. Soils with brittle stress-strain relationships are more prone to general shear failure.

Figure 2.1(a) also depicts the variance in foundation settlement and load per unit area, q. The settling increases as the load per unit area increases during the early loading period. The soil supporting the foundation will collapse at a specific point, i.e., when the load per unit area equals qu. This load per unit area is referred to as the foundation's ultimate bearing capacity.

2.3.2 Local shear failure

Similar to general shear failure, local shear failure is defined by the diagonal downward movement of a well-defined soil wedge beneath a foundation, but with an increased depth of downward movement that causes the slip surfaces within the soil structure beyond the foundation edges to fade before they are visible at ground level. This failure mode can go unnoticed because it only slightly swells the ground surface. This failure mode exhibits a transitional failure mode between general and punching shear failure due to the behavior of strong soil compression directly beneath the foundation and upward movement of the soil surrounding the foundation.

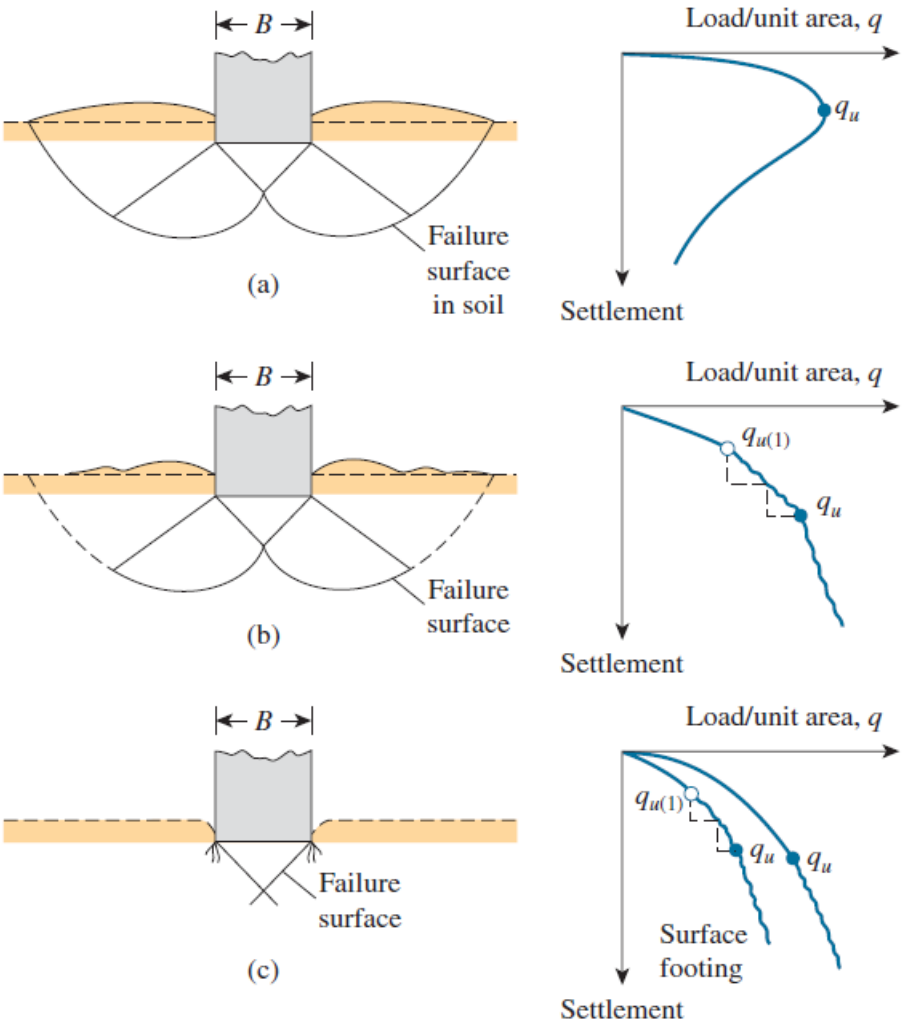

Figure 2.1: Nature of bearing capacity failure in soil. (a) general shear failure: (b) Local Shear Failure: (c) Punching shear failure (redrawn after (Vesić, 1973))

Sharp jerks will accompany the foundation movement as soon as the load per unit area on the foundation equals $q_{u(1)}$ (refer to load settlement plot in Figure 2.1(b)). The first failure load is known as $q_{u(1)}$, and it is lower than the final failure load per area, q_u. This is the most typical type of failure in soil constructions having a plastic stress-strain relationship.

2.3.3 Punching shear failure

When a well-defined wedge of soil beneath a foundation undergoes substantial compression in addition to vertical shearing, punching shear failure occurs. There is minimal, if any, ground surface indication of failure because the ground just below the footing collapses and the soil on either side of the foundation has no effect. Footing stability, or the absence of rotation, is typically preserved throughout failure (Das &

Sivakugan, 2018). The load settling plot will essentially follow a linear pattern beyond the ultimate failure load, qu., as illustrated in Figure 2.1. (c). This kind of collapse is common in soil constructions when the shearing planes are poorly defined, and the stress-strain relationship is very variable.

2.4 Bearing Capacity Theories

Since settlement calculations inherently account for the other failure modes, in practice, the general shear failure situation is usually investigated.(Coduto, 2001). (Karl Terzaghi, 1943) proposed a reasonable approach to predicting a foundation's bearing capability, which is as follows:

For a square footing:

$$q_u = 1.3cN_c + \sigma_z N_q + 0.4\gamma B N_\gamma$$

For a strip footing:

$$q_u = cN_c + \sigma_z N_q + 0.5\gamma B N_\gamma$$

Where, c is the soil cohesion; σ_z is the vertical stress at the base of the foundation; γ is the unit weight of soil; B is the width of the foundation; N_c, N_q and N_γ are non-dimensional bearing capacity factors.

2.5 Footings' bearing capacity in a multi-layered soil profile.

A multi-layered soil profile's bearing capacity is contingent upon a number of parameters, such as the composition and thickness of each soil layer as well as the type of footing being utilized. The bearing capacity is a crucial aspect of foundation design, ensuring the stability and safety of structures.

There are several ways to determine a footing's carrying capacity on a multi-layered soil profile, including the following:

Terzaghi's Bearing Capacity Theory: This approach is frequently applied to determine a shallow foundation's bearing capacity on a single soil layer. It can be extended to multi-layered soil profiles by considering the characteristics of each layer and their respective depths.

Boussinesq's Theory: This theory considers the influence of multiple layers on bearing capacity by calculating stress distribution through the layers. It's more complex but allows for a more detailed analysis of multi-layered soil profiles.

Finite Element Analysis (FEA): FEA is a numerical technique for soil profile and complex structure analysis. It can account for various soil properties and layering effects to calculate the bearing capacity of footings on multi-layered soil profiles with high accuracy.

Empirical Methods and Codes: Various empirical formulas and building codes provide simplified guidelines for estimating bearing capacity based on soil types, depths, and foundation types. These methods might simplify the calculation process but may not consider all nuances of multi-layered soil behavior.

The property of the uppermost layer alone is sufficient to appropriately assess the bearing capacity and settlement behavior of the foundation over layered soils if the thickness of the uppermost soil layer is noticeably greater than the width of the foundation. However, if the width of the foundation is similar to the thickness of the uppermost soil layer, lower soil layers within the foundation's zone of impact must be included for a realistic calculation of bearing capacity..(Poulos et al., 2001).

2.6 Arching in the soil

Arching happens because of pressure transferring from a flexible or yielding section of soil to an adjacent area that is less yielding or more rigid. When a segment of the soil yields under pressure, it tries to shift from its initial position. However, this movement is countered by the interface between the yielding and more stable sections. As a result, the pressure on the yielding section diminishes, while the pressure on the less yielding areas intensifies. Consequently, the soil forms an arch-like structure over the yielding section, redirecting the load to the sturdier sections, which act as support points.

2.7 Bearing Capacity of footings above the underground voids

As was previously indicated, complex natural and anthropogenic processes produce Underground void with variable engineering qualities. The investigation of the stability of the footing above voids can be found from 1980s.

(Baus, 1980), investigated stability of shallow continuous footings with varying the footing size, footing depth, void size, void shape, and the elevation of a soil-rock boundary

relative to the location of the void. The design curves for silty clay soil were presented which may serve as a basis for sizing the foundation.

(Badie & Wang, 1984)studied the stability of Spread Footing Above the void in clay using theoretical analysis and model test.it found that footing shape, soil property and void size affects the critical region for the bearing capacity. Moreover, the Df/B ratio above 2.4 shows no influence in the clay.

(Wang & Badie, 1985)Examine how void affects the stability of a shallow foundation with a three-dimensional finite element program. The clay used was commercially available Kaolinite. orientation of the continuous void was examined in both perpendicular and parallel directions which shows that parallel direction is more critical than the perpendicular direction and the critical depth also varies according to the footing width and voids parameter.

(Wang & Hsieh, 1987)used the upper bound theorem of the limit analysis to examine the collapse load of the strip footing over the circular void. The mechanism of failure was purposed, namely mechanism A, Mechanism B and Mechanism C.

(Azam et al., 1991)investigated how well strip footing performed on a layered soil deposit with void. The study concentrated on the impact of layered layer soil with voids in the bearing capacity and the effect of bedrock on that capacity. The result shows the variation in the strength due to void location, depth to bedrock and layer characteristics.

(Kiyosumi et al., 2007)The yielding pressure of spread footing over the voids has been well examined. The effect of presence of single and multiple voids with reduction factor has been established.

(Sireesh et al., 2009)investigated, using a series of laboratory-scale tests, the bearing capacity of circular footing on a geocell-sand mattress covering a clay bed with voids. The study shows the increase of bearing capacity up to 40 times than without geocell sand mattress if adequate mattress is provided.

(Kiyosumi et al., 2011)carried out the 1G model test on the stiff ground with void to determine the strip footing's bearing capacity. According to the observation, a single void can have one of three failure scenarios. Specifically, void failure without bearing failure, void failure with bearing failure, and bearing failure with void failure.

(Lee et al., 2014)used Plaxis 2d program to investigate the undrained stability of surface strip footing with single and dual void on clay. the study showed that the failure mode is governed by roof, wall, and combined failure mechanisms.(Lee et al., 2015) further investigated how the load inclination affected the spread footing's ability to support loads over voids.

(Lavasan et al., 2016)Using Plaxis software, numerically analyze the bearing capacity and failure processes of a shallow strip foundation above the two voids. This study also shows that the variation of bearing capacity with respect to size and location of the voids.

(Zhou et al., 2018) investigated the strip footing's bearing capacity via discontinuity layout optimization on c-ϕ soils with square voids. The results show the effect of void is more dormant in c-ϕ soils than the undrained soil.

(Xiao, Zhao, Zhao, et al., 2018) conducted finite element limit analysis on rock mass with voids. The results showed that parameters like intact rock strength, unit weight, location of void size of void affect the bearing capacity which are presented in charts.

(Xiao, Zhao, & Zhao, 2018) studied the undrained stability of strip footing using finite element limit analysis on two layered clays. Effect of single and multiple voids with respect to top layer thickness, location, size, width, height and spacing has been evaluated.

(Wu, Zhao, Zhang, et al., 2020) conducted finite element limit analysis on eccentrically loaded strip footing above voids in rock masses which also support the parameter which affects the bearing capacity as location, size, length to width ratio as influential factor.

(Wu, Zhao, Zhao, et al., 2020) also conducted finite element limit analysis in c-ϕ soils with upper bound theorem and Lower bound theorem. which also supports the parameter that influences the bearing capacity, such as position, size, and length to width ratio as an influential factor.

(Wu et al., 2021) investigated the stability of the voids system with random soils using Radom adaptive finite element limit analysis. The soil's spatial variability is described by the random field theory, and Monte-Carlo simulations are used to determine the failure probability.

(Benbouza et al., 2023)examined how strip footing behaves above a void in sandy soil. The outcome shows that void presence lowers bearing capacity and that void has no influence above a Critical value for D/B.

2.8 Numerical modeling by Finite Element Method

Computational modeling, commonly referred to as numerical modeling, is a method used in a variety of scientific and technical domains to replicate challenging real-world processes. It entails developing a computer program that, by breaking a system or phenomena down into smaller components or steps and solving equations iteratively, approximates the behavior of the system or phenomenon. Researchers and analysts can analyze systems that might be too costly, risky, or difficult to study directly.

Finite Element Analysis (FEA) is a numerical method that breaks down large structures and systems into smaller components known as finite Elements in order to study the behavior of these elements. Each finite element is joined by the joint called ‘node’. Finite element analysis includes the process like Discretization, Mathematical modeling, equation formulation, assembly, solving the system and post processing.

To arrive at the answer for the complete construction, the attributes of the elements are formulated and merged. In terms of displacement at the element's nodes, the shape functions are chosen to approximate the variation in displacement inside an element. The nodal displacement will also be used to express the stresses and strains within an element. The equations of equilibrium for the element are derived using the virtual displacement approach, and the nodal displacement will be the equations' unknowns. The equilibrium equations are calculated for the nodal displacement after the boundary conditions are put in place. The stresses and strains are calculated using the element characteristics from the nodal displacement values for each element. Therefore, in this Finite Element Method, emphasis is primarily placed on the formulation of properties of the constituent elements rather than solving the problem for the complete structure in one operation.

The FEM has many advantages of its own. Some of them are given below:

1. FEM is applicable to a wide range of fields and physical scenarios, making it a versatile tool for different types of simulations.
2. FEM’s ability to break down complex shapes into smaller elements allows accurate modeling of intricate and irregular geometries.
3. FEM's approach of dividing structures into elements permits precise analysis of specific areas, capturing localized behaviors.
4. FEM supports mesh refinement in critical regions, enhancing accuracy in those areas while maintaining efficiency elsewhere.

5. FEM accommodates various types of boundary constraints, enabling realistic modeling of real-world scenarios.
6. FEM offers a selection of element types that can be chosen to match the problem's characteristics, optimizing accuracy.
7. FEM handles interconnected physical effects, allowing simulations of systems with multiple interacting phenomena.
8. FEM can accurately simulate materials with nonlinear behaviors, such as plasticity, enabling realistic representations.
9. FEM software provides tools for visualizing stress, deformation, and other results, aiding in understanding system behavior.
10. FEM reduces reliance on physical prototypes and experiments, saving costs associated with materials and testing.
11. FEM efficiently explores how changes in design parameters affect a system's behavior, aiding in optimization.
12. FEM assists in understanding complex systems, providing insights and data for research and development purposes.

3. METHODOLOGY

This section includes a summary of the methods used to complete the analysis as well as a presentation of the findings. A flow chart, like the one in Figure 3.1 below, can be used to briefly convey the entire process.

The research was conducted in different stages.

a. Literature review and data acquisition: In this part of the study, the main goal was to gather the data that would be needed for input into the FE program, including the parameters of silty sandy soil and a literature analysis to identify the correlations that would be useful in processing the data collected to prepare it for input. This section also includes a brief review of the literature on earlier research on similar that are comparable.

b. Processing of data for input: This phase processed all the data from step a, considering both the mathematical and empirical relationships found in many books and literatures, and prepared the data for modeling.

c. Input data: In order to model the problem in FE software, data from publications and literatures that were analyzed in step b were combined with additional relevant data obtained through mathematical and empirical relationships.

d. Run the model: A parametric investigation was conducted using several numerical models that were created taking various variables into account.

e. Output data: After the model was successfully run in the FE program, output data were collected, including the soil's ultimate carrying capacity, settlement, deformation, and stress.

f. Processing of the output data: All the outputs from step e are arranged and processed in this phase so that they are presentable and include the necessary verification for the results to be validated. The outcomes are then collated and contrasted with various parametric outcomes.

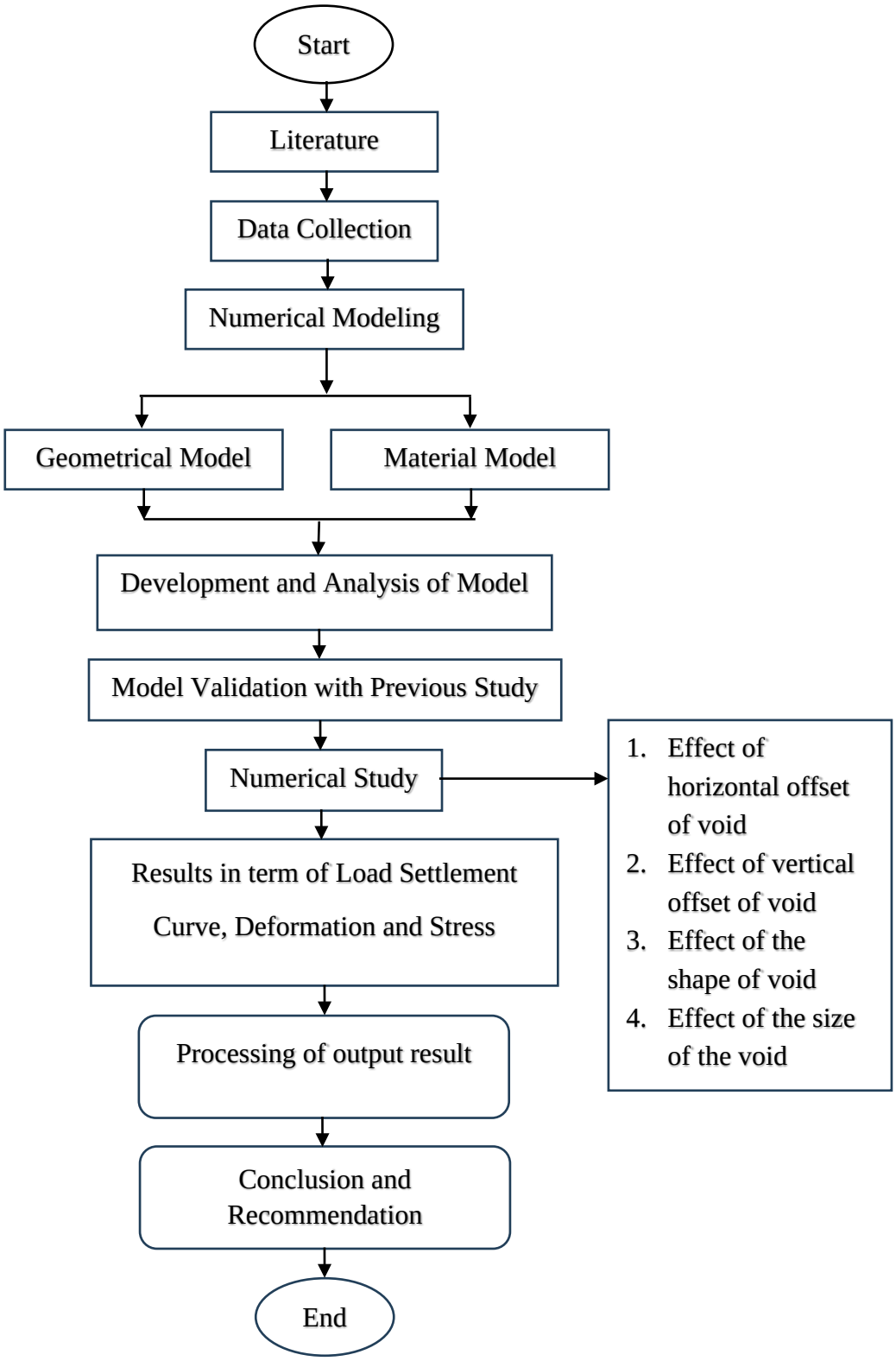

Figure 3.1: Algorithm used in the process to finish the study.

3.1 Material Model

3.1.1 Soil Constitutive Model

In geotechnical engineering, a soil constitutive model is a mathematical representation that explains the mechanical behavior of soil under various loading and deformation scenarios. Soil, a complex substance, exhibits non-linear behavior and frequently demonstrates anisotropic and time-dependent characteristics. Additionally, it displays irreversible behavior under stress. Constitutive models aim to capture these complexities by providing equations or algorithms that relate stress (forces) and strain (deformations) for different loading scenarios. There are various types of soil constitutive models, each designed to capture specific aspects of soil behavior. Some common types include:

A. Elastic Models: These models presuppose that the behavior of the soil is linearly elastic, which implies that the relationship between stress and strain is linear. Pure elastic models are only useful for relatively small deformations since most soils display non-linear behavior at higher strains. Examples of elastic models include linear elastic and nonlinear elastic. In the linear elastic model, the value of the modulus remains constant irrespective of magnitude of stress and strains while in nonlinear elastic, the nonlinear curve is represented by mathematical functions such as hyperbola, parabola, splines, and Ramberg-Osgood(R-O).
B. Plastic Models: Beyond the elasticity of the soil, plastic models focus on plastic deformations (permanent deformations). These models frequently include yield surfaces, which specify the upper boundary beyond which plastic deformation takes place. Examples of plastic models include the Cam-Clay model and the Modified Cam-Clay model.
C. Elastoplastic Models: Aspects of both elastic and plastic behavior are combined in these models. They consider the ideas of plasticity for higher strains and elasticity for smaller strains. A popular elastoplastic model for describing soil behavior in both drained and undrained circumstances is the Mohr-Coulomb model.
D. Critical State Models: These models are based on the idea of the soil's critical state, which denotes the condition in which the soil reaches its highest density and shear strength. The models are frequently applied to sands and gravels and are intended to represent soil behavior around critical state.

E. Hyperelastic Models: These models are used for soft soils and are based on the theory of elasticity for materials that undergo very large deformations. Hyperelastic models are often used to describe the behavior of organic materials and peat.

Soil failure in a three-dimensional condition of stress is incredibly difficult in addition to the behavior of the soil. Various models have emerged in recent years to represent the stress-strain relationship and failure patterns of soils. Each of these models possesses its own limitations and drawbacks, often contingent upon their specific applications. For this research, the Mohr-Coulomb model has been selected.

Mohr-Coulomb model

As a first-order model, the elastic-plastic Mohr-Coulomb model is frequently used to simulate behavior in general. The Mohr-Coulomb model is both straightforward and suitable for a three-dimensional stress space model, requiring only two strength parameters to characterize the plastic behavior. Mohr-Coulomb requires five input parameters: ϕ and c for soil plasticity, which establishes the failure criteria; ψ as an angle of dilatancy; and E and ν for soil elasticity, as determined by Hooke's law. In addition to the five model parameters mentioned above, most soil deformation issues depend heavily on the initial state of the soil. Selection of Ko-values must be used to create the initial soil stresses. This model can be used to examine the stability of embankments, slopes, shallow foundations, and dams. (Ti et al., 2009).

Basic parameters for Mohr- Coulomb model

As previously mentioned, the Mohr-coulomb model requires five parameters in total, which can be acquired from various correlations and simple laboratory procedures. Below is a list of the parameters along with their standard units.

Table 3.1: Parameter for Mohr-Coulomb model

Symbol	Description	Unit
E	Young’s Modulus	kN/m^2
ν	Poisson’s Ratio	-
φ	Friction Angle	°
c	Cohesion	kN/m^2

ψ	Dilatancy Angle	°

3.1.2 Acquisition of Soil Parameters

The SPT tests conducted at lamachaur, Pokhara metropolitan City-19 were obtained from site investigations report through geotechnical reports. The visual classification of the soil and the SPT values at each 1.5-meter depth interval were recorded in the borehole logs. The SPT values are according to IS 2131-1981.

Correction for SPT N value to N60

the SPT value is corrected for various factor such as:

a. Sampler type (C_S)
b. Rod length (C_R)
c. Borehole Diameter (C_B)
d. Energy Ratio (C_E)

$N_{60}=N\times C_E\times C_B\times C_R\times C_S/0.6$

Where,

N=Measured penetration number

N_{60}= Standard Penetration number correction for field condition

Correlation between Standard Penetration Number and Modulus of Elasticity

Modulus of Elasticity for sandy soil by (Farrent, 1963) based on Terzaghi and pecks loading,

$$E_s = \frac{7.5 \times \frac{8}{9} \times N_{60} \times 95.76}{100}$$

Or, Modulus of Elasticity for silty sand by (Schultze & Menzenbach, 1961) as

$$E_s = 100 \times \frac{24 + 5.3 \times N_{60}}{100}$$

Later correlation was used for modulus of elasticity.

Correlation of ϕ and Standard Penetration Number

Angle of Internal friction, as described by (Wolff, 1989) is

$$\emptyset = 27.1 + 0.3 \times N_{60} - 0.00054 \times {N_{60}}^2$$

Table 3.2: Value range for Poisson's ratio, ν (Ranjan & Rao, 2011)

Type of soil	**ν**
Clay, saturated	0.4 – 0.5
Clay, unsaturated	0.1 – 0.3
Sandy clay	0.2 – 0.3
Silt	0.3 – 0.35
Sand(dense) Coarse Fine grained	0.3 – 0.4 0.15 0.25
Concrete	0.15

For Sandy soil, the value of Poisson's ratio is taken as 0.25.

The dilatancy angle ψ, is specified in degrees. Both the density and the friction angle affect the sand's dilatancy. For ϕ value greater than 30° dilatancy angle may be calculated using Ψ = φ - 30°,

Whereas, for sands with φ < 30 the dilatancy angle is mostly zero.

The soil parameters as per the requirement of study are considered as tabulated below:

Table 3.3: Parameters considered in soil model.

Parameters	**Soil**
unit weight of soil (kN/m^3)	18 kN/m^3
Saturated unit weight of soil(kN/m^3)	20kN/m^3
Friction angle of soil, φ	34 ^{o}
Young's modulus of elasticity (MN/m$^{2)}$	14.6MN/m^2

Poisson's ratio	0.25
Dilatancy angle Ψ	4 ^{o}
Cohesion	70 kN/m^2
Failure criteria	Mohr-Coulomb
Type of material model	drained condition

3.1.3 Acquisition of Foundation Parameters

The foundation was modeled as continuous surface footing with plain strain, elastic, and isometric behavior. The parameters are derived from (Kiyosumi et al., 2007)

Table 3.4: Foundation Material Properties

Parameter	Values
Normal Stiffness (EA) kN/m	3×10^7
Flexural Rigidity (EI) kN/m^2/m	2×10^4
Equivalent Thickness, m	0.2
Poisson’s Ratio	0.1

3.2 Geometric model

The geometrical parameters along with the optimization of problem model size, mesh convergence analysis and boundary condition in accordance with different literatures are considered and the following parameters are used in this study.

3.2.1 Geometrical parameter

The geometrical parameters of the numerical model are expressed below.

Table 3.5: Model geometry

Geometrical Parameters	Values
Width of footing (B)	2 m
Width of analysis soil (W_d)	20B (40m)
Depth of analysis soil (D_d)	15B (30m)
Shape of Void	Circular, Square, Rectangular

Size of Void (D or W)	0.5, 1.0,1.5 ,2.0 and 3m
Water table below the ground level	1m to 15m
Vertical position of Void (y)	B, 2B, 3B, 4B, 5B and 6B (from the base of footing to crest of void)
Horizontal position of void(x)	0B, 1B, 2B, 3B and 4B (from the center of foundation to the center void)

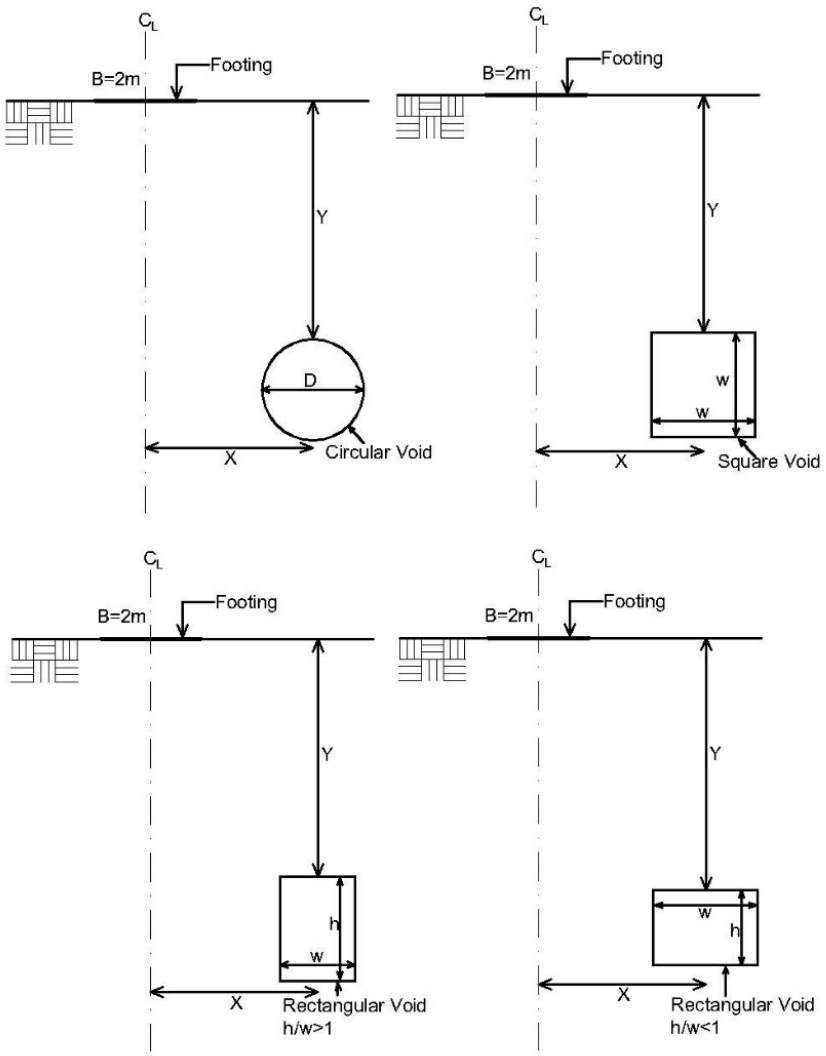

Figure 3.2: Schematic view of footing and voids

3.2.2 Optimization of model for analysis

The study model is optimized for size i.e., width and depth to produce a well-performing model for additional model analysis. For avoiding any boundary effect different literature

has been consulted(Kiyosumi et al., 2007; Lee et al., 2014; Wu et al., 2021; Wu, Zhao, Zhang, et al., 2020; Xiao, Zhao, & Zhao, 2018; Xiao, Zhao, Zhao, et al., 2018).The width is kept at 20B and depth at 15B.

3.2.3 Meshing effect analysis

Predictions of deflections/displacements, stresses, natural frequencies, temperature distributions, etc. are common in engineering designs. To improve the behavior of the materials, these parameters are utilized to iterate on the geometry and/or material properties. Traditional approaches, including hand calculations, idealized physical models, and used straightforward equations to find solutions. The problem is oversimplified by these approximations, and an analytical solution can only offer conservative estimates. The goal of FEM and other numerical approaches, as opposed to hand computations, is to provide an engineering study that is comprehensive and takes into consideration many details. The body is divided into smaller pieces by FEM, which enforces continuity of displacements at these element borders to prevent the outcome of FEA from being impacted by changing the mesh size.

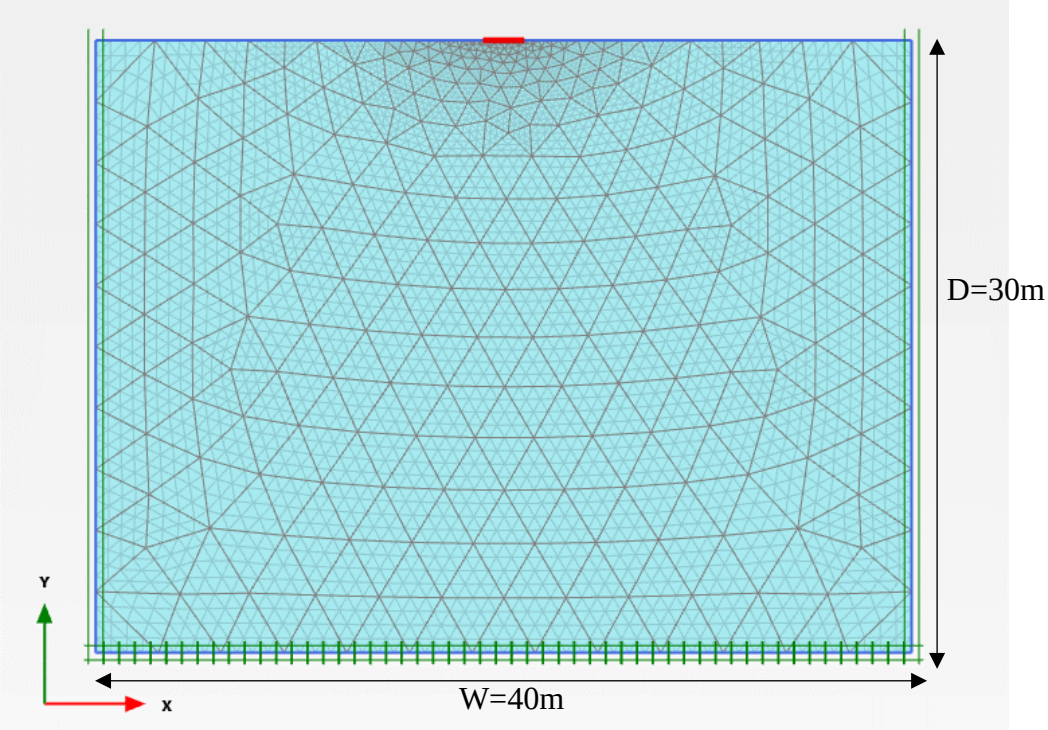

Figure 3.3: Typical mesh for numerical analysis

To determine how many nodes and elements are appropriate, the numbers of element and nodes varied in the range of 168-1433,336-2821,542-4509,1192-9797 and 2154-17581

respectively for no-void case, and 188-1593,338-2837,524-4365,1008-8325 and 1826-14957 respectively for void case as preliminary trail. Triangle elements with 15 nodes are used for meshing. Figure 3.3 shows a typical triangular element. Additionally, the mesh configuration around the footing and void was changed to 0.05 for the footing and 0.7071 for the voids. This was done to acquire sensitive data near the direct influence of the foundation and the soil void. It was confirmed that the variation in the obtained result and yielding settlement when the element exceeds 1192. Hence fine mesh was used for no-void condition while for the void condition, medium mesh was found to be enough.

3.2.4 Boundary condition

By restricting the horizontal and vertical displacement on the bottom boundary and keeping the vertical borders normally constrained, the boundary condition of the model is made to be compatible with the actual soil condition. The behavior of the ground surface under various parametric variations is examined without restriction at the upper soil boundary.

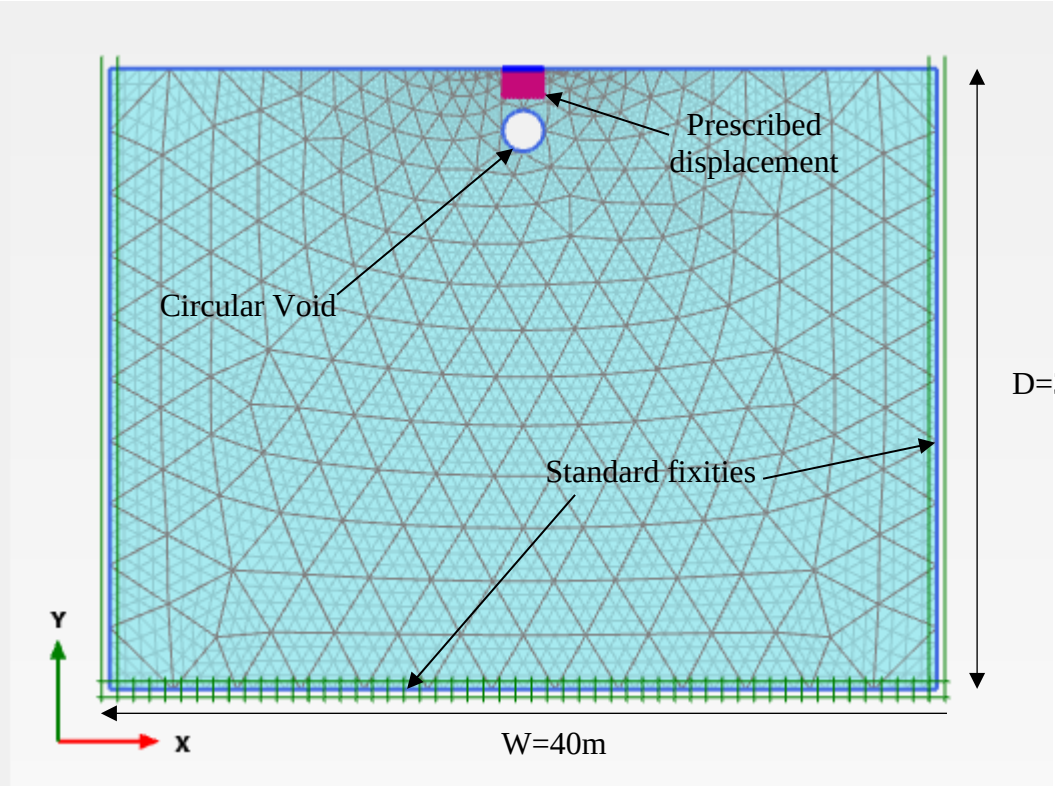

Figure 3.4: Geometrical model of strip footing with void.

3.3 Numerical modeling

The bearing capacity was examined using finite element-based software. The goal of the current research is to determine the maximum bearing capacity of strip footings sitting on silty sandy soils that have continuous voids of different shapes. 20B x 15B was the geometry of the finite element soil model used for the investigation. With the use of triangular elements with 15 nodes, the soil domain was discretized. Strip footing is regarded as rigid. Therefore, there is consistent settlement across all the nodes on the footing. For static analysis, this is obtained through uniform prescribed displacement. A 2m wide strip footing was used. To avoid the boundary effect brought on by loading, the soil field was modeled with dimensions of 40 m in width and 30 m in depth. Figure 3.4 displays the geometric model that was used for the analysis.

3.4 Test Procedure

The numerical model's input data includes variables such as the subsurface void's vertical and horizontal position, size, and shape. For parametric analysis, a total of 16 sets of different void shape and size models with 30 sets of different horizontal and vertical location of the void with respect to the foundation has been considered. Figure 3.5 shows the schematic diagram of models performed for parametric analysis.

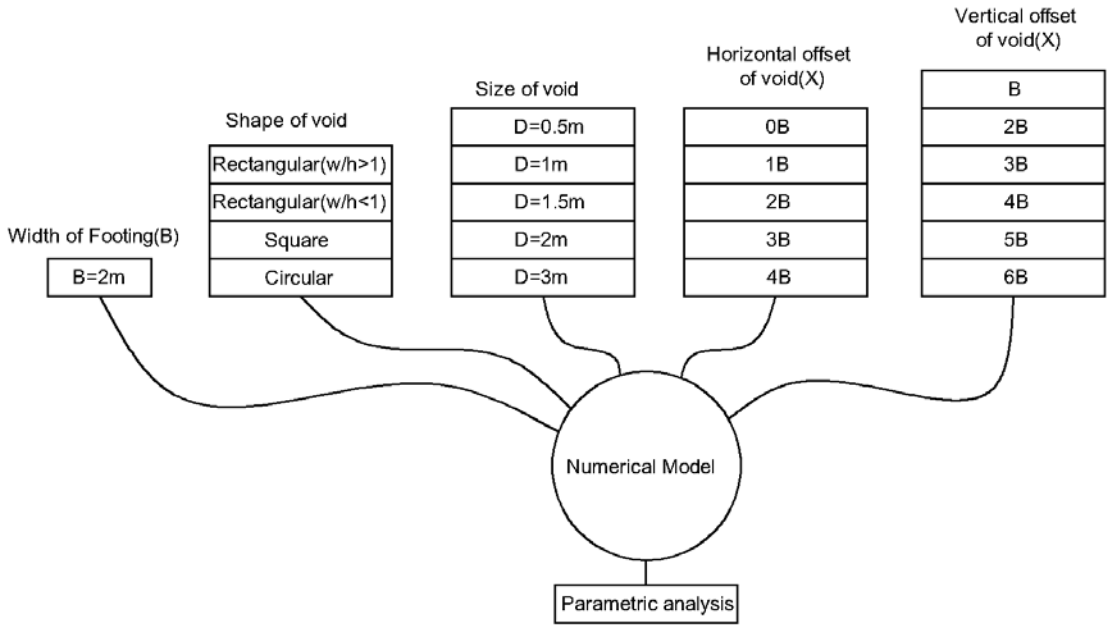

Figure 3.5: Schematic illustration for parametric analysis displaying numerical models with various geometric and material properties.

3.5 Application of load to models

Calculations were made using the loading input as staged construction and the plastic analysis calculation type for static analysis. The load was applied to the model through the prescribed displacement.

3.6 Output

Load settling curves are produced after analysis of the output results. Utilizing the load-settlement curves, the maximum bearing capacity is determined in accordance with (IS:1888-1982, 1983) shown in Figure 3.6. The results obtained from the finite element (FE) simulation depict the settlement and displacement patterns of the soil, along with the plastic failure occurring due to the applied load, as illustrated in Figure 3.7 (a) and (b) respectively. These outcomes showcase the deformation of the soil beneath the foundation.

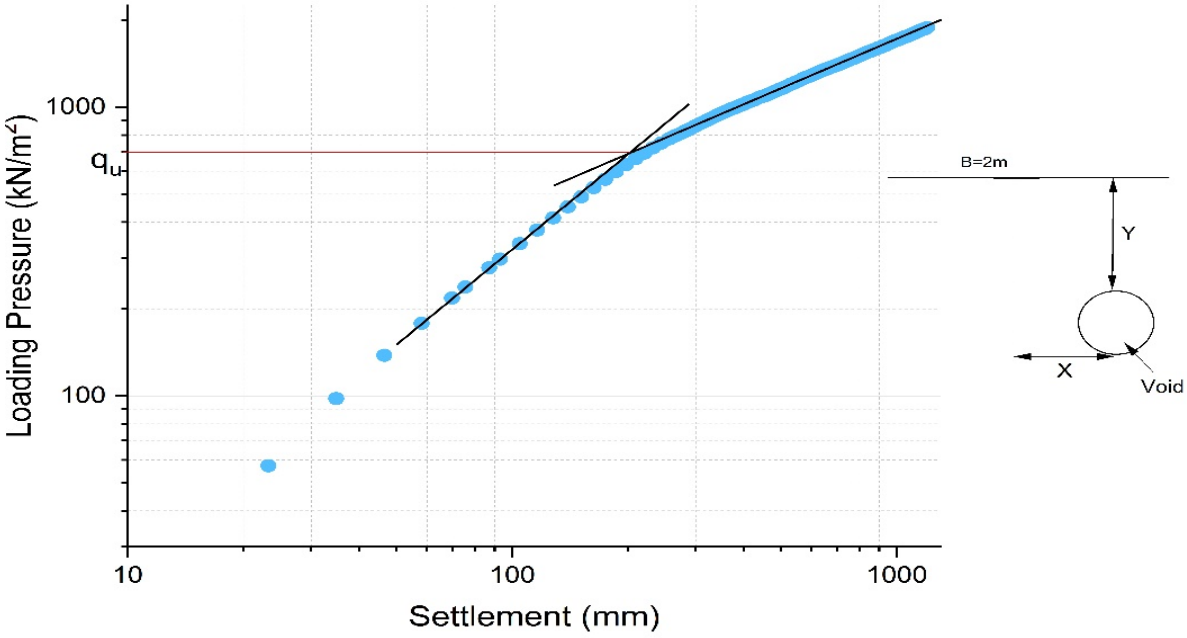

Figure 3.6: Load-settlement curve

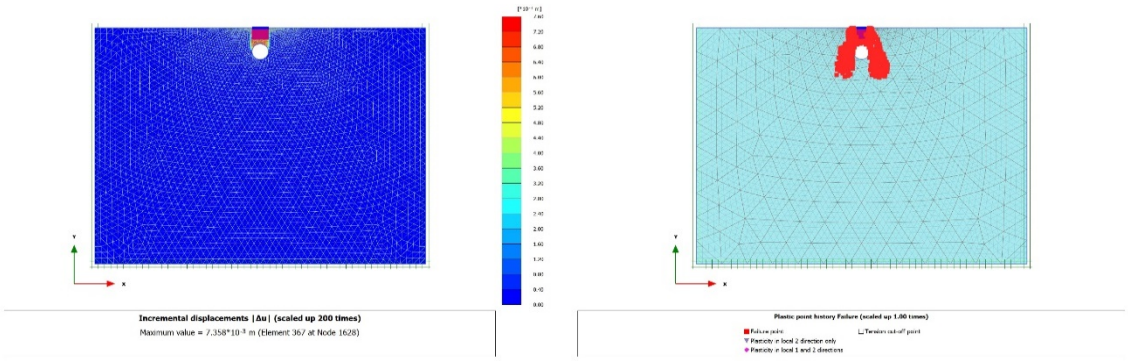

(a) (b)

Figure 3.2: Deformation behavior of soil under the foundation; (a) Displacement of soil elements, (b) plastic Compressive failure of soil under the foundation

4. RESULT AND DISCUSSION

This section presents and discusses the simulation findings. This study includes FE models with different material and geometrical parameters, which are mentioned in Table 3.3, 3.4 and 3.5. The first part includes model validation while the second part includes parametric analysis. The ultimate bearing capacity of each model is calculated using the model output (load settlement curve), and the results are shown in ANNEX A. Additionally, ANNEX B tabulates and displays each model's ultimate bearing capacity.

4.1 Numerical Model and its Validation:

The result obtained from FE software is compared with various literature. For the purpose of this study (Kiyosumi et al., 2007) has been used as comparison model.(Kiyosumi et al., 2007) examined the yielding pressure of spread footing on calcareous sediments above several voids in the Japanese Okinawa region. The effect of square void of size 2m x 2m on the yielding pressure and settlement with variation in horizontal and vertical distribution as well as effect of presence of multiple voids and the progress of failure has been studied. A typical model similar to that of (Kiyosumi et al., 2007) us shown in fig 4.1

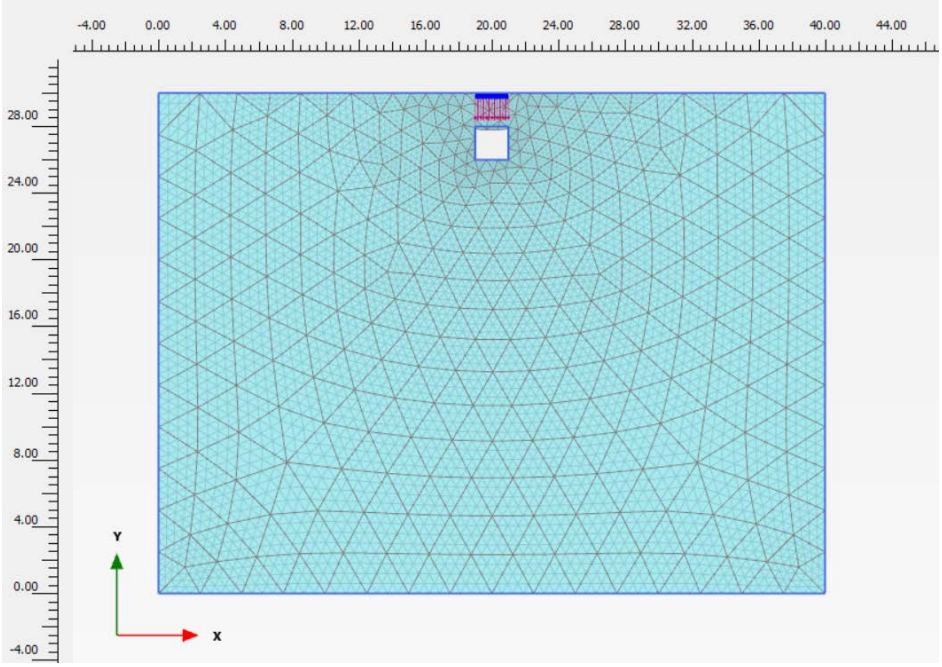

Figure 4.1: Typical Mesh Model as of (Kiyosumi et al., 2007)

4.1.1 Material Model

The material properties of soil of the model used is given in the table below:

Table 4.1: Material properties of soil used as of (Kiyosumi et al., 2007).

Physical properties	**Value**
Submerged unit weight, γ' (kN/m^3)	9.0
Poisson's Ratio, ν	0.3
Young's Modulus, E (kN/m^2)	4.9 x 10^5
Cohesion, c (kN/m^2)	980
Internal friction angle, φ (deg)	26.5
Dilatancy angle, ψ (deg)	0
Tensile Strength, σ_t (kN/m^2)	490

The material properties of footing of the model used in given in table:

Table 4.2: Material properties of Spread footing used as of (Kiyosumi et al., 2007).

Physical properties	**Value**
Submerged unit weight, γ' (kN/m^3)	14
Poisson's Ratio, ν	0.1
Young's Modulus, E (kN/m^2)	3 x 10^7

Table 4.3: Geometric properties used as of (Kiyosumi et al., 2007)

Geometric Property	**Value**
Width of Footing, B (m)	2.0
Size of Void, W (m)	2.0
Horizontal offset of Void, X (m)	0.0
Depth of Void, Y (m)	3.0

The double logarithmic plot's relationship between the loading pressure and footing settlement was compared below for the no-void condition and for a square void that was 2 m wide and 3 m deep from the base of the footing.

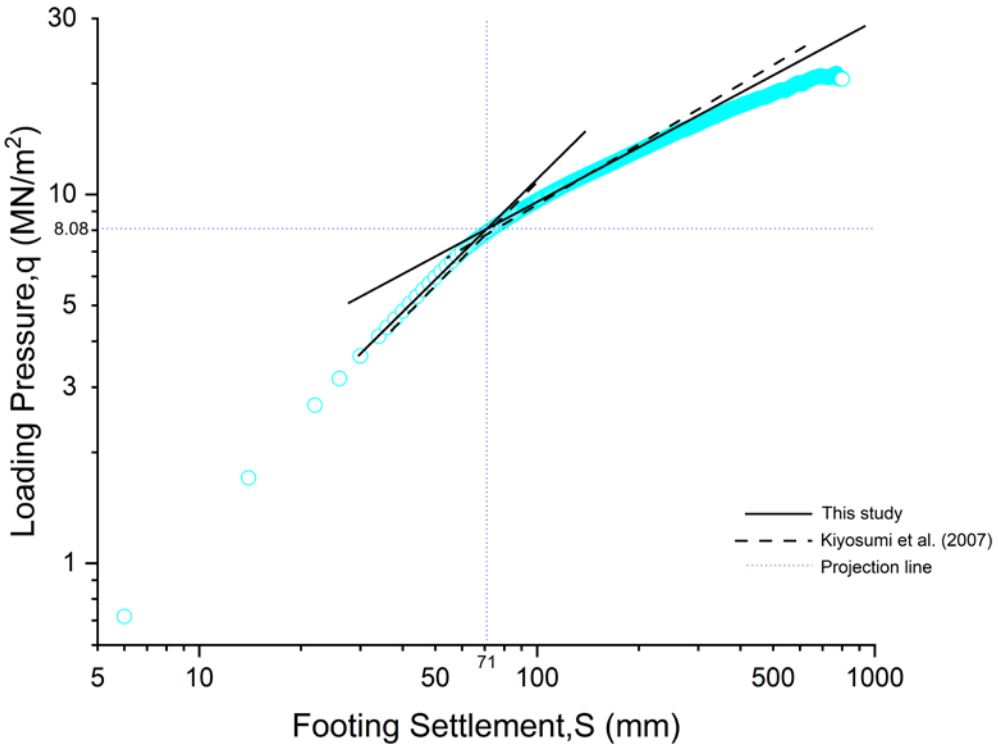

Figure 4.2: Relationship between loading pressure and footing settlement for no void

Figure 4.2 depicts the relationship between the footing settlement and the loading pressure under no-void conditions. Additionally, Figure 4.3 illustrates the relationship between the footing settlement and the loading pressure for soil with a square void of 2 m in width beneath the foundation at a depth of 3 m. When the loading pressure against displacement relationship from Figures 4.2 and 4.3 from this study's model and that of (Kiyosumi et al., 2007) are compared, the agreement between the two is extremely good with only minor differences. The discrepancy in non-void condition is about 3.6% while for void condition, discrepancy is about 0.14%.The validation of the numerical model employed in this work is concluded by the little deviation obtained and the close agreement between the results of (Kiyosumi et al., 2007) and the model.

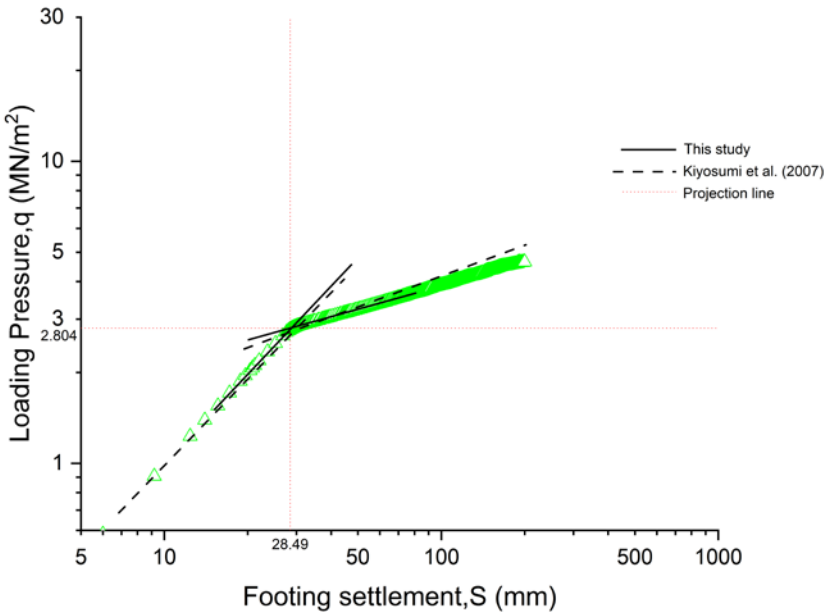

Figure 4.3: Relationship between loading pressure and footing settlement for void

4.2 Parametric studies

Parametric study has been carried out by varying the position, shape and size of the void.

4.2.1 Effect of position of underground void

The performance of the foundation is significantly influenced by the void's placement with respect to it. The void at various points in the soil domain beneath the foundation has been simulated to assess various situations. After analyzing these models, bearing capacity—that is, the load settlement curve—was determined.

4.2.1.1 Effect of vertical offset (Y)

To determine the degree to which the void's vertical position or depth beneath the foundation base has an impact, FE models with void at various depths have been simulated. Further, ultimate bearing capacity as determined by the load settlement curve at different depths of void keeping the shape of the void as circle are shown in Figure 4.4 (a), (b), (c),(d) and (e).

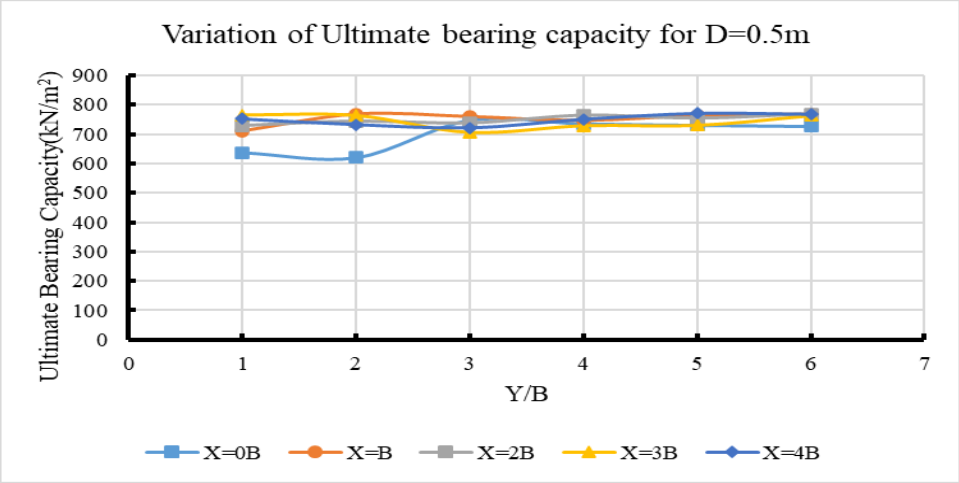

Figure 4.4(a): Effect of circular void(D=0.5m) with varying void depth(Y) upon bearing capacity of foundation for different horizontal offset(X) of void.

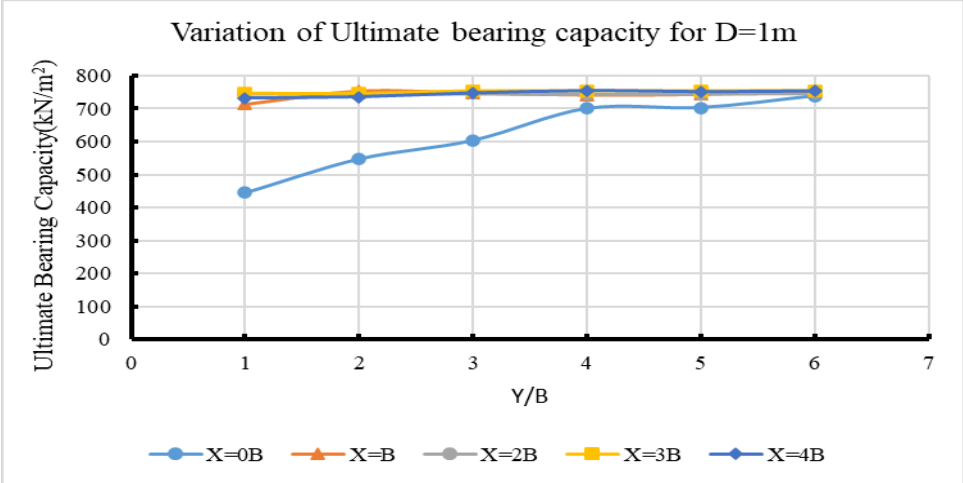

Figure 4.4(b): Effect of circular void(D=1.0m) with varying void depth(Y) upon bearing capacity of foundation for different horizontal offset(X) of void.

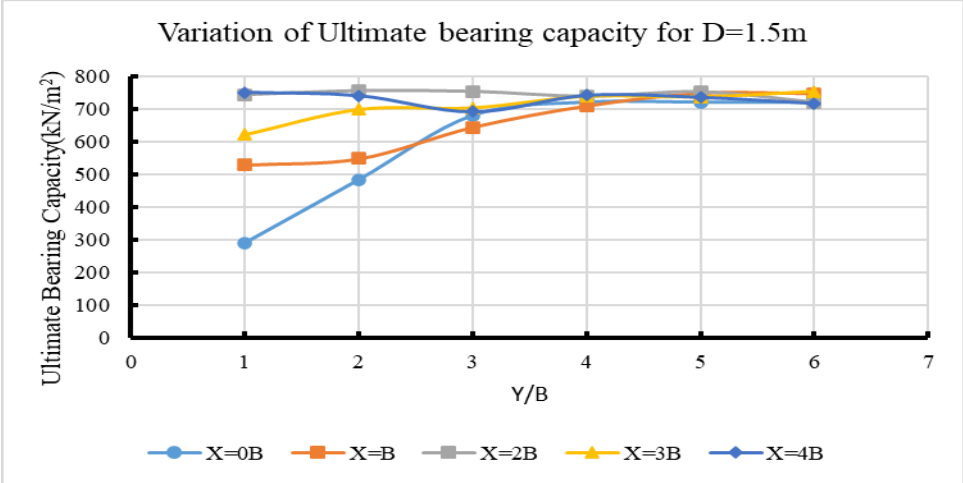

Figure 4.4(c): Effect of circular void (D=1.5m) with varying void depth(Y) upon bearing capacity of foundation for different horizontal offset of void(X).

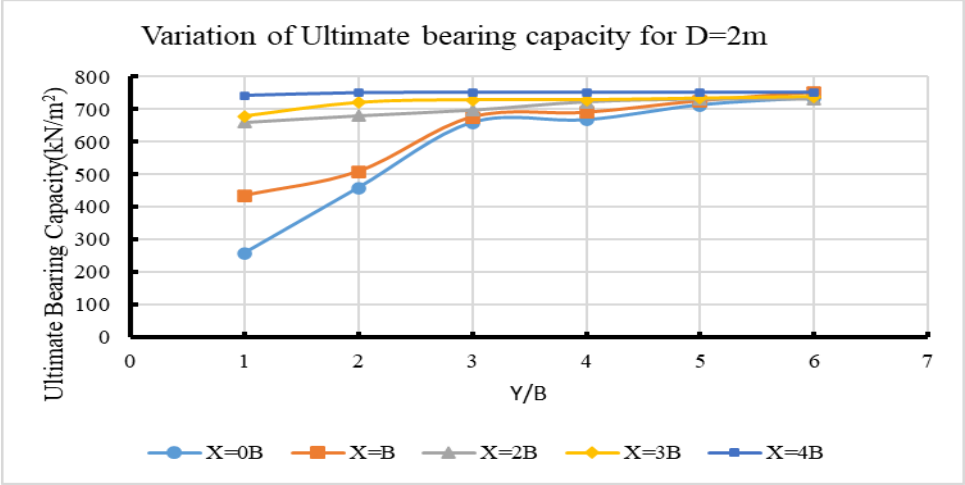

Figure 4.4(d): Effect of circular void(D=2.0m) with varying void depth(Y) upon bearing capacity of foundation for different horizontal offset(X) of void.

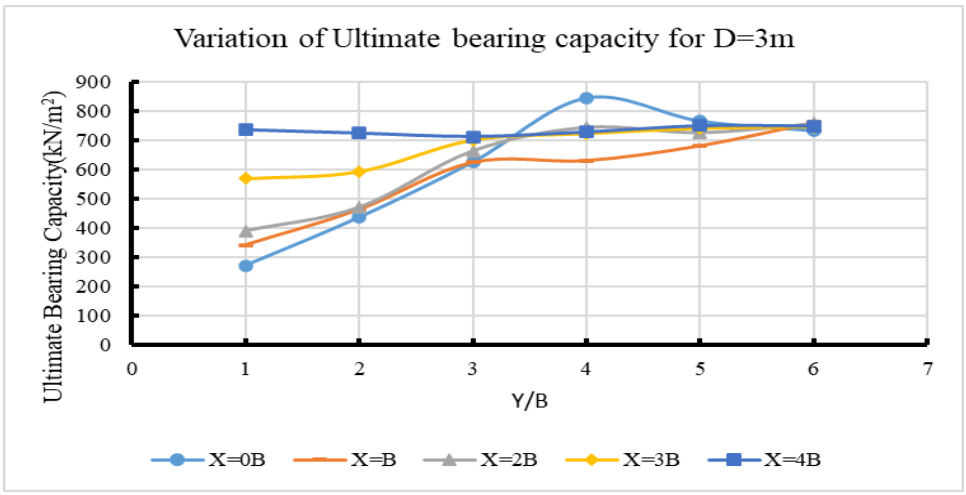

Figure 4.4(e): Effect of circular void (D=3.0m) with varying void depth(Y) upon bearing capacity of foundation for different horizontal offset of void(X).

The findings show that the biggest reduction in bearing capacity occurs when the void is located closest to the footing base. The ultimate bearing capacity also reduces when the footing's distance from the subsurface void's crest diminishes. Furthermore, the influence of void decreases when it is located farther down from the footing's base. This occurs depending on the size of the void. The effect of the shape is also expected to change the critical depth, the depth up to which the effect of the void can be observed. The change in void size for the critical depth can be seen in fig 4.4 (a), (b), (c), (d) and (e). where 0.5m diameter void influence can be seen up to depth of 3B while for 3m diameter void the depth has increase to 4B or up to 5B as well. As a result, the analysis's conclusion shows that there is a critical depth beneath the footing where the existence of void has a major impact on the footing's performance.

It is evident from Figure 4.4(a),(b),(c), and (d) that the reduction in bearing capacity varies depending on the depth of the void. Figure 4.4 makes it evident that the consequences of a void's presence decrease in proportion to the void's size. The results also show that, in addition to depth, the horizontal position of the void with respect to the foundation is a major factor in how well the foundation performs. The bearing capacity is most affected by the void's presence when it is closest to the foundation. This could be the case because, in the vicinity of the foundation, void failure happens first, followed by bearing failure; as depth increases, the failure transitions to void and bearing failure, and ultimately to only bearing failure.

Among the circular, rectangular and square voids, circular voids are more stable that other two, although the expected output will follow the same pattern, but the value of the bearing capacity will be less for those two cases.

4.2.1.2 Effect of horizontal offset of the void (x)

A void at different horizontal offsets from the foundation center has been simulated to examine the degree to which the void's horizontal position in relation to the foundation center affects the foundation's performance.

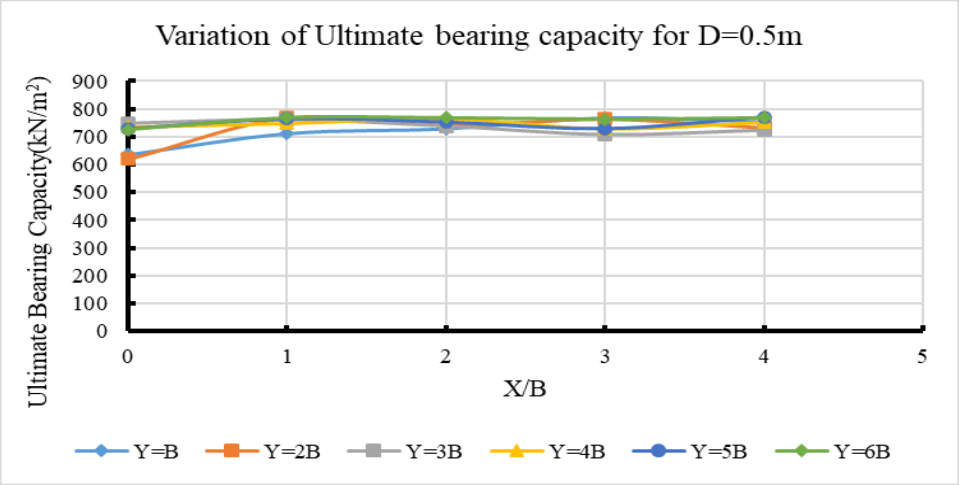

Figure 4.5(a): Effect of circular void(D=0.5m) with varying horizontal offset(X) upon bearing capacity of foundation for different vertical offset(Y) of void.

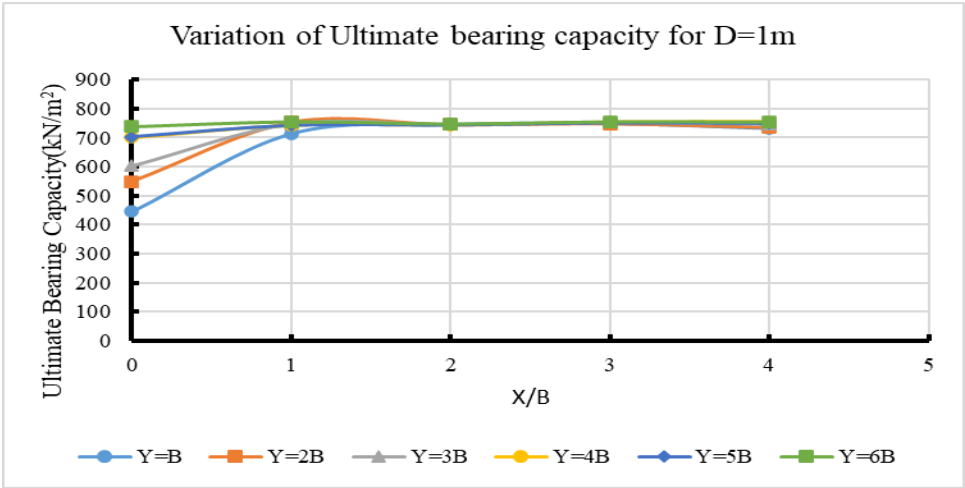

Figure 4.5(b): Effect of circular void(D=1.0m) with varying horizontal offset(X) upon bearing capacity of foundation for different vertical offset(Y) of void.

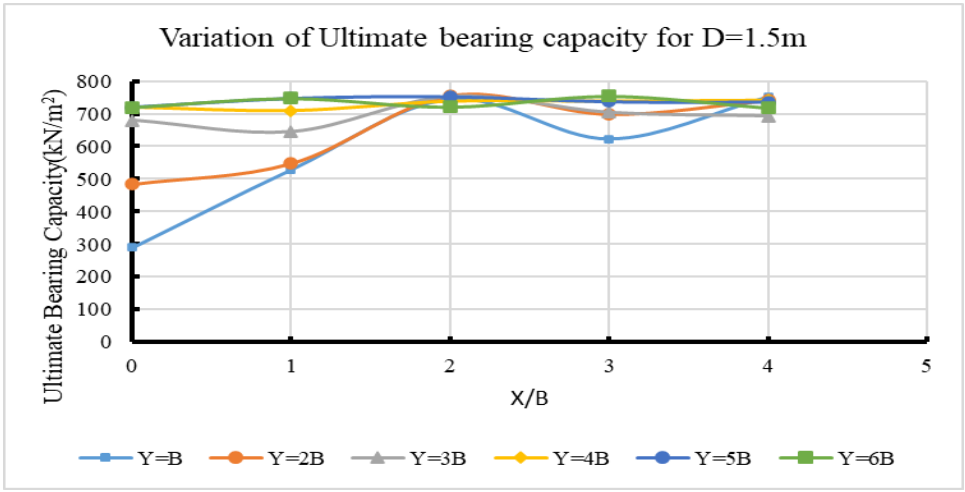

Figure 4.5(c): Effect of circular void (D=1.5m) with varying horizontal offset(X) upon bearing capacity of foundation for different vertical offset(Y) of void.

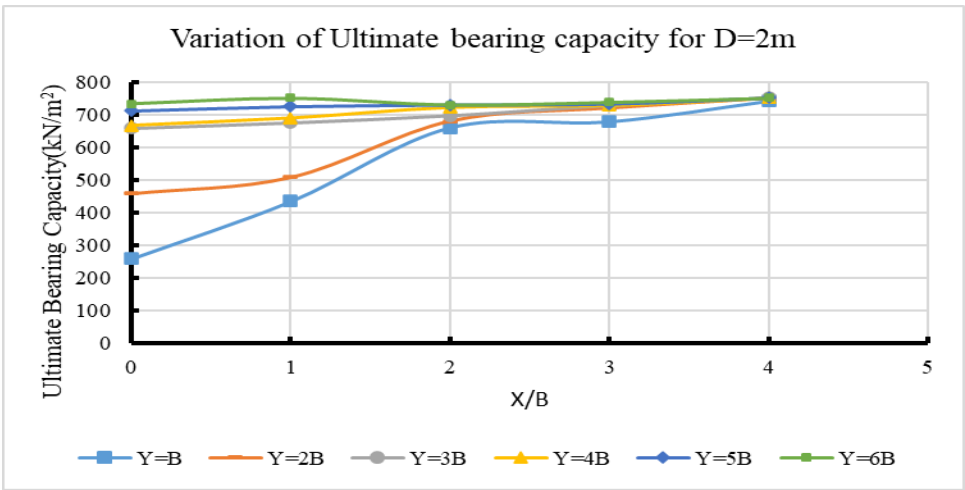

Figure 4.5(d): Effect of circular void(D=2.0m) with varying horizontal offset(X) upon bearing capacity of foundation for different vertical offset(Y) of void.

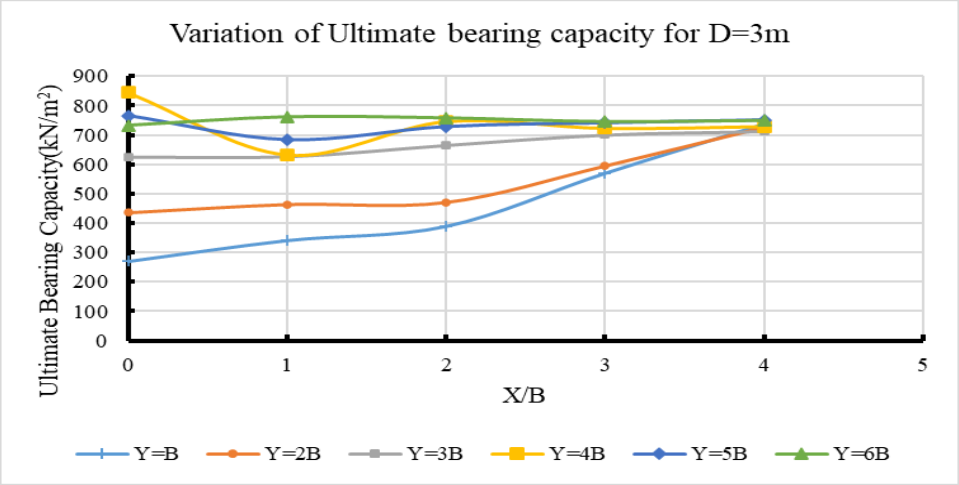

Figure 4.5(e): Effect of circular void (D=3.0m) with varying horizontal offset(X) upon bearing capacity of foundation for different vertical offset(Y) of void.

Furthermore, Figure 4.5(a), (b), (c), (d) and (e) demonstrate the ultimate bearing capacity as determined by the load settlement curve at various void positions while maintaining the void's circular shape.

The ultimate bearing capacity reduces as the footing's distance from the void decreases, and the highest reduction in bearing capacity occurs when the void is close to the footing, according to the research. Furthermore, the influence of the void decreases when it is positioned farther from the footing's center. This happens in accordance with the void's size, as seen in Figure 4.5(a), (b), (c), (d), and (e). As a result, the analysis's conclusion shows that the footing is surrounded by a location. The presence of void will only materially impair footing performance if it is found in this area.

It is evident from Figure 4.5(a), (b), (c), (d), and(e) that the decrease in bearing capacity is not uniform with regard to the void's horizontal offset. The bearing capacity decreases with increasing void size. The results also show that, in addition to its horizontal position, the vertical position of the void in the soil domain is crucial to the foundation's performance. The void's existence has the biggest impact on bearing capacity when it is at the closest level of the footing (i.e., at y=B). Furthermore, as the horizontal offset increases, the effect continues to decrease until a certain point, depending on the size of the void, at which point it becomes constant. Depending on the void's size, the critical width—the farthest distance at which its influence can be observed—varies from 2B to 5B.

4.2.2 Effect of size of void

A circular-shaped void with varying dimensions has been simulated to examine the extent to which the void's size affects the foundation's performance. Furthermore, Figure 4.6(a), (b), (c), (d), (e) and (f). demonstrate the ultimate bearing capacity as determined by the load settlement curve for various circular void sizes.

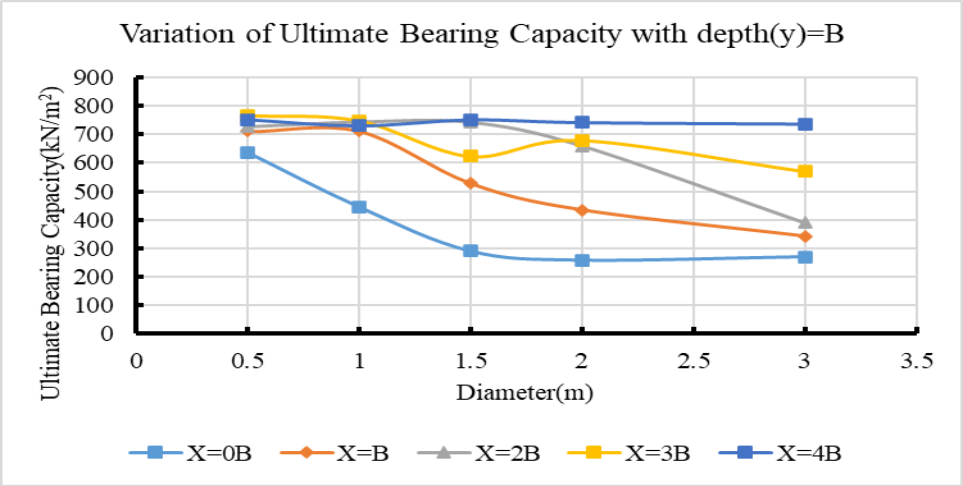

Figure 4.6(a): Effect of Vertical offset(Y=B) with varying void size(D) upon bearing capacity of foundation for different Horizontal offset(X) of void.

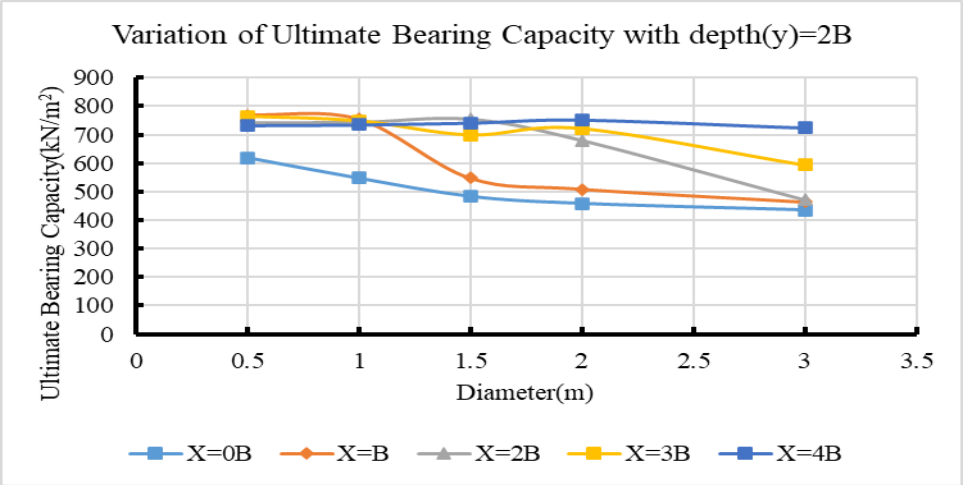

Figure 4.6(b): Effect of Vertical offset(Y=2B) with varying void size(D) upon bearing capacity of foundation for different Horizontal offset(X) of void.

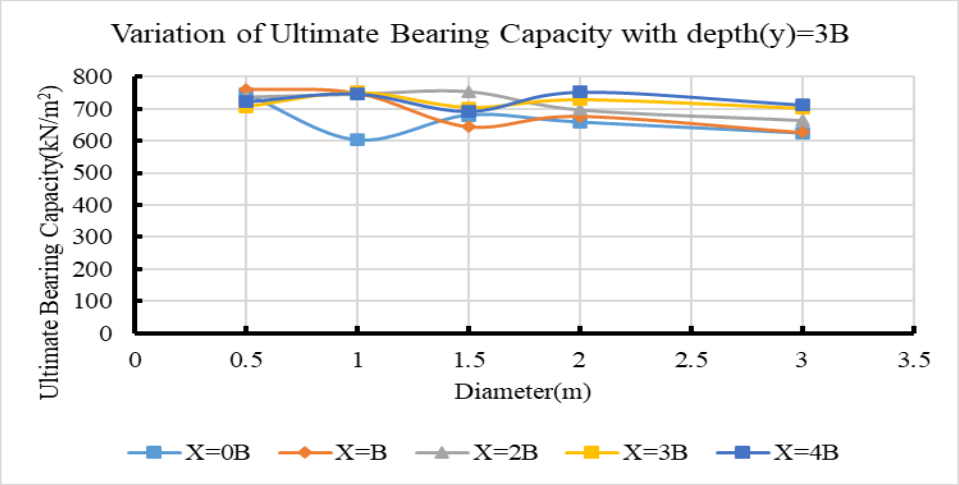

Figure 4.6(c): Effect of Vertical offset(Y=3B) with varying void size(D) upon bearing capacity of foundation for different Horizontal offset(X) of void.

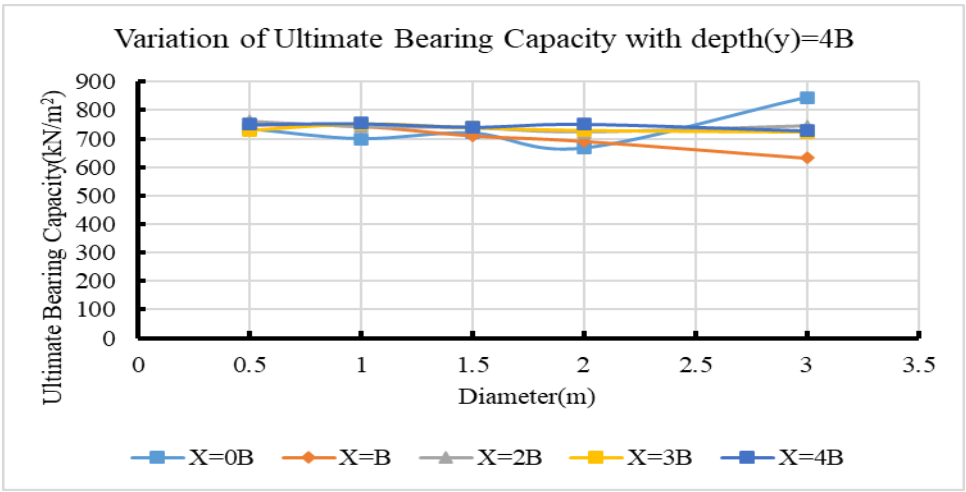

Figure 4.6(d): Effect of Vertical offset(Y=4B) with varying void size(D) upon bearing capacity of foundation for different Horizontal offset(X) of void.

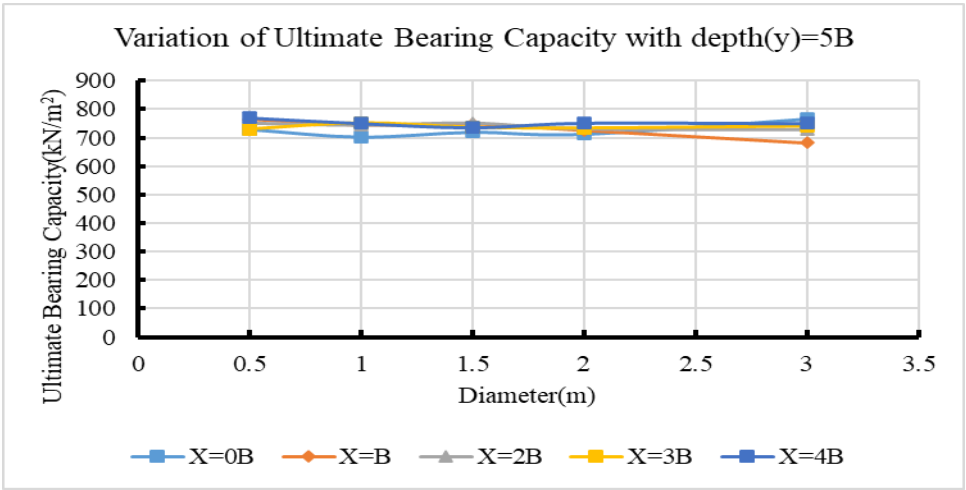

Figure 4.6(e): Effect of Vertical offset(Y=5B) with varying void size(D) upon bearing capacity of foundation for different Horizontal offset(X) of void.

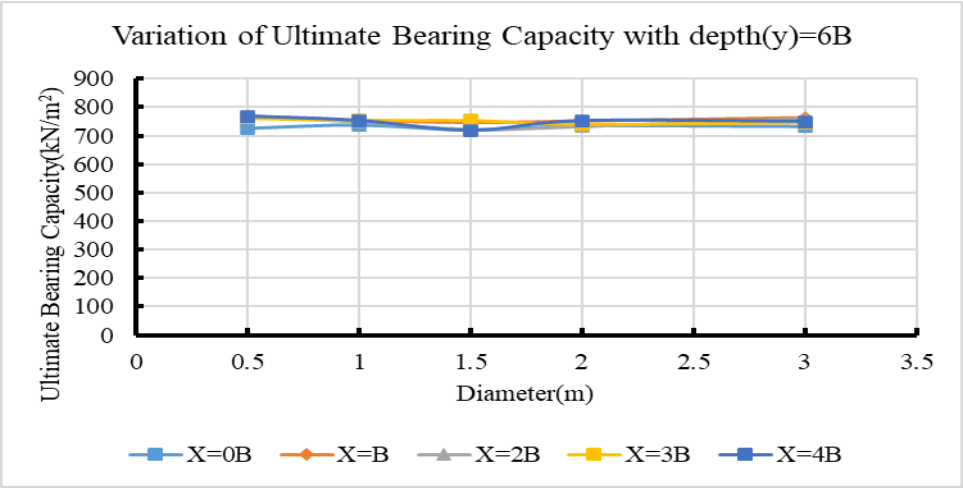

Figure 4.6(f): Effect of Vertical offset(Y=6B) with varying void size(D) upon bearing capacity of foundation for different Horizontal offset(X) of void.

The findings show that as void size increases, the ultimate bearing capacity decreases, with the largest void showing the greatest reduction in bearing capacity (fig. 4.6The greatest void in this study has a diameter of only three meters, yet the bearing capacity trend with regard to void size clearly illustrates a pattern of decreasing ultimate bearing capacity as void size increases. Furthermore, the influence of the void decreases with a reduction in size. The analysis's conclusion is that there is a crucial void size, and that when the void's size surpasses this dimension, its presence will have a substantial impact on the footing's performance based on its horizontal and vertical offset with regard to the foundation.

It is evident from Figure 4.6(a), (b), (c), (d), (e), and (f) that the reduction in bearing capacity varies depending on the size of the soil void. It can be noticed from the results that the position of the void with respect to the foundation in the soil domain plays major function in the performance of the foundation, as closer the void and larger the void is located to the foundation, greater will be its influence. The void's existence has less impact if it is farther away than the critical area surrounding the foundation. As observed in Figure 4.6(e) and (f), the presence of a void, regardless of size or location, has no effect on the bearing capacity when it is deeper than the critical depth. This could be due to the fact that the failure surface and stress only reach the so-called critical zone—the region around the foundation outside of which the presence of void has no bearing on the functionality of the foundation.

4.2.3 Effect of void shape

To investigate the effect of the void shape, shapes such as circular, square and rectangle voids have been simulated. The size of the voids is varied for different shapes and the comparison has been made by making the widest portion same. Moreover, for rectangular void both the cases horizontal and vertical has been study.

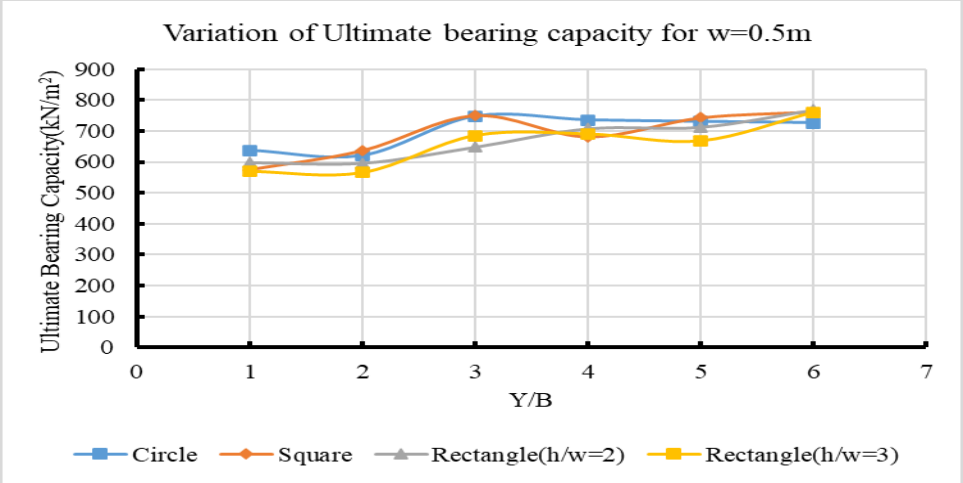

Figure 4.7(a): Effect of Different shape of void having top width or diameter(W=0.5m) with varying vertical offset(Y) and Horizontal offset(X=0) for different shapes

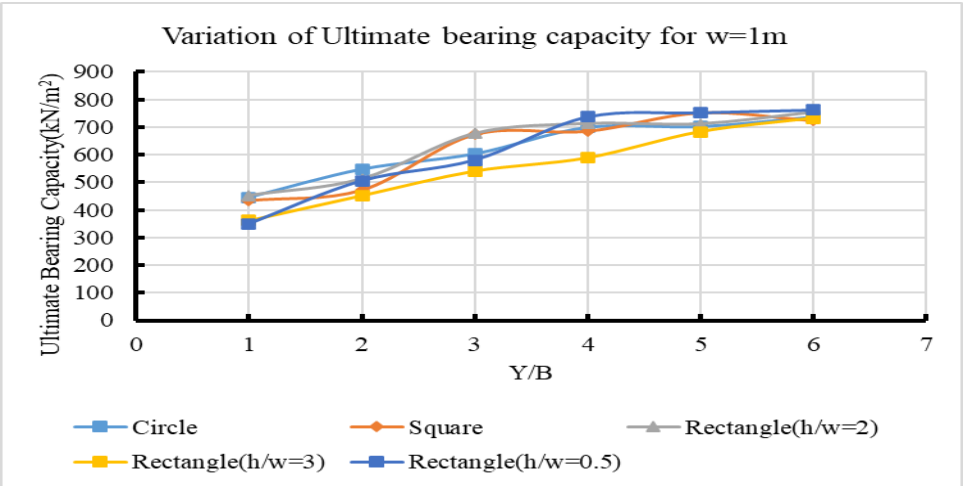

Figure 4.7(b): Effect of Different shape of void having top width or diameter(W=1m) with varying vertical offset(Y) and Horizontal offset(X=0) for different shapes

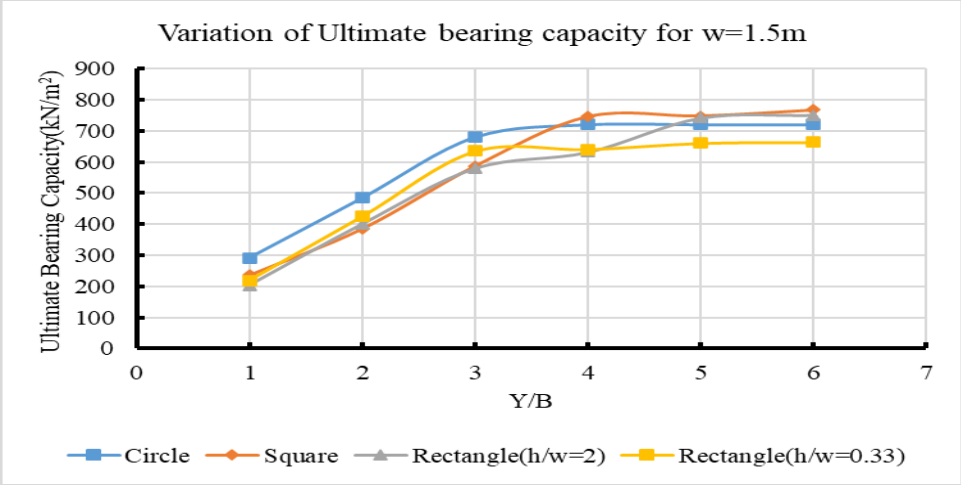

Figure 4.7(c): Effect of Different shape of void having top width or diameter(W=1.5m) with varying vertical offset(Y) and Horizontal offset(X=0) for different shapes

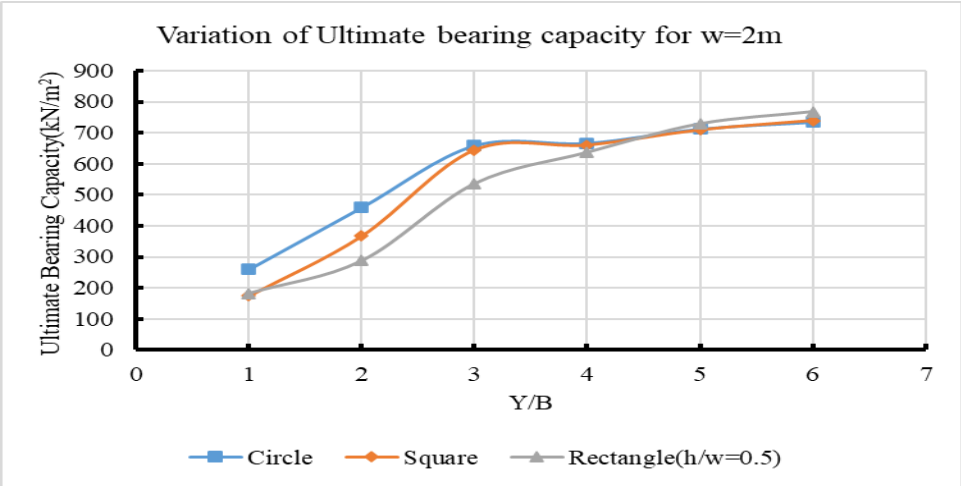

Figure 4.7(d): Effect of Different shape of void having top width or diameter(W=2m) with varying vertical offset(Y) and Horizontal offset(X=0) for different shapes

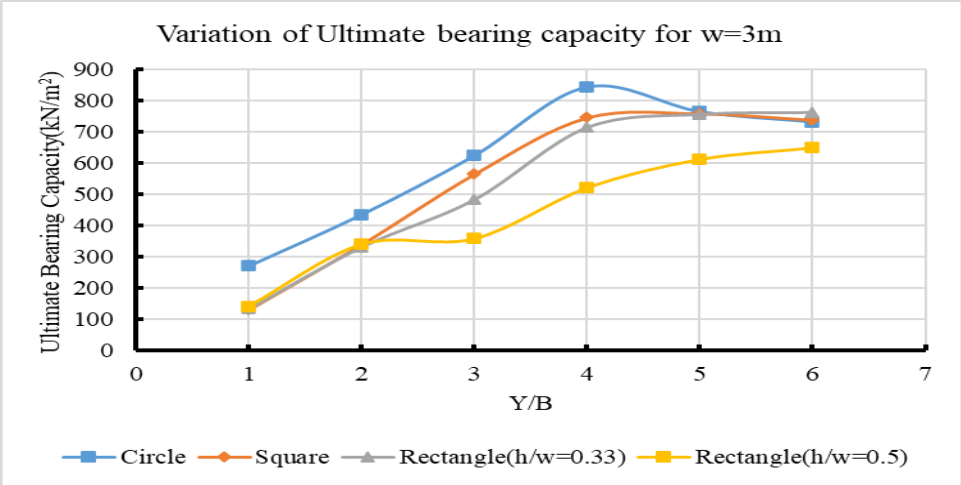

Figure 4.7(e): Effect of Different shape of void having top width or diameter(W=3m) with varying vertical offset(Y) and Horizontal offset(X=0) for different shapes

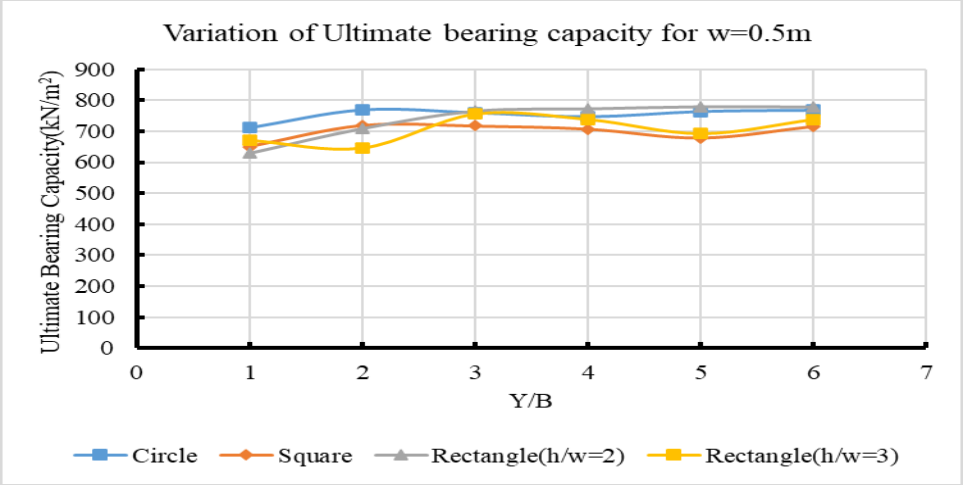

Figure 4.8(a): Effect of Different shape of void having top width or diameter(W=0.5m) with varying vertical offset(Y) and Horizontal offset(X=B) for different shapes

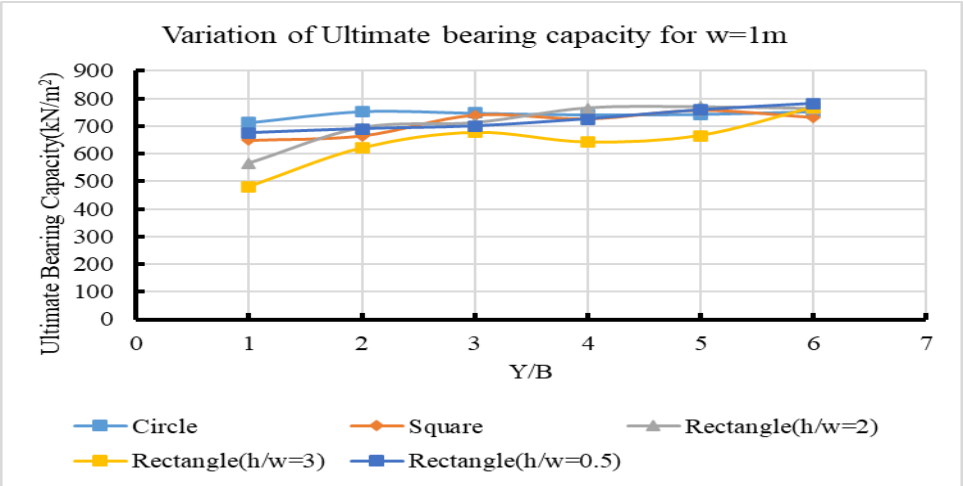

Figure 4.8(b): Effect of Different shape of void having top width or diameter(W=1m) with varying vertical offset(Y) and Horizontal offset(X=B) for different shapes

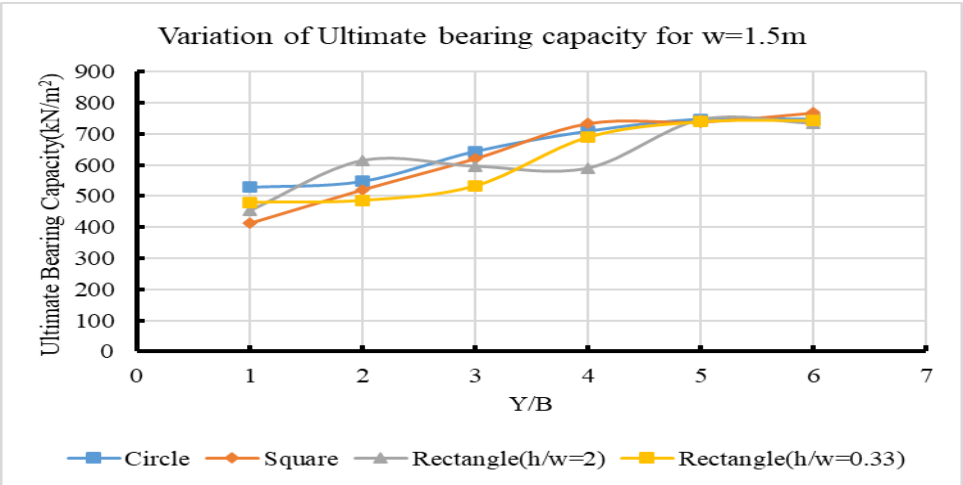

Figure 4.8(c): Effect of Different shape of void having top width or diameter(W=1.5m) with varying vertical offset(Y) and Horizontal offset(X=B) for different shapes

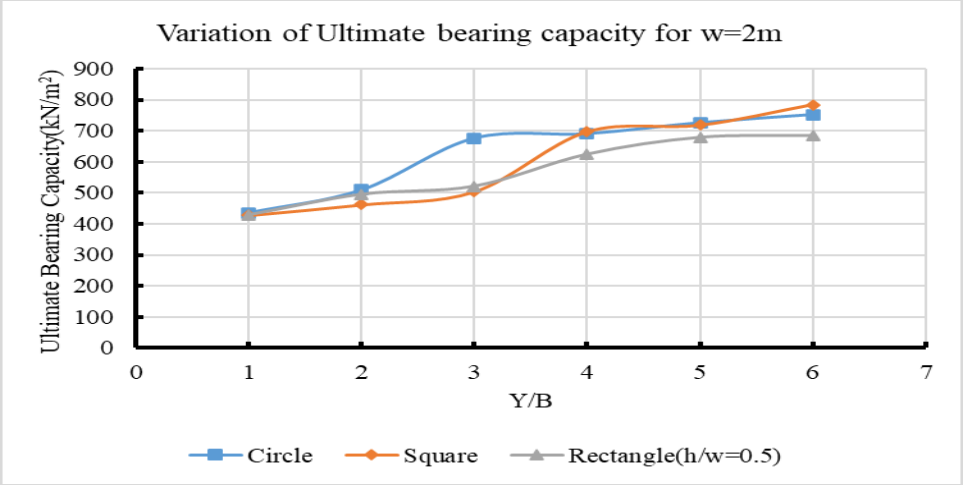

Figure 4.8(d): Effect of Different shape of void having top width or diameter(W=2m) with varying vertical offset(Y) and Horizontal offset(X=B) for different shapes

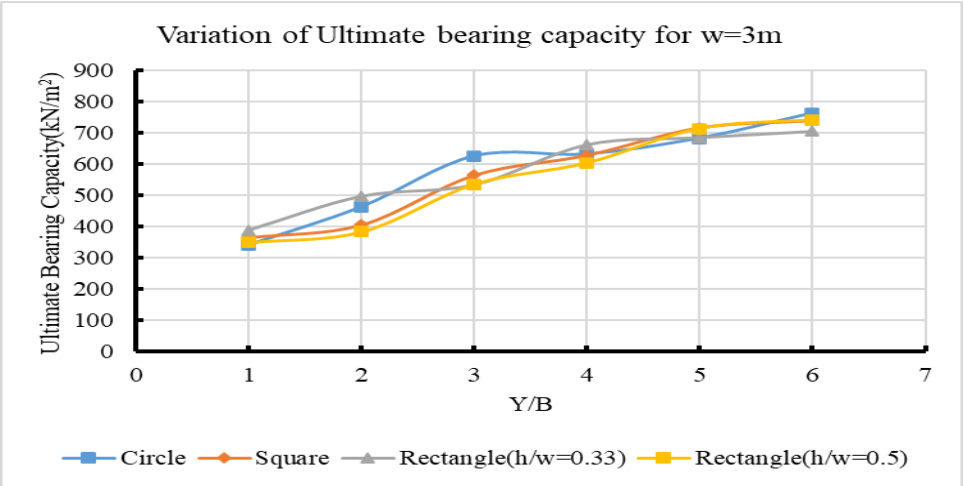

Figure 4.8(e): Effect of Different shape of void having top width or diameter(W=3m) with varying vertical offset(Y) and Horizontal offset(X=B) for different shapes

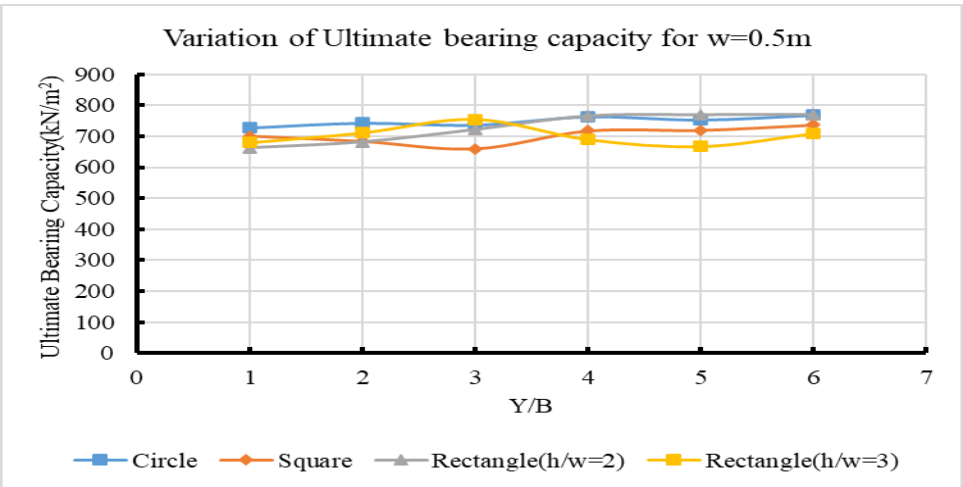

Figure 4.9(a): Effect of Different shape of void having top width or diameter(W=0.5m) with varying vertical offset(Y) and Horizontal offset(X=2B) for different shapes

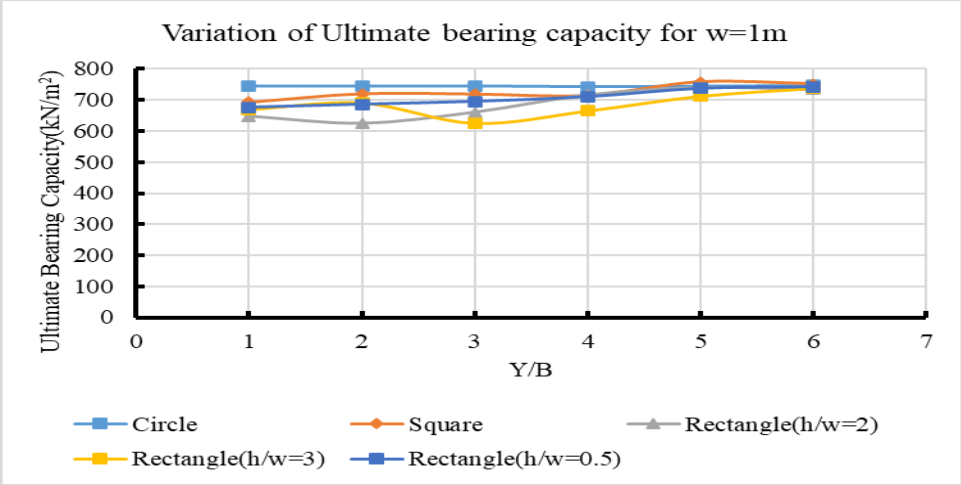

Figure 4.9(b): Effect of Different shape of void having top width or diameter(W=1m) with varying vertical offset(Y) and Horizontal offset(X=2B) for different shapes

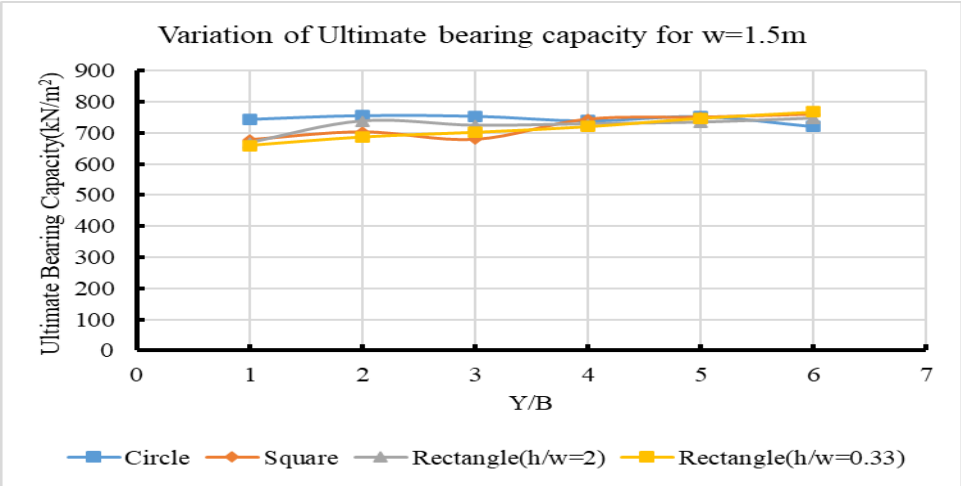

Figure 4.9(c): Effect of Different shape of void having top width or diameter(W=1.5m) with varying vertical offset(Y) and Horizontal offset(X=2B) for different shapes

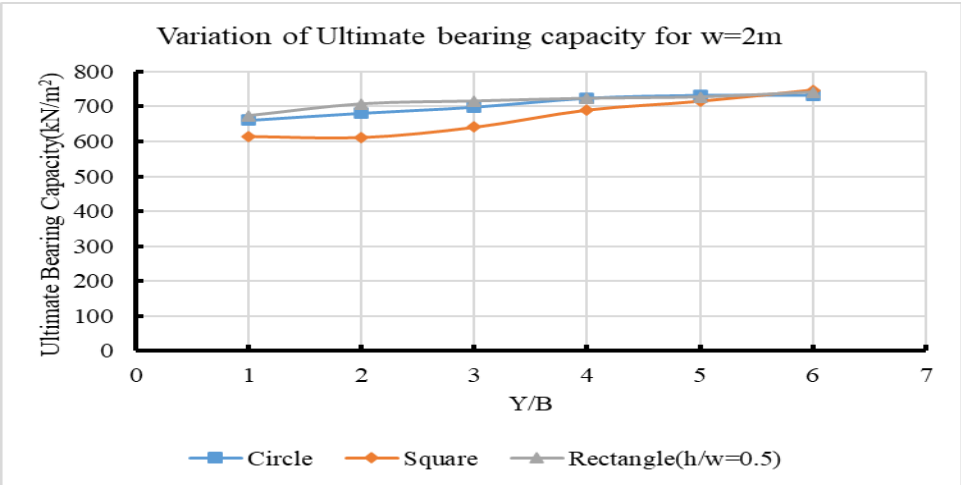

Figure 4.9(d): Effect of Different shape of void having top width or diameter(W=2m) with varying vertical offset(Y) and Horizontal offset(X=2B) for different shapes

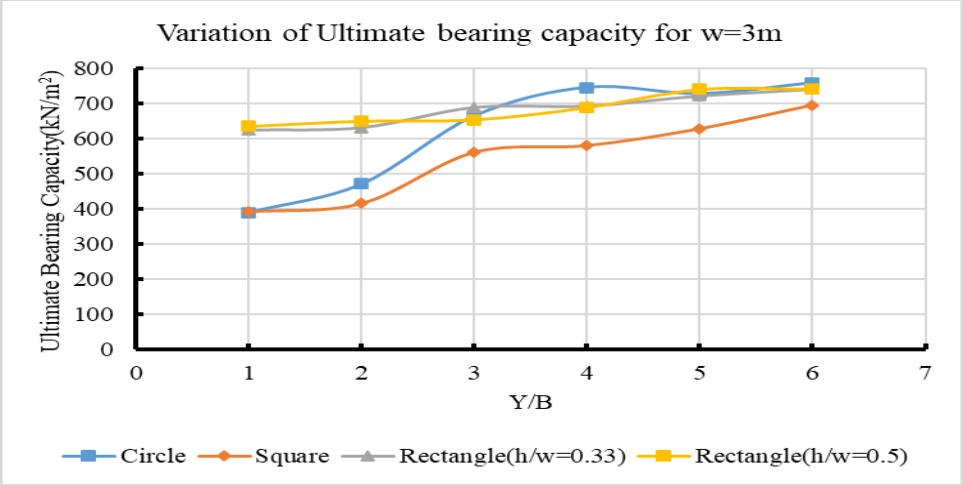

Figure 4.9(e): Effect of Different shape of void having top width or diameter(W=3m) with varying vertical offset(Y) and Horizontal offset(X=2B) for different shapes

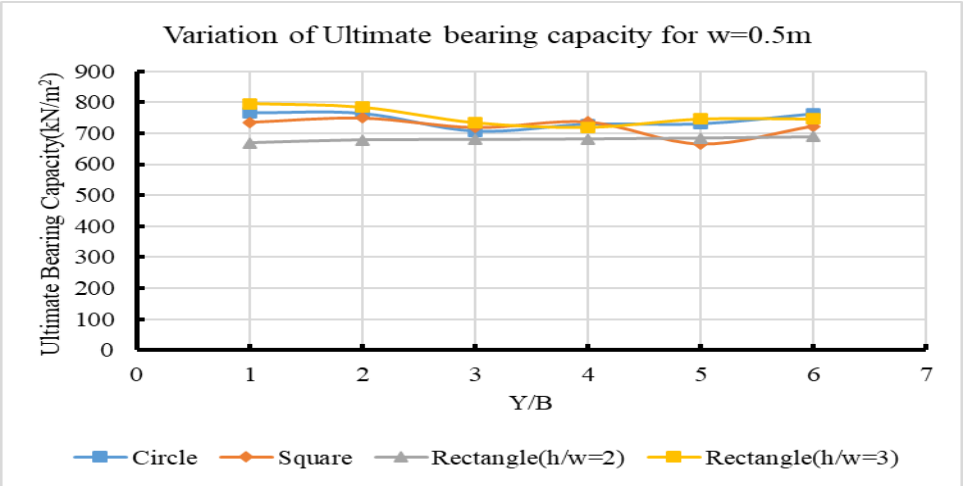

Figure 4.10(a): Effect of Different shape of void having top width or diameter(W=0.5m) with varying vertical offset(Y) and Horizontal offset(X=3B) for different shapes

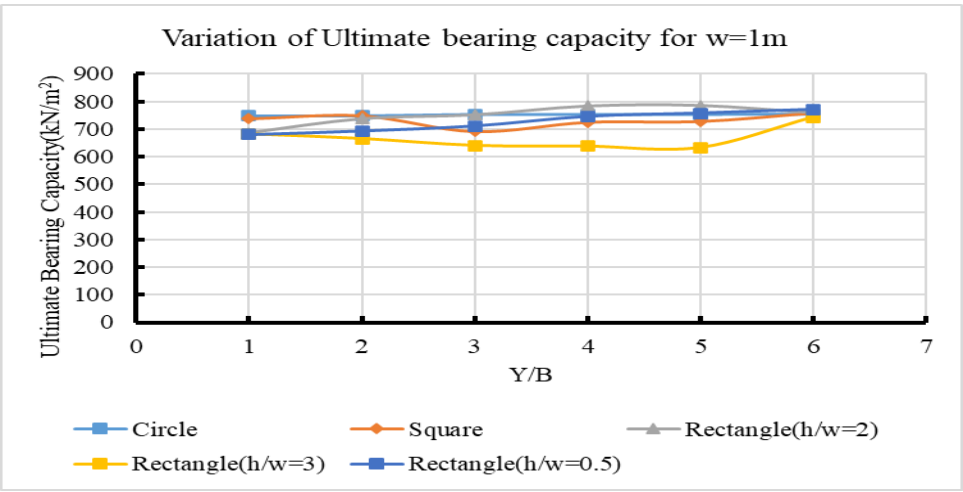

Figure 4.10(b): Effect of Different shape of void having top width or diameter(W=1m) with varying vertical offset(Y) and Horizontal offset(X=3B) for different shapes

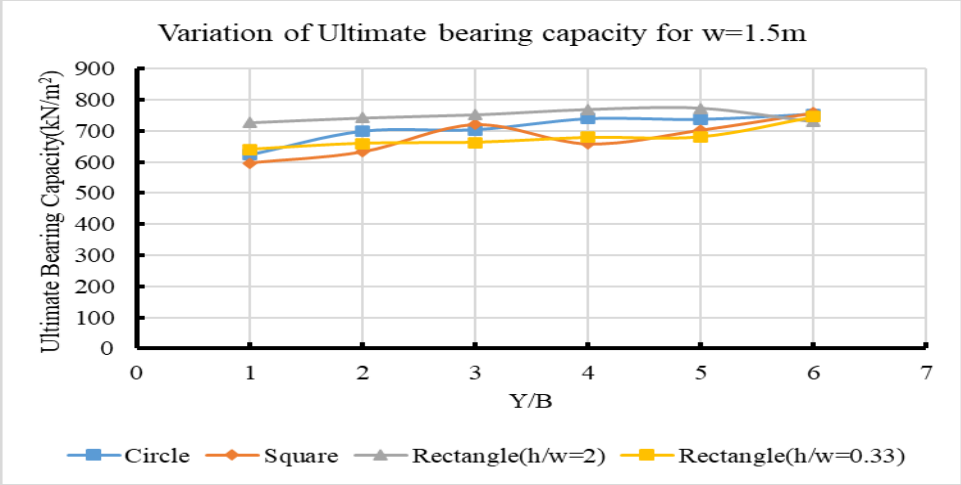

Figure 4.10(c): Effect of Different shape of void having top width or diameter(W=1.5m) with varying vertical offset(Y) and Horizontal offset(X=3B) for different shapes

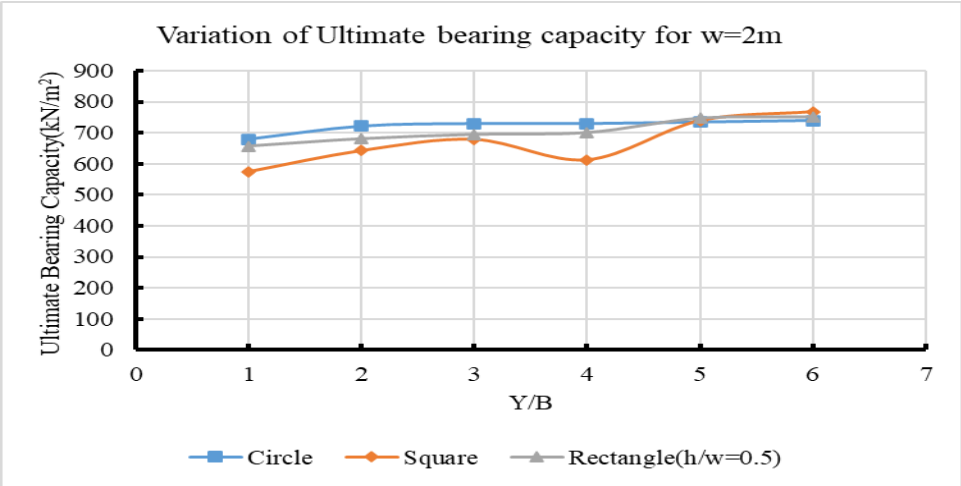

Figure 4.10(d): Effect of Different shape of void having top width or diameter(W=2m) with varying vertical offset(Y) and Horizontal offset(X=3B) for different shapes

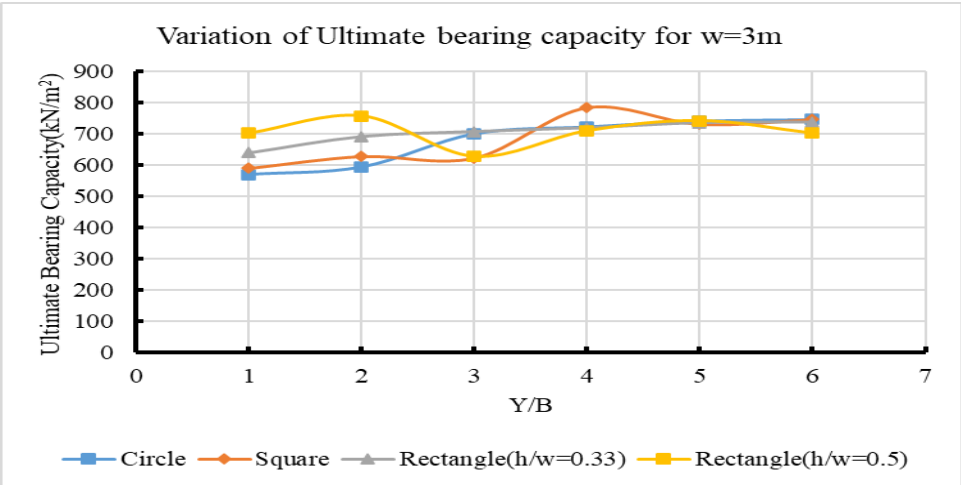

Figure 4.10(e): Effect of Different shape of void having top width or diameter(W=3m) with varying vertical offset(Y) and Horizontal offset(X=3B) for different shapes

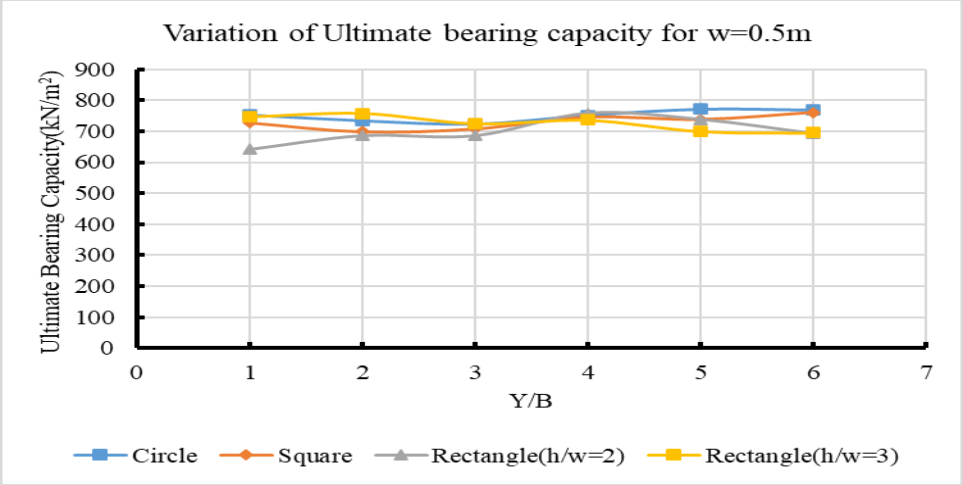

Figure 4.11(a): Effect of Different shape of void having top width or diameter(W=0.5m) with varying vertical offset(Y) and Horizontal offset(X=4B) for different shapes

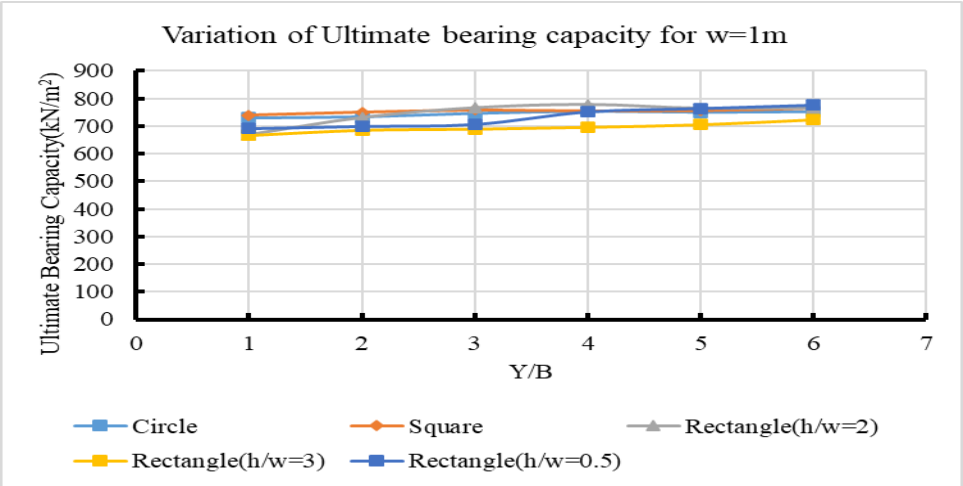

Figure 4.11(b): Effect of Different shape of void having top width or diameter(W=1m) with varying vertical offset(Y) and Horizontal offset(X=4B) for different shapes

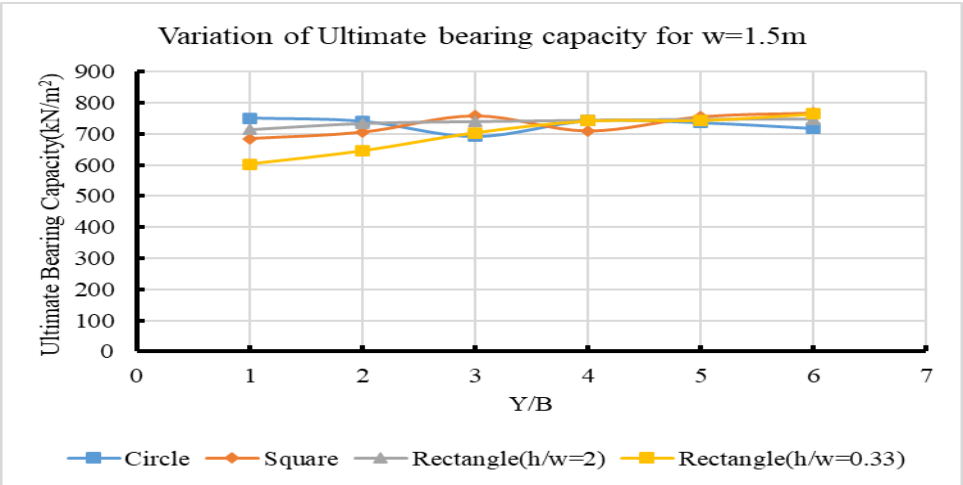

Figure 4.11(c): Effect of Different shape of void having top width or diameter(W=1.5m) with varying vertical offset(Y) and Horizontal offset(X=4B) for different shapes

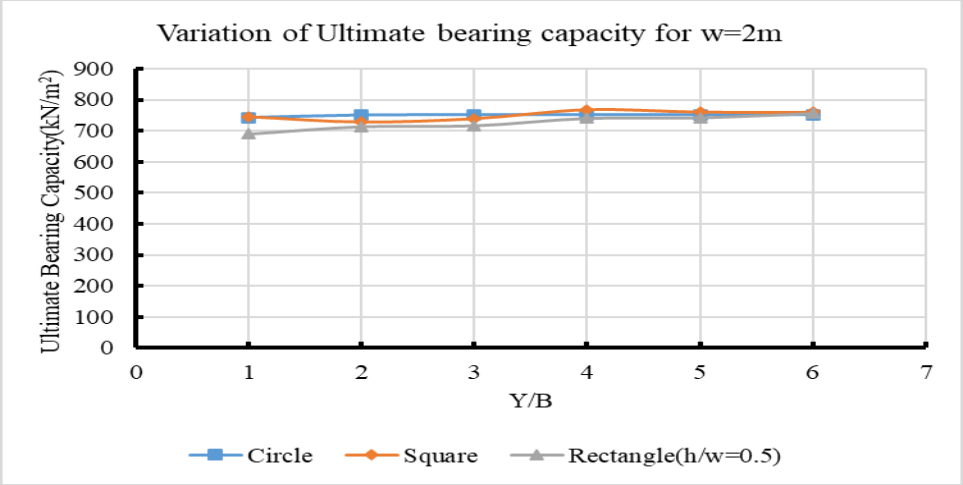

Figure 4.11(d): Effect of Different shape of void having top width or diameter(W=2m) with varying vertical offset(Y) and Horizontal offset(X=4B) for different shapes

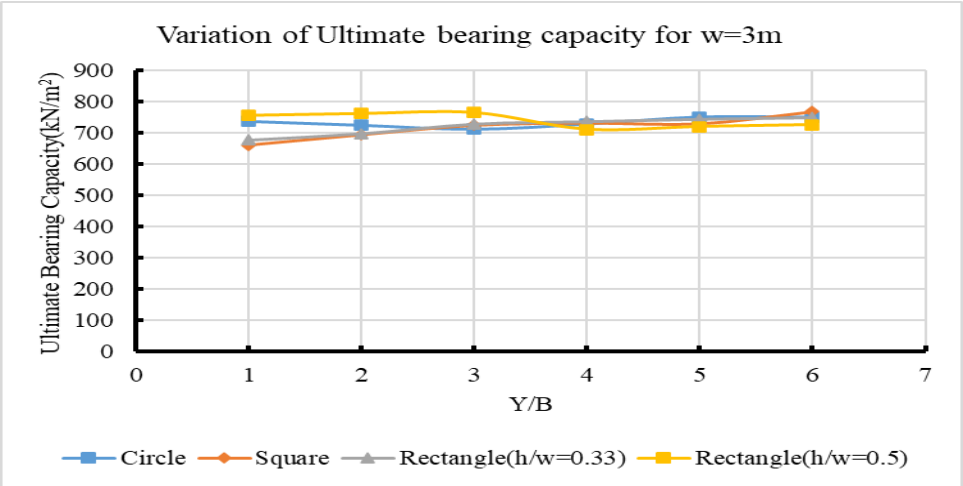

Figure 4.11(e): Effect of Different shape of void having top width or diameter(W=3m) with varying vertical offset(Y) and Horizontal offset(X=4B) for different shapes

As we can see in figure 4.7, the outcome shows that for the zero-horizontal offset, the final bearing capacity reduces as the depth of the void location grows. The bearing capacity is mostly unaffected by the void's shape because it increases as depth does similar for all types of shape. However, upon closer inspection it can be found that the circular void has more bearing capacity than the square and rectangular void when the total unsupported length is same. This phenomenon is due to more arching effect of circular voids than square and rectangle. Moreover, when the size of the void increases the critical depth for the bearing capacity decreases which is rational to the previous finding regarding the circular void.

Because the bearing capacity increases as depth of void location increases, the shape of the void has very little effect on it. However, upon closer inspection it can be found that the rectangular voids which have height to width ratio greater than 1 seem to have lower bearing capacity although the total unsupported length is same. Figure 4.8, Figure 4.9, and Figure 4.10 illustrate this occurrence. Moreover, when the size of the void increases the critical depth for the bearing capacity decreases which is rational to the previous finding regarding the circular void.

From figure 4.7, figure 4.8, figure 4.9, figure 4.10 and figure 4.11, the ultimate bearing capacity increases with the increase the horizontal offset. Although the result is uniform indicating that the decrease in the bearing capacity is non uniform and the reduction is more when the position of the void is near the foundation. The effect of the void decreases when the increase in the vertical offset and horizontal offsets.

4.2.4 Effect of presence of ground water table.

The effect of water table in the bearing capacity has been studied by varying the depth of ground water for one meter to fifteen meter from the ground surface. For the purposes of this study, the shape of void is restricted to circular void and the range of the opening varies form 1.5m to 3m i.e.(diameter(D/W)=1.5m,2m and 3m).

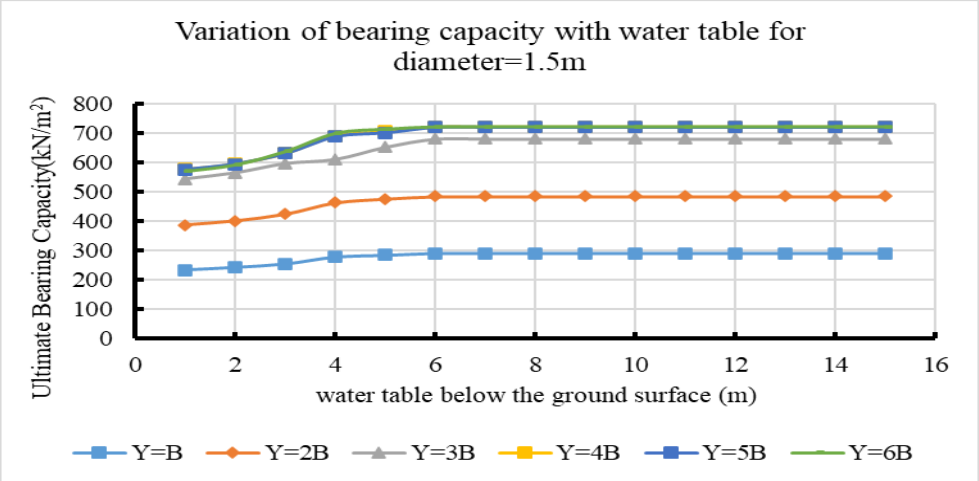

Figure 4.12(a): Effect of variation of water table from 1m to 15m on bearing capacity of with horizontal offset(X=0) for Circular shape of void having diameter(D=1.5m)

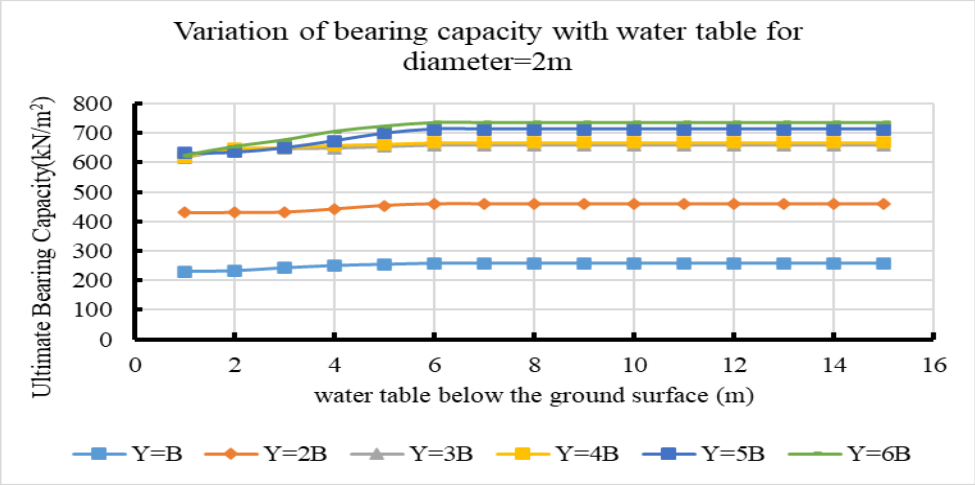

Figure 4.12(b): Effect of variation of water table from 1m to 15m on bearing capacity of with horizontal offset(X=0) for Circular shape of void having diameter(D=2m)

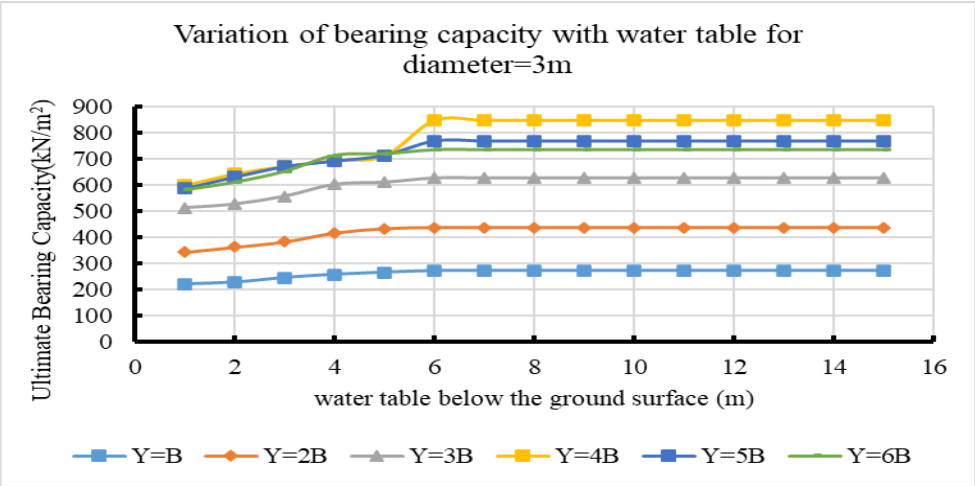

Figure 4.12(c): Effect of variation of water table from 1m to 15m on bearing capacity of with horizontal offset(X=0) for Circular shape of void having diameter(D=3m)

Figure 4.12 indicates the effect of water table in the bearing capacity of the strip footing when there is present of the void. From figure 4.12(a), (b) and (c), the bearing capacity has decreased when the water table is near the foundation and the bearing capacity gradually increases when the water table goes down. The effect of the water table is seen up to the depth of 6m from the top of the surface i.e., 3B for the top of the surface. When the water table is below 3B, the bearing capacity remains the same as that of the non-water table condition. As the unit weight is reduced due to presence of water table.

Moreover, the size of the void has no effect on the bearing capacity with present of ground water table as the decrease in the bearing capacity is similar irrespective of the size of the void i.e., the decrease in bearing capacity can be seen up to the depth of 3B, irrespective

of the size of the void and the location of the void. From previous findings, it can also be said that the shape of the void also does not have significant effect on bearing capacity with the water table i.e., the decrease in bearing capacity due to water table is similar irrespective of the shape of the void.

4.2.5 Effect of presence of void on deformation and failure zone.

The effect of presence of underground void poses unfavorable and unpredictable reduction in bearing capacity. The cause of such unfavorable conditions can be studies trough the deformation and compressive failure surface. expected output may be compressive failure zone will connect to the void without the formation of active wedge in the region where reduction of bearing capacity is found and when the active wedge is formed below the footing the effect void diminishes.

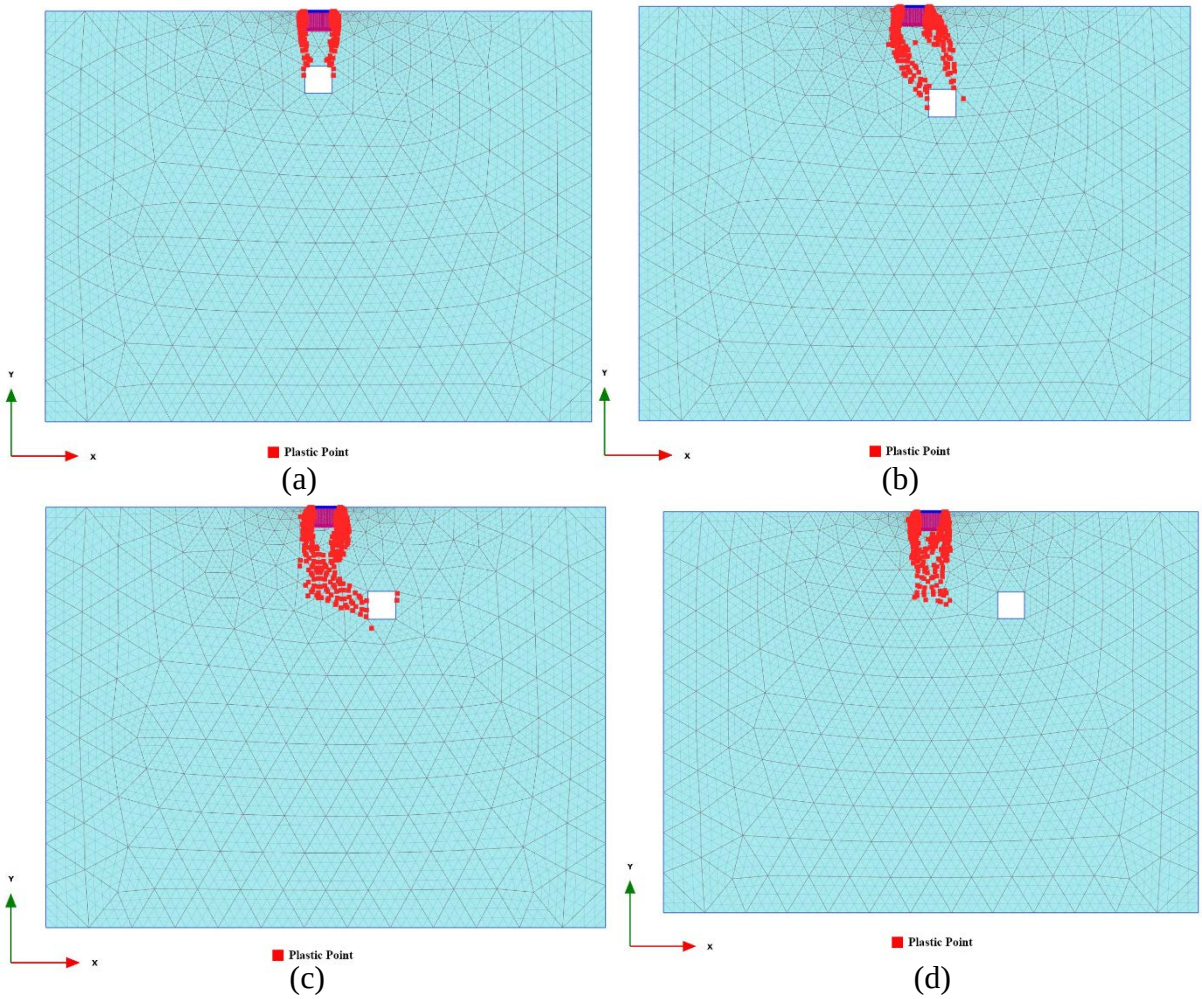

Figure 4.13: Failure model of the soil due to presence of void. (a) Roof Failure, (b) combined failure, (c) Side wall failure and (d) wedge Failure

There are four common types of failure models, as shown in figure 4.13(a), (b), (c), and (d). The primary failure model for a void that is directly below the foundation—that is, without any horizontal offset—is roof failure since the failure is brought on by the collapse of the void's roof. Moreover, when the void is slightly offset then the combined failure of roof and slide wall is likely to occur when can be termed as combined failure. And when the void has larger offset, slide wall failure is likely to occur. Finally, when the void is far enough i.e., away from the critical depth or critical width the wedge failure will occur which is characterized by the formation of wedge like structure below the foundation.

5. CONCLUSIONS AND RECOMMENDATIONS

5.1 Conclusion

The purpose of this study was to evaluate how underground voids affected the surface strip foundation's ability to support loads in silty sandy soil. In this investigation parametric analysis has been performed to perceive the extent of effect of size, location, and shape of the void in the bearing capacity under foundation load. Below is a summary of some of the study's key findings:

- There is a critical depth below the foundation. When the void is present within or at this depth, the performance of the foundation will be significantly affected. The bearing capacity of the foundation is drastically reducing as the depth of void from the base of the foundation decreases. The depth of the critical zone varies for the different sizes. For diameter or width equal to 0.5m the critical depth is 3B, similarly for 1m and 1.5m it’s 4B, for 2m its 5B and for 3m its 6B.
- There is a horizontal zone of influence around the foundation. When the void is present within or at this distance, the performance of the foundation will be significantly affected. The bearing capacity of the foundation is drastically reducing as the void lies within this zone of influence. The critical horizontal offset at which the effect void is significant depends on the size and shape of the void. The critical horizontal for diameter of 0.5m,1m,1.5m,2m,3m are 2B,3B,3B,4B,4B respectively.
- The size of void greatly influences the bearing capacity behavior of the sub-soil. The bearing capacity of the soil decreases as the size of void increases and vice versa. The effect of void is more prominent for larger void than that for smaller ones for the respective position of void. When the void is present at B depth for the foundation effect of all the sizes of void can be seen, moreover when the void is at 2B effect of 0.5m width void diminishes and on every increase of B, there effect of 1m,1.5m,2m and 3m effect diminishes.
- The effect of shape of the void does not have any effect on the bearing capacity of the foundation, circular, square and rectangular voids have similar effects on the bearing capacity. However, if the rectangular void with h/w ratio greater than 1 is present at certain offset of foundation then the then is reduction of bearing capacity due to sidewall failure rather than roof failure.

- The failure of the void can be categorized into three as roof failure, side wall failure and combined failure. The mode of failure depends on the location of the void. voids which are directly below the foundation (i.e., X=0) fail by roof failure, void which are at the offset of X=2B fails by wall failure and void which are at X=Bm fails by combined failure. These are the values for circle with diameter(D)=2m.

The bearing capacity of the soil varies with the proximity of the void to the foundation, as demonstrated by the outcomes of several numerical model analyses.

5.2 Recommendation

There are significant limits to this research, making it far from perfect. Following are some suggestions for upcoming work.:

- This study is limited to a single layered soil only, which is not favorable for the wide range of soil type present in nature. Hence similar study can be carried out for with multiple layers soils.
- Although void is assumed to be continuous and in a single location at a time for the study, such regular heterogeneity is impracticable in nature. So, the effect of multiple voids and their interaction can be carried out.
- Only continuous strip foundation is the subject of this investigation. Thus, comparable research can be done for alternative footing configurations. Moreover, a 3-dimensional approach can be engaged with the presence of void of different lengths at various random 3D locations.
- Other than this, research is limited to bearing capacity calculations made in cases where the void runs parallel to the strip footing. However, the void can be pointed in any direction. Therefore, the effect of perpendicular voids can be executed.
- The arching effect of the voids is not fully understood, So mechanism of arching in the soil due to presence of the void can be further analyzed.

REFERENCES

Azam, G., Hsieh, C., & Wang, M. (1991). Performance of strip footing on stratified soil deposit with void. *Journal of Geotechnical Engineering*, *117*(5), 753-772.

Badie, A., & Wang, M. (1984). Stability of spread footing above void in clay. *Journal of Geotechnical Engineering*, *110*(11), 1591-1605.

Baus, R. L. (1980). *The stability of shallow continuous footings located above voids*. The Pennsylvania State University.

Benbouza, A., Mansouri, T., & Abbeche, K. (2023). Behavior of Strip Footing/s above Void in Sandy Soil. *Engineering, Technology & Applied Science Research*, *13*(1), 10039-10044.

Bowles, J. E. (1997). *Foundation Analysis and Design*. The McGrawHill Companies. Inc.

Das, B. M., & Sivakugan, N. (2018). *Principles of foundation engineering*. Cengage learning.

Farrent, T. (1963). The prediction and field verification of settlement in cohesionless soils. Proceedings of the 4th Australia-New Zeland conference on soil mechanics and foundation engineering,

Gautam, P., Pant, S. R., & Ando, H. (2000). Mapping of subsurface karst structure with gamma ray and electrical resistivity profiles: a case study from Pokhara valley, central Nepal. *Journal of Applied Geophysics*, *45*(2), 97-110.

IS:1888-1982. (1983). Method of Load Test on Soils. In *IS:1888 -1982*. New Delhi: Indian Standards Institution.

Jain, S., Nusari, M., Shrestha, R., & Mandal, A. (2023). Use of RCC pile, anchor bolt and geogrid for building construction on the unstable slope. *Geoenvironmental Disasters*, *10*. https://doi.org/10.1186/s40677-023-00243-8

Kiyosumi, M., Kusakabe, O., & Ohuchi, M. (2011). Model Tests and Analyses of Bearing Capacity of Strip Footing on Stiff Ground with Voids. *Journal of Geotechnical and Geoenvironmental Engineering*, *137*(4), 363-375. https://doi.org/10.1061/(asce)gt.1943-5606.0000440

Kiyosumi, M., Kusakabe, O., Ohuchi, M., & Le Peng, F. (2007). Yielding pressure of spread footing above multiple voids. *Journal of Geotechnical and Geoenvironmental Engineering*, *133*(12), 1522-1531.

Lavasan, A. A., Talsaz, A., Ghazavi, M., & Schanz, T. (2016). Behavior of Shallow Strip Footing on Twin Voids. *Geotechnical and Geological Engineering*, *34*(6), 1791-1805. https://doi.org/10.1007/s10706-016-9989-6

Lee, J. K., Jeong, S., & Ko, J. (2014). Undrained stability of surface strip footings above voids. *Computers and Geotechnics*, *62*, 128-135. https://doi.org/10.1016/j.compgeo.2014.07.009

Lee, J. K., Jeong, S., & Ko, J. (2015). Effect of load inclination on the undrained bearing capacity of surface spread footings above voids. *Computers and Geotechnics*, *66*, 245-252. https://doi.org/10.1016/j.compgeo.2015.02.003

Poulos, H. G., Carter, J. P., & Small, J. C. (2001). Foundation and Retaining Structures - Research and Practise (theme Lecture). Proceeding the 15th International Conference on Soil Mechanics and Geotechnical Engineering, Istanbul, Turkey.

R.M. Pokhrel, T. K., R.Kuwano,G. Chairo and T. Katagiri. (2015). *Site Investigation of sinkhole damage in the armala area pokhara Nepal(printed).pdf* International Conference on Geotechnical Engineering,

Ranjan, G., & Rao, A. (2011). *Basic and applied soil mechanics*. New Age International.

Schultze, E., & Menzenbach, J. (1961). SPT and Compressibility of Soils. *V ICSMFE, Paris*.

Schwanghart, W., Bernhardt, A., Stolle, A., Hoelzmann, P., Adhikari, B., Andermann, C., Tofelde, S., Merchel, S., Rugel, G., Fort, M., & Korup, O. (2016). *Schwanghart etal 2016 SCIENCE*.

Sireesh, S., Sitharam, T. G., & Dash, S. K. (2009). Bearing capacity of circular footing on geocell–sand mattress overlying clay bed with void. *Geotextiles and Geomembranes*, *27*(2), 89-98. https://doi.org/10.1016/j.geotexmem.2008.09.005

Terzaghi, K. (1943). *Theoretical soil mechanics*. J. Wiley and Sons

Chapman and Hall.

Terzaghi, K. (1943). *Theoritical Soil Mechanics*. John Wiley & Sons.

Ti, K. S., Huat, B. B., Noorzaei, J., Jaafar, M. S., & Sew, G. S. (2009). A review of basic soil constitutive models for geotechnical application. *Electronic Journal of Geotechnical Engineering*, *14*, 1-18.

Vesić, A. S. (1973). Analysis of ultimate loads of shallow foundations. *Journal of the Soil Mechanics and Foundations Division*, *99*(1), 45-73.

Wang, M., & Badie, A. (1985). Effect of underground void on foundation stability. *Journal of Geotechnical Engineering*, *111*(8), 1008-1019.

Wang, M., & Hsieh, C. (1987). Collapse load of strip footing above circular void. *Journal of Geotechnical Engineering*, *113*(5), 511-515.

Wolff, T. F. (1989). Pile capacity prediction using parameter functions. Predicted and observed axial behavior of piles: results of a pile prediction symposium,

Wu, G., Zhao, H., & Zhao, M. (2021). Undrained stability analysis of strip footings lying on circular voids with spatially random soil. *Computers and Geotechnics*, *133*. https://doi.org/10.1016/j.compgeo.2021.104072

Wu, G., Zhao, M., Zhang, R., & Liang, G. (2020). Ultimate bearing capacity of eccentrically loaded strip footings above voids in rock masses. *Computers and Geotechnics*, *128*. https://doi.org/10.1016/j.compgeo.2020.103819

Wu, G., Zhao, M., Zhao, H., & Xiao, Y. (2020). Effect of Eccentric Load on the Undrained Bearing Capacity of Strip Footings above Voids. *International Journal of Geomechanics*, *20*(7). https://doi.org/10.1061/(asce)gm.1943-5622.0001710

Xiao, Y., Zhao, M., & Zhao, H. (2018). Undrained stability of strip footing above voids in two-layered clays by finite element limit analysis. *Computers and Geotechnics*, *97*, 124-133. https://doi.org/10.1016/j.compgeo.2018.01.005

Xiao, Y., Zhao, M., Zhao, H., & Zhang, R. (2018). Finite Element Limit Analysis of the Bearing Capacity of Strip Footing on a Rock Mass with Voids. *International Journal of Geomechanics*, *18*(9). https://doi.org/10.1061/(asce)gm.1943-5622.0001262

Zhou, H., Zheng, G., He, X., Xu, X., Zhang, T., & Yang, X. (2018). Bearing capacity of strip footings on c–φ soils with square voids. *Acta Geotechnica*, *13*(3), 747-755. https://doi.org/10.1007/s11440-018-0630-0

ANNEX A: LOAD SETTLEMENT CURVE

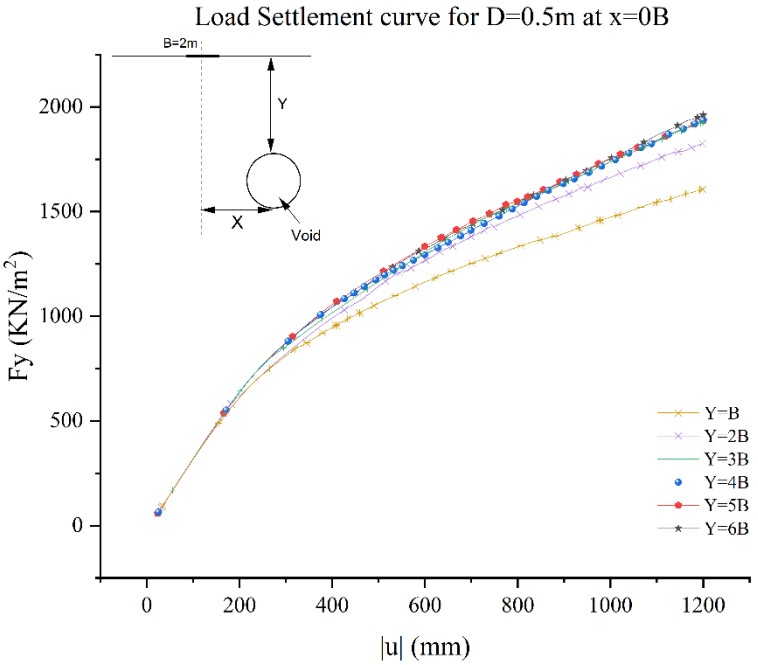

(a)

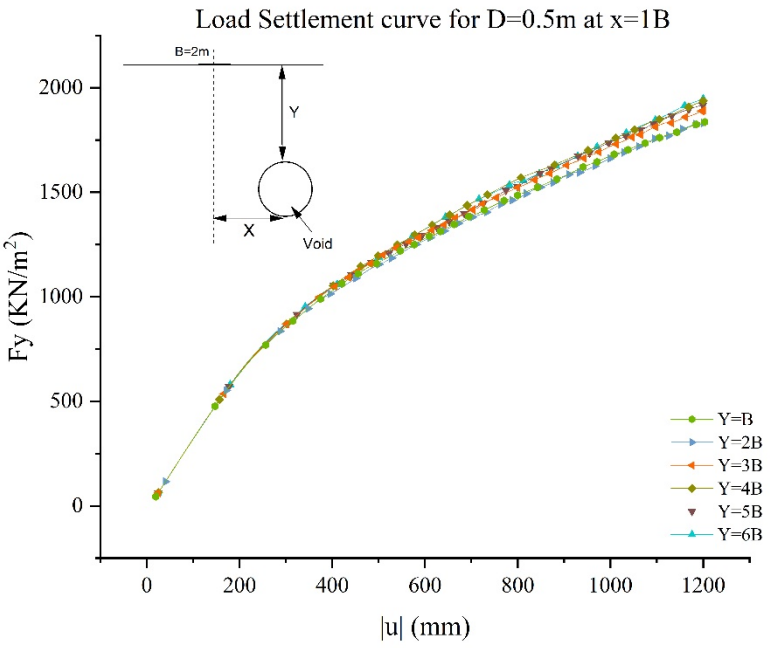

(b)

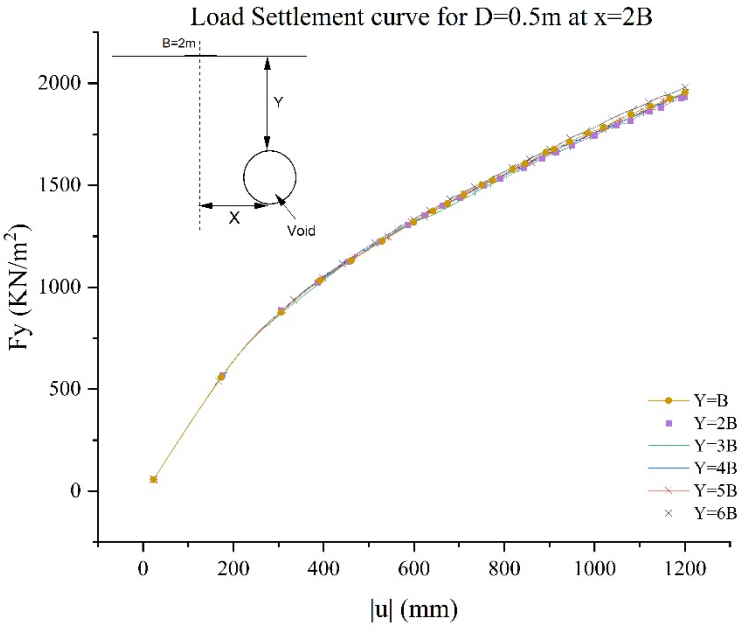
Load Settlement curve for D=0.5m at x=2B
B=2m
Y
X
Void
Fy (KN/m²)
|u| (mm)
Y=B
Y=2B
Y=3B
Y=4B
Y=5B
Y=6B

(c)

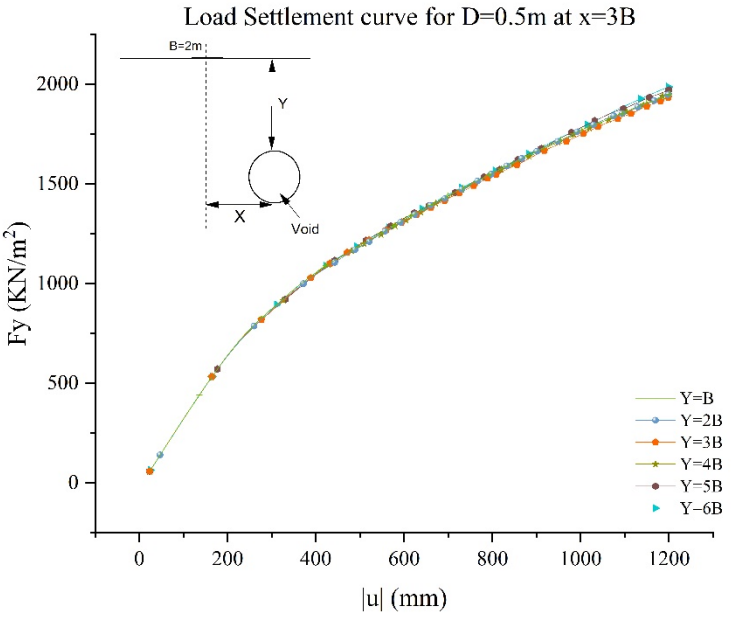
Load Settlement curve for D=0.5m at x=3B
B=2m
Y
X
Void
Fy (KN/m²)
|u| (mm)
Y=B
Y=2B
Y=3B
Y=4B
Y=5B
Y=6B

(d)

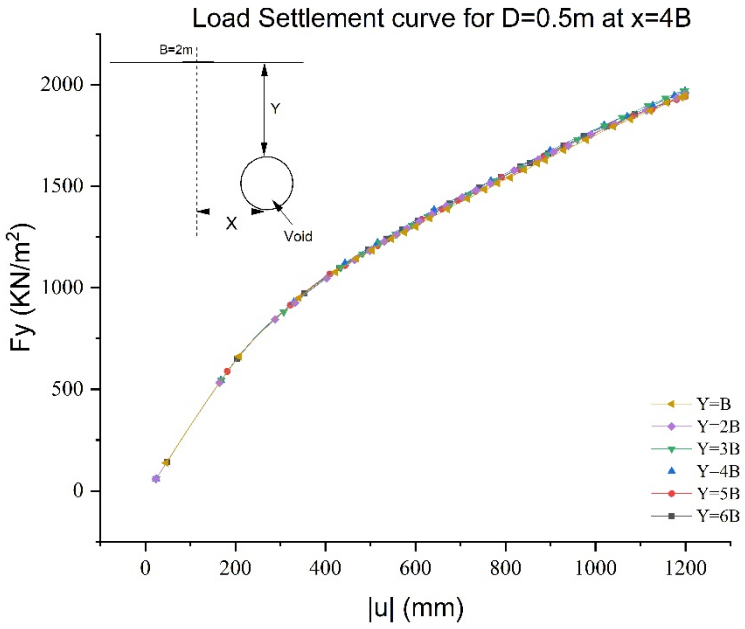

(e)

Figure A.1: Stress Load-Settlement Curve for a void of diameter, D=0.5m for variation in depth of void (y) at horizontal offset (x) as (a) x=0B, (b) x=B, (c) x=2B, (d) x=3B and (e) x=4B

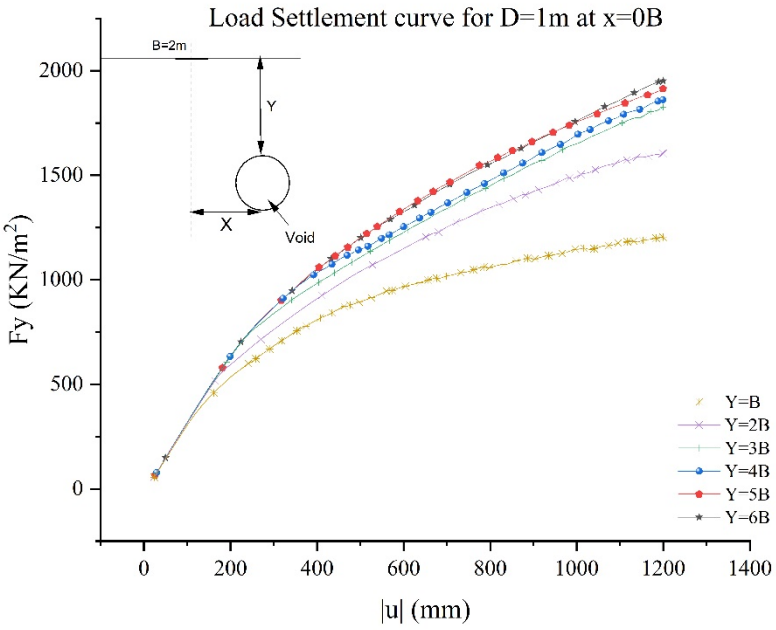

(a)

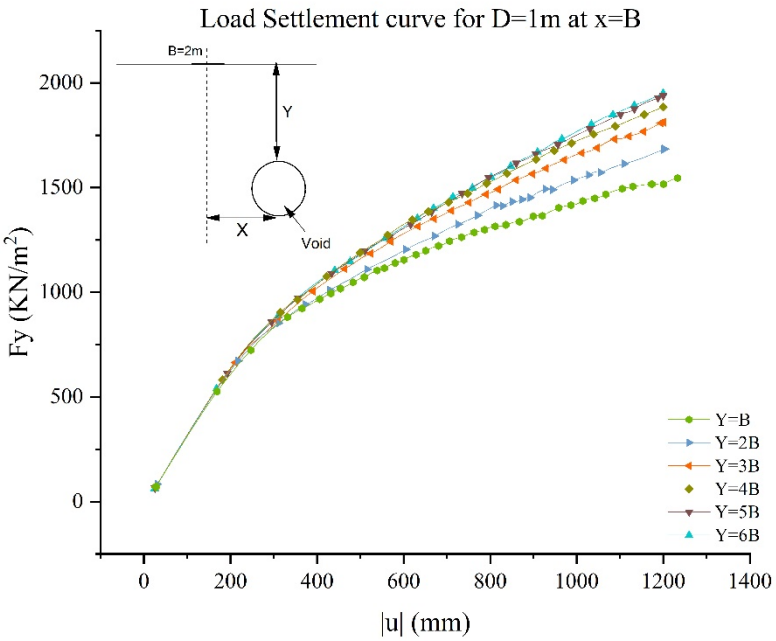
Load Settlement curve for D=1m at x=B
B=2m
Y
X
Void
Fy (KN/m^2)
|u| (mm)
Y=B
Y=2B
Y=3B
Y=4B
Y=5B
Y=6B

(b)

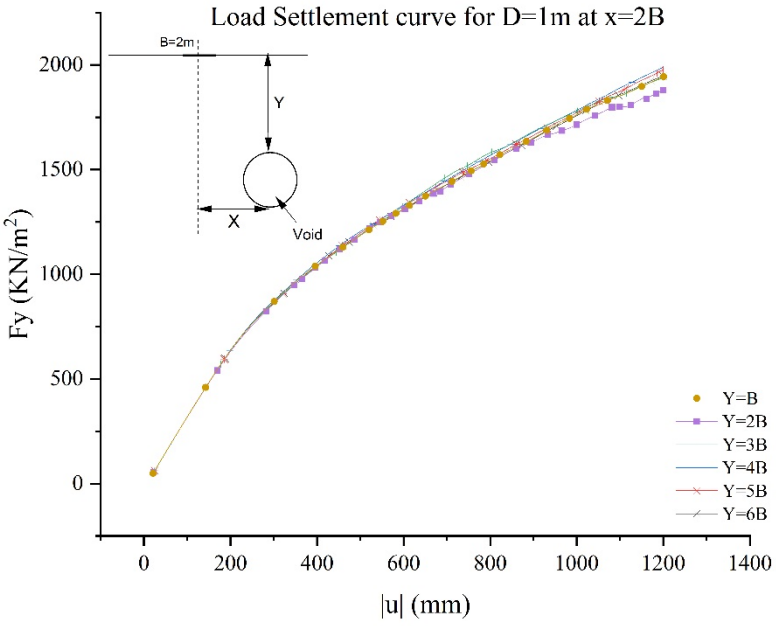
Load Settlement curve for D=1m at x=2B
B=2m
Y
X
Void
Fy (KN/m^2)
|u| (mm)
Y=B
Y=2B
Y=3B
Y=4B
Y=5B
Y=6B

(c)

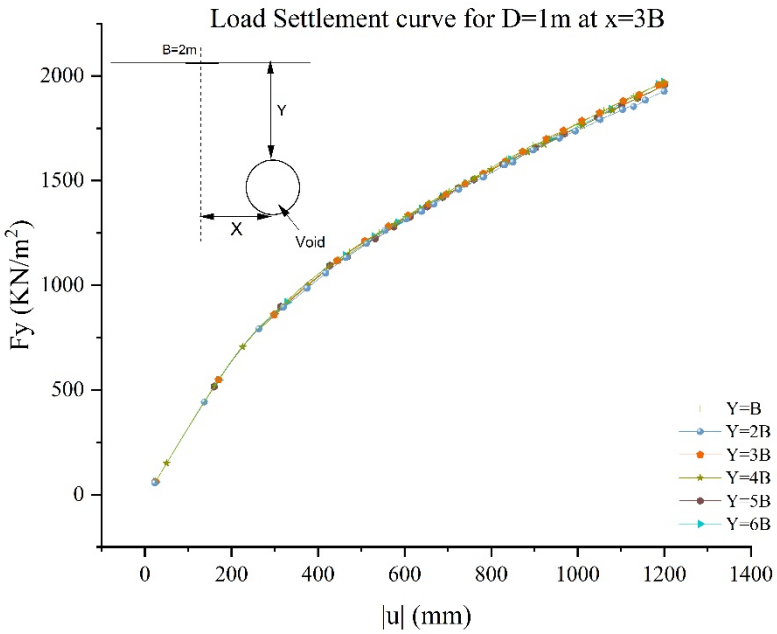

(d)

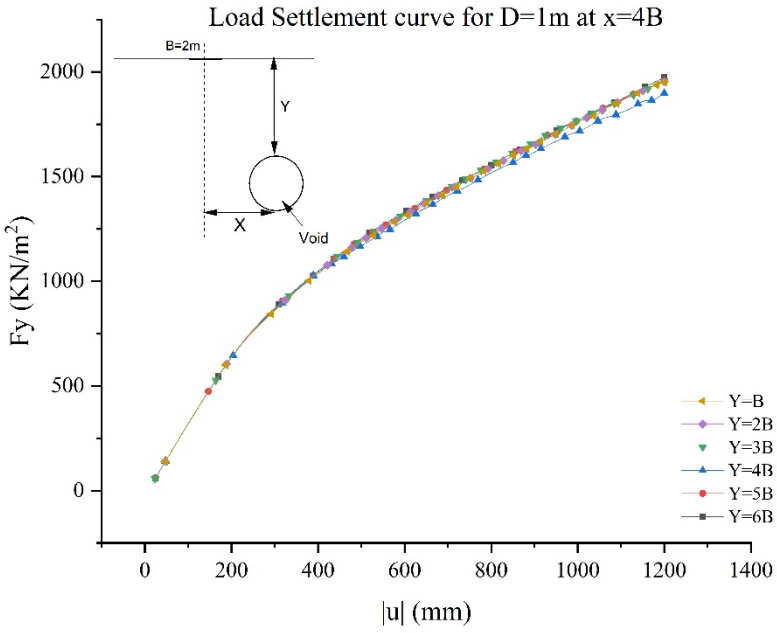

(e)

Figure A.2: Stress Load-Settlement Curve for a void of diameter, D=1m for variation in depth of void (y) at horizontal offset (x) as (a) x=0B, (b) x=B, (c) x=2B, (d) x=3B and (e) x=4B

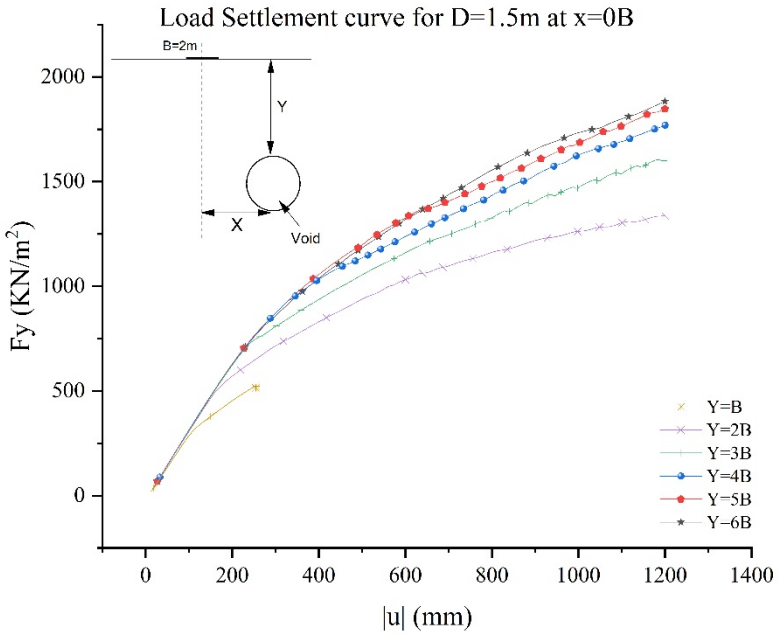
Load Settlement curve for D=1.5m at x=0B
B=2m
Y
X
Void
Fy (KN/m²)
|u| (mm)
0
500
1000
1500
2000
0
200
400
600
800
1000
1200
1400
Y=B
Y=2B
Y=3B
Y=4B
Y=5B
Y=6B

(a)

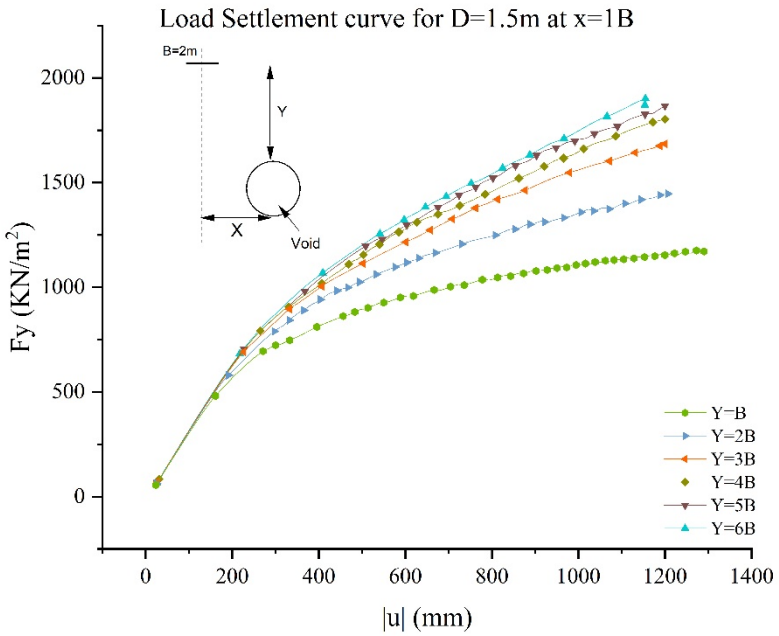
Load Settlement curve for D=1.5m at x=1B
B=2m
Y
X
Void
Fy (KN/m²)
|u| (mm)
0
500
1000
1500
2000
0
200
400
600
800
1000
1200
1400
Y=B
Y=2B
Y=3B
Y=4B
Y=5B
Y=6B

(b)

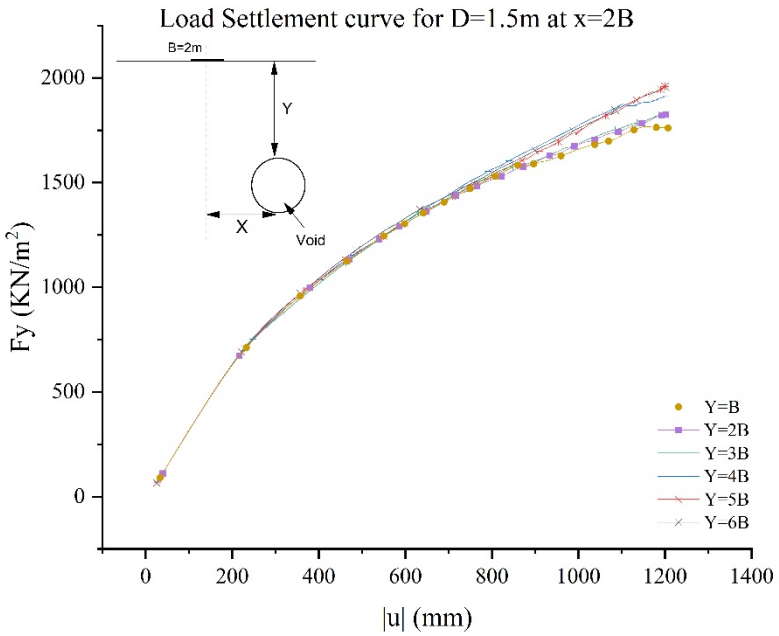
Load Settlement curve for D=1.5m at x=2B
B=2m
Y
X
Void
Fy (KN/m^2)
|u| (mm)
Y=B
Y=2B
Y=3B
Y=4B
Y=5B
Y=6B

(c)

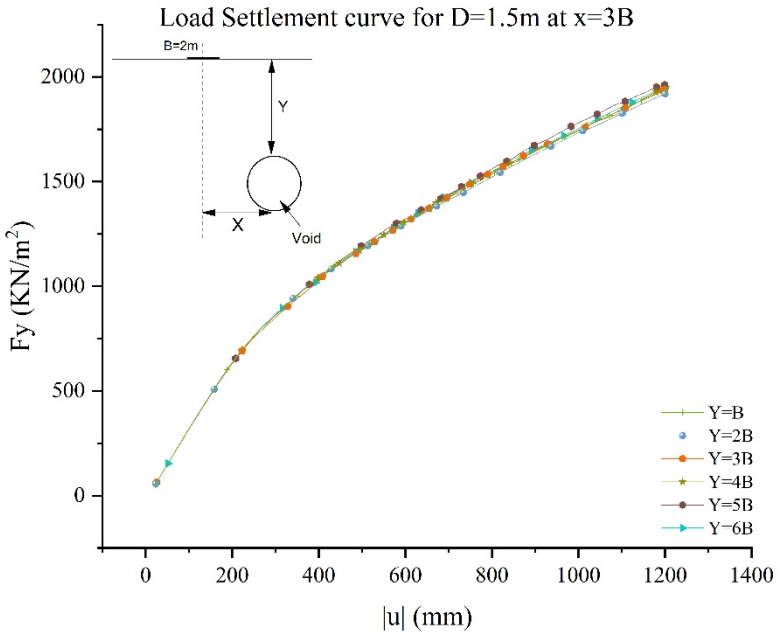
Load Settlement curve for D=1.5m at x=3B
B=2m
Y
X
Void
Fy (KN/m^2)
|u| (mm)
Y=B
Y=2B
Y=3B
Y=4B
Y=5B
Y=6B

(d)

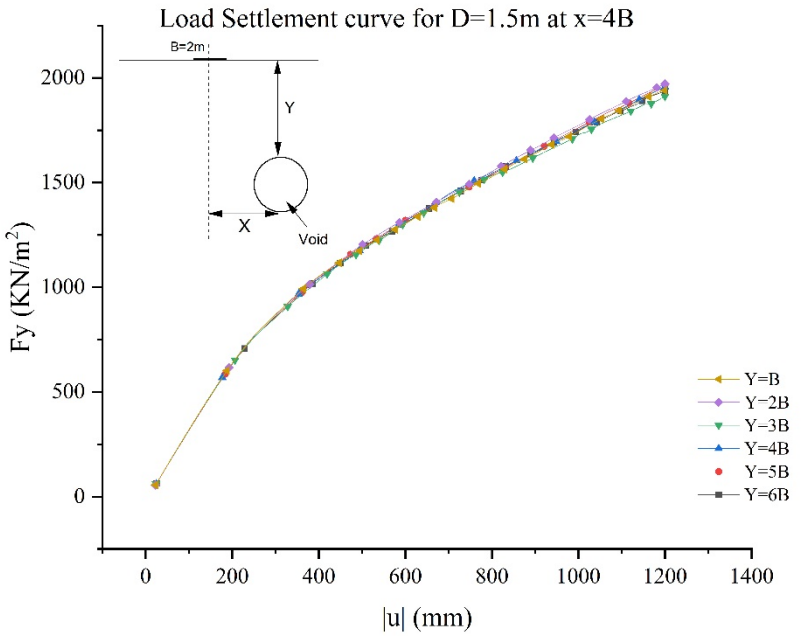

(e)

Figure A.3: Stress Load-Settlement Curve for a void of diameter, D=1.5m for variation in depth of void (y) at horizontal offset (x) as (a) x=0B, (b) x=B, (c) x=2B, (d) x=3B and (e) x=4B

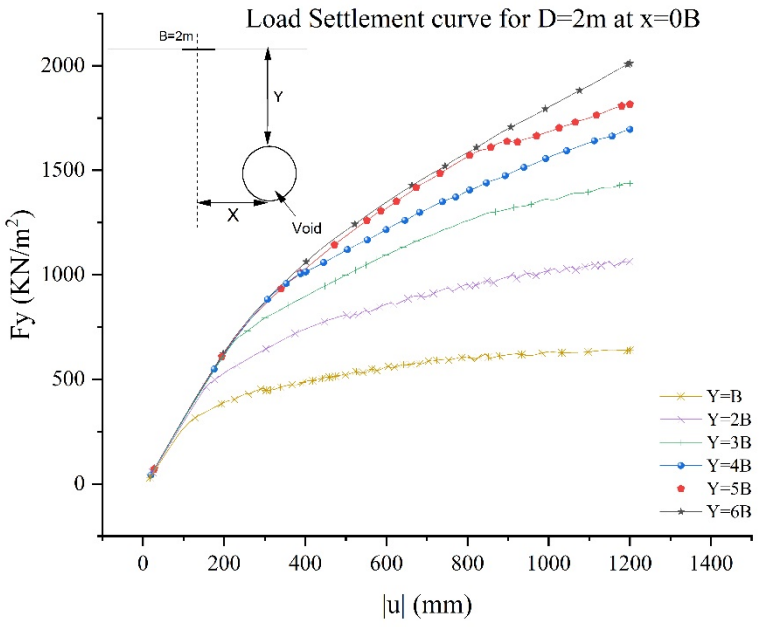

(a)

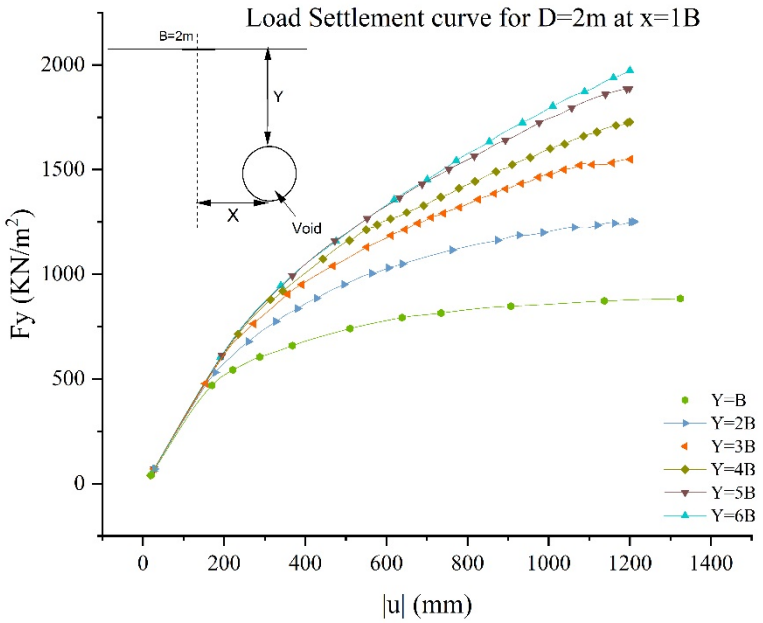
Load Settlement curve for D=2m at x=1B
B=2m
Y
X
Void
Fy (KN/m^2)
|u| (mm)
0
500
1000
1500
2000
0
200
400
600
800
1000
1200
1400
Y=B
Y=2B
Y=3B
Y=4B
Y=5B
Y=6B

(b)

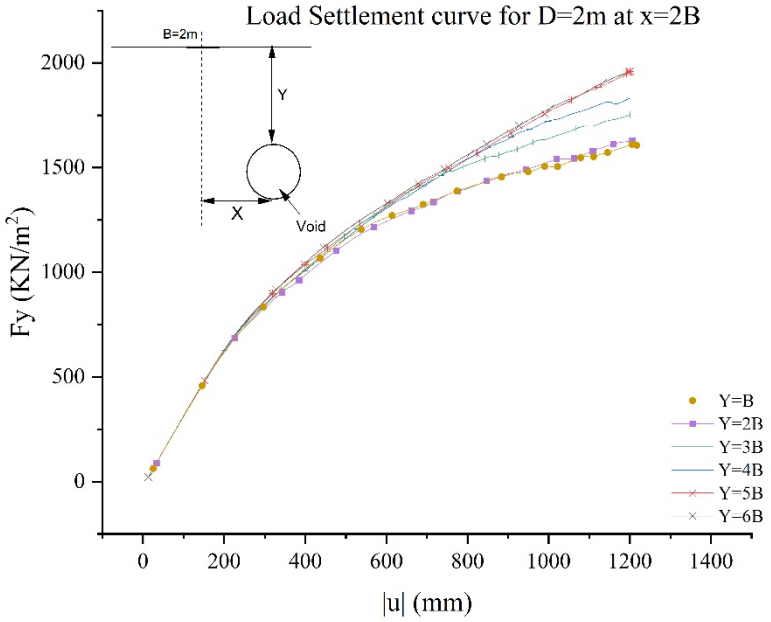
Load Settlement curve for D=2m at x=2B
B=2m
Y
X
Void
Fy (KN/m^2)
|u| (mm)
0
500
1000
1500
2000
0
200
400
600
800
1000
1200
1400
Y=B
Y=2B
Y=3B
Y=4B
Y=5B
Y=6B

(c)

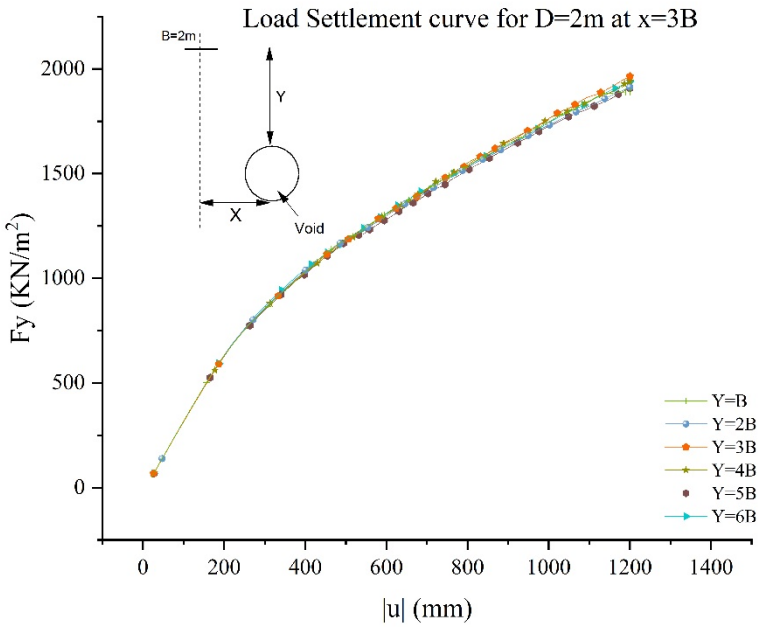

(d)

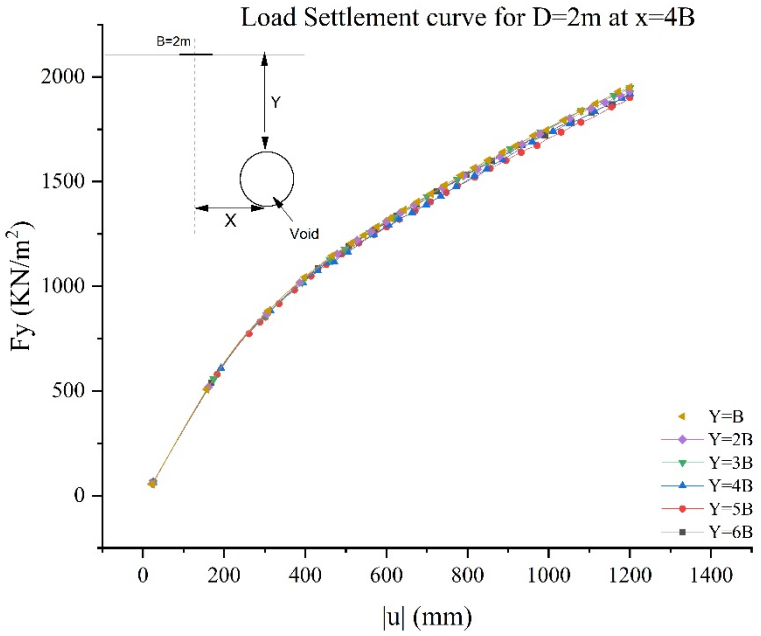

(e)

Figure A.4: Stress Load-Settlement Curve for a void of diameter, D=2m for variation in depth of void (y) at horizontal offset (x) as (a) x=0B, (b) x=B, (c) x=2B, (d) x=3B and (e) x=4B

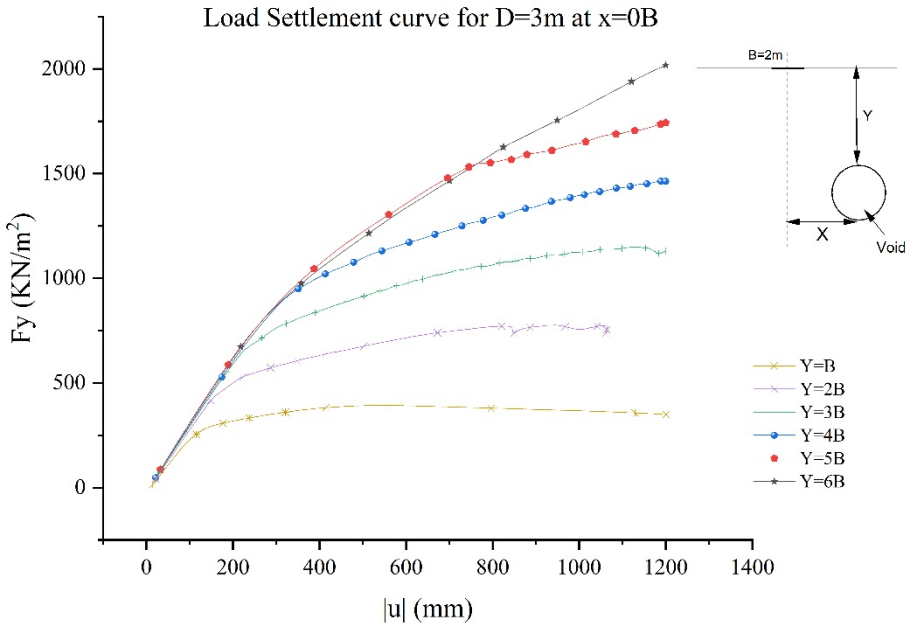
Load Settlement curve for D=3m at x=0B
Fy (KN/m²)
|u| (mm)
0
500
1000
1500
2000
0
200
400
600
800
1000
1200
1400
B=2m
Y
X
Void
Y=B
Y=2B
Y=3B
Y=4B
Y=5B
Y=6B

(a)

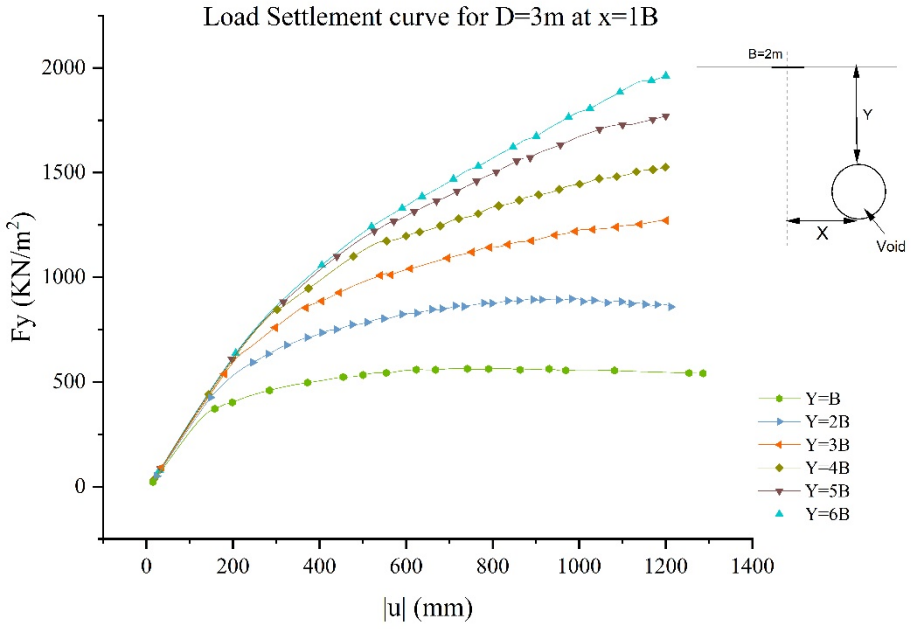
Load Settlement curve for D=3m at x=1B
Fy (KN/m²)
|u| (mm)
0
500
1000
1500
2000
0
200
400
600
800
1000
1200
1400
B=2m
Y
X
Void
Y=B
Y=2B
Y=3B
Y–4B
Y=5B
Y=6B

(b)

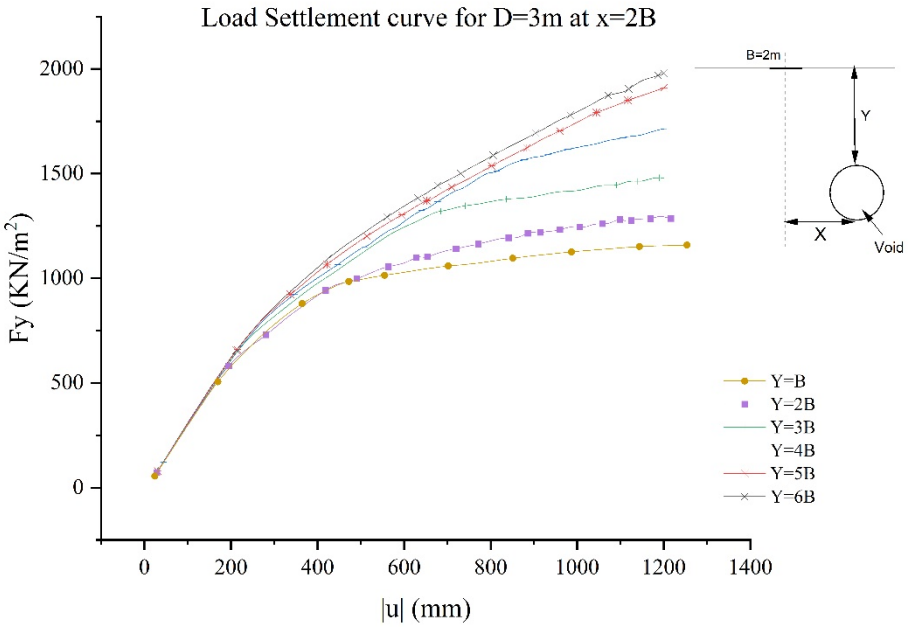
Load Settlement curve for D=3m at x=2B
Fy (KN/m²)
|u| (mm)
B=2m
Y
X
Void
Y=B
Y=2B
Y=3B
Y=4B
Y=5B
Y=6B

(c)

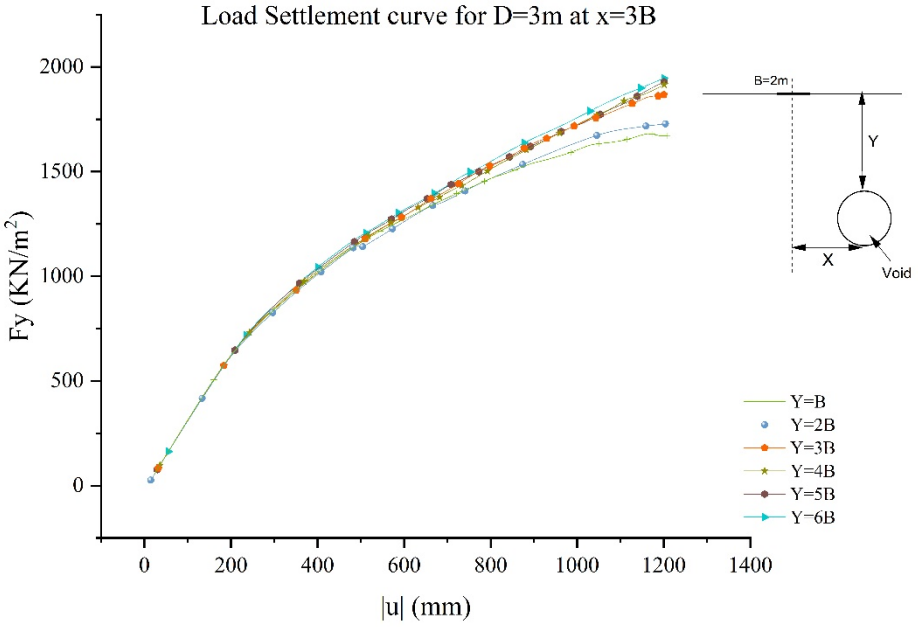
Load Settlement curve for D=3m at x=3B
Fy (KN/m²)
|u| (mm)
B=2m
Y
X
Void
Y=B
Y=2B
Y=3B
Y=4B
Y=5B
Y=6B

(d)

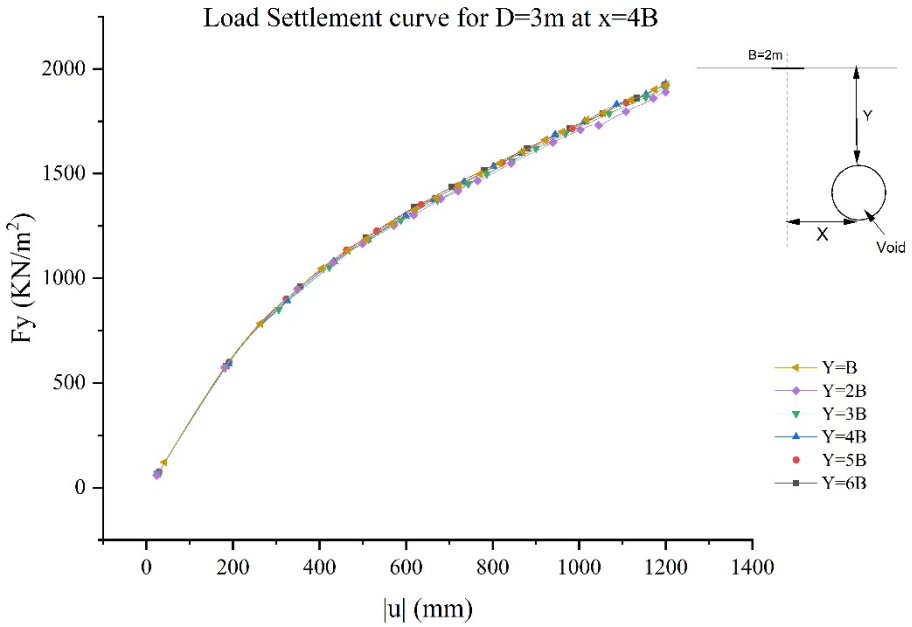

(e)

Figure A.5: Stress Load-Settlement Curve for a void of diameter, D=3m for variation in depth of void (y) at horizontal offset (x) as (a) x=0B, (b) x=B, (c) x=2B, (d) x=3B and (e) x=4B

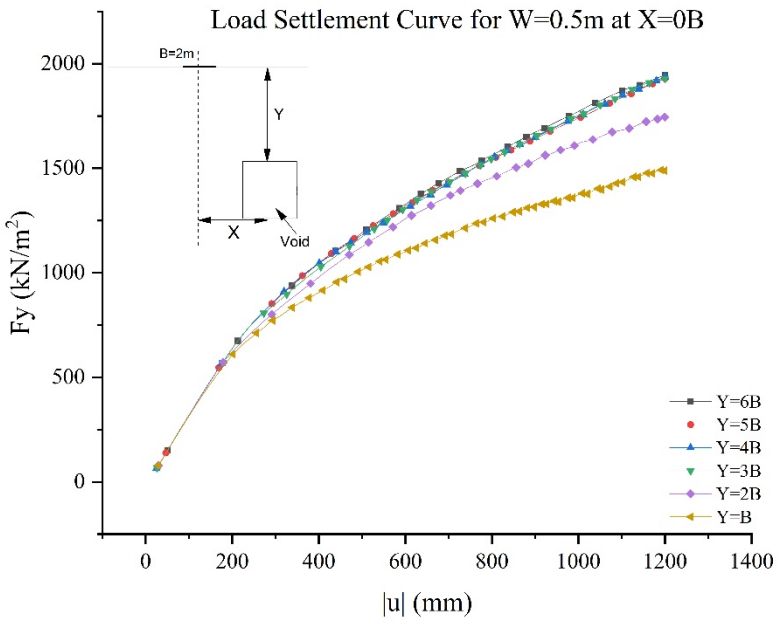

(a)

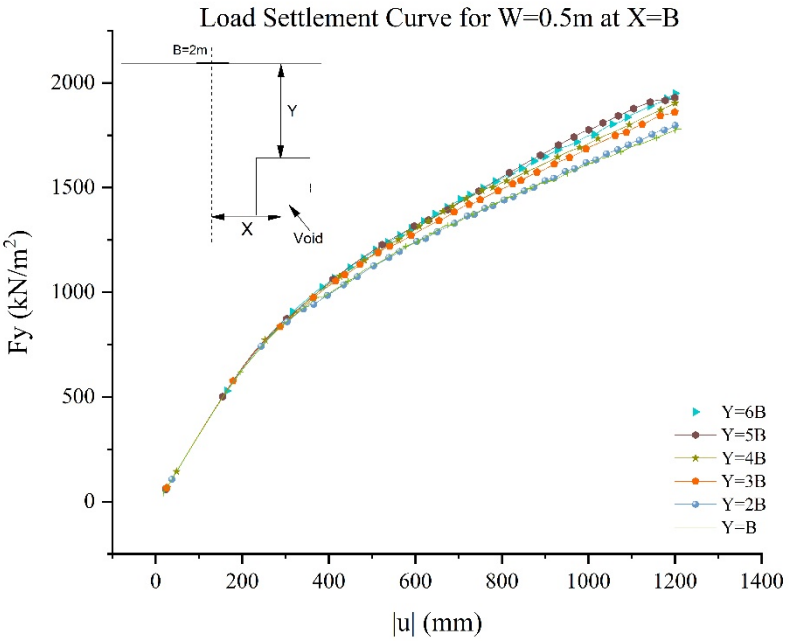
Load Settlement Curve for W=0.5m at X=B
B=2m
Y
X
Void
Fy (kN/m^2)
|u| (mm)
Y=6B
Y=5B
Y=4B
Y=3B
Y=2B
Y=B

(b)

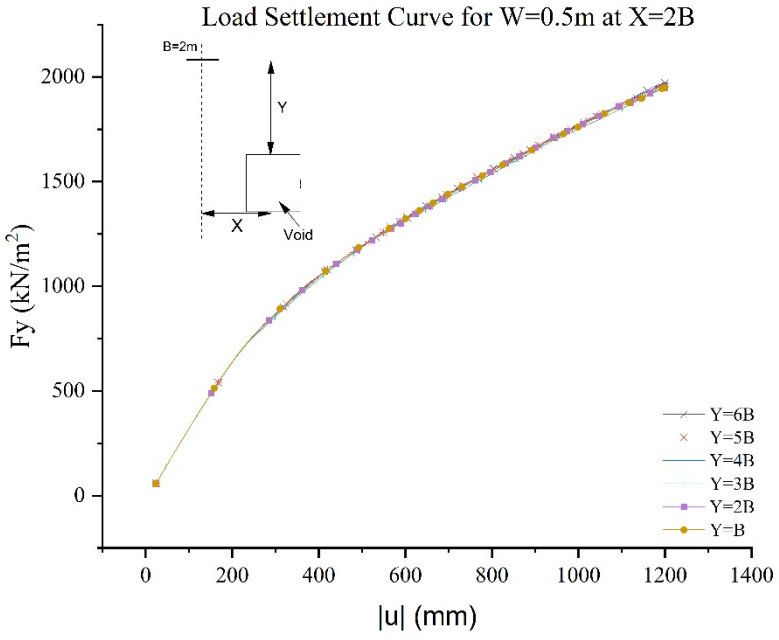
Load Settlement Curve for W=0.5m at X=2B
B=2m
Y
X
Void
Fy (kN/m^2)
|u| (mm)
Y=6B
Y=5B
Y=4B
Y=3B
Y=2B
Y=B

(c)

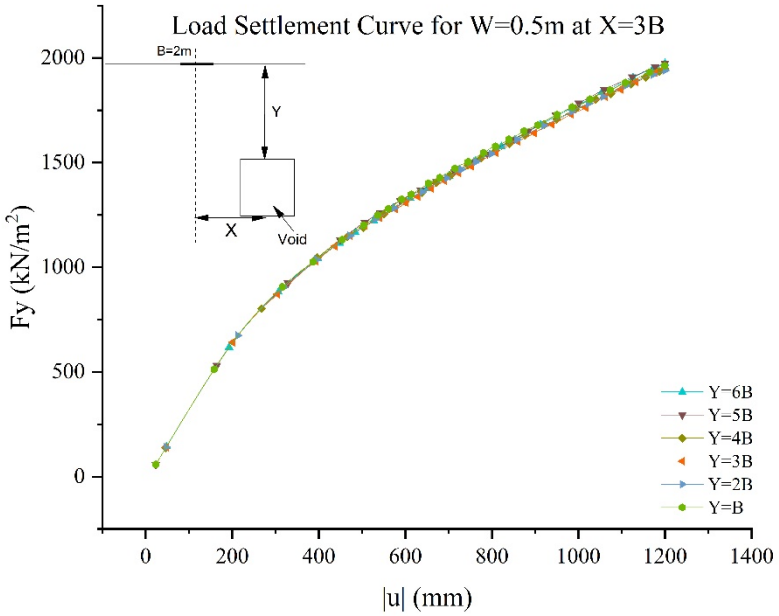

(d)

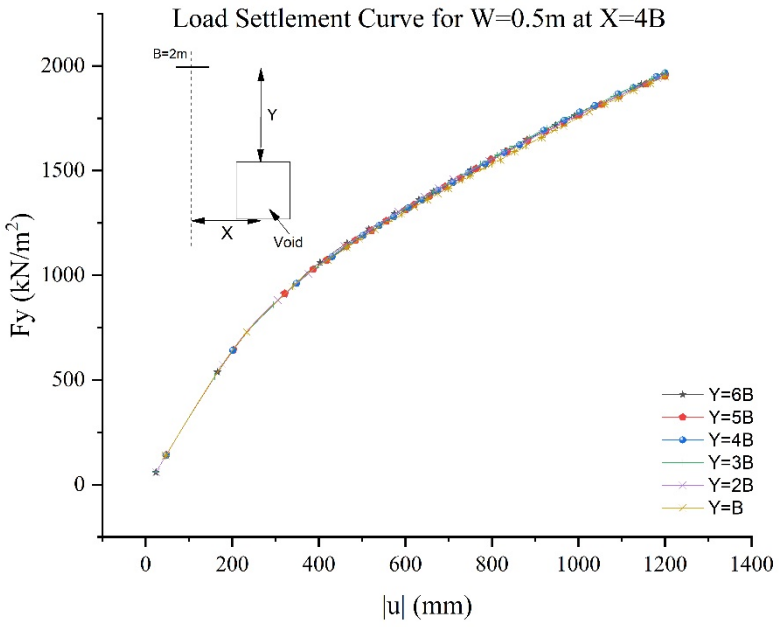

(e)

Figure A.6: Stress Load-Settlement Curve for a square void, W=0.5m for variation in depth of void (y) at horizontal offset (x) as (a) x=0B, (b) x=B, (c) x=2B, (d) x=3B and (e) x=4B

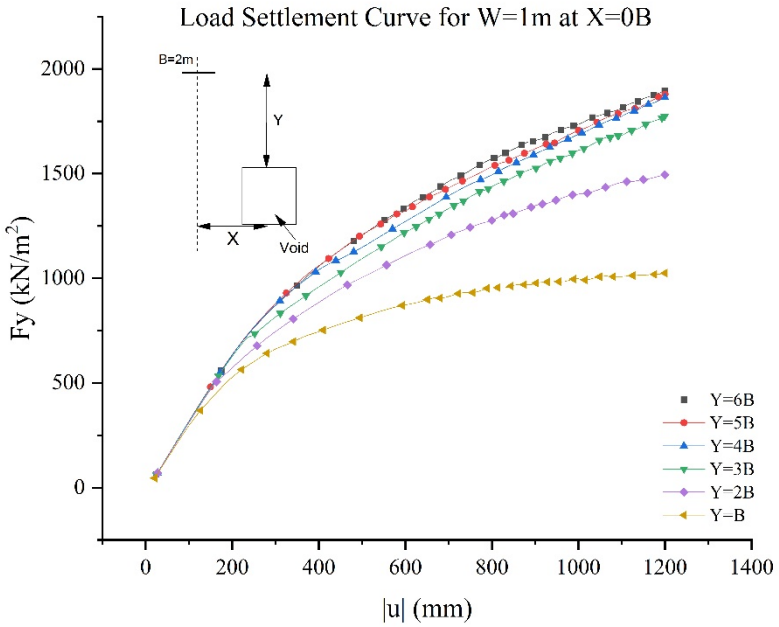
Load Settlement Curve for W=1m at X=0B
B=2m
Y
X
Void
Fy (kN/m²)
|u| (mm)
Y=6B
Y=5B
Y=4B
Y=3B
Y=2B
Y=B

(a)

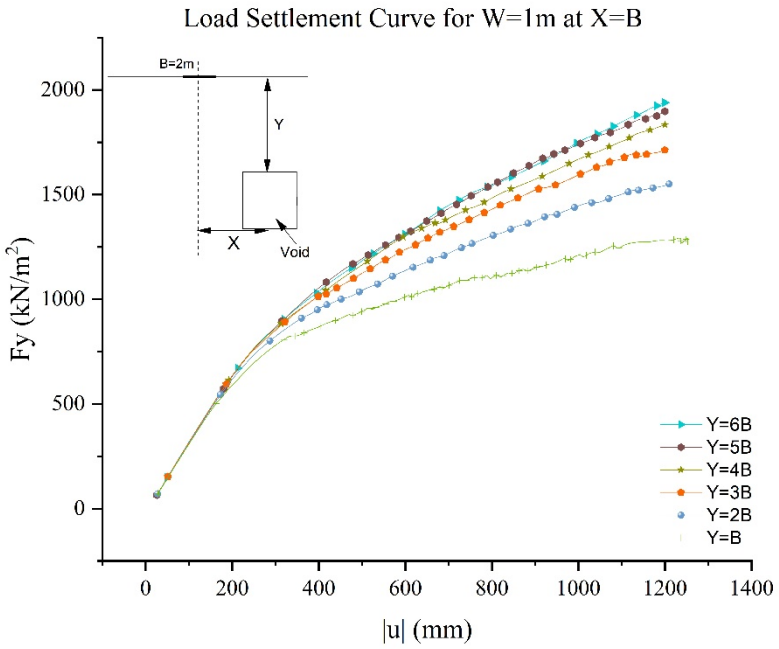
Load Settlement Curve for W=1m at X=B
B=2m
Y
X
Void
Fy (kN/m²)
|u| (mm)
Y=6B
Y=5B
Y=4B
Y=3B
Y=2B
Y=B

(b)

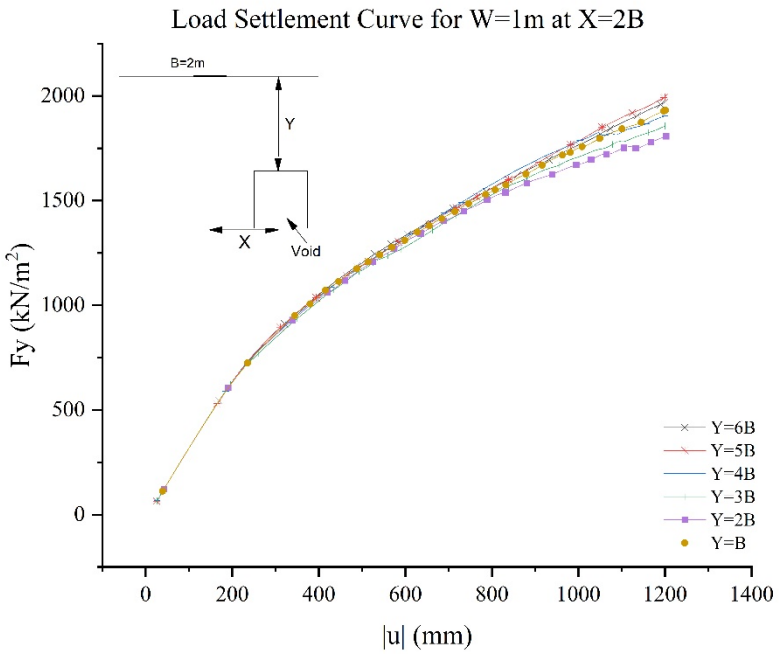
Load Settlement Curve for W=1m at X=2B
B=2m
Y
X
Void
Fy (kN/m²)
|u| (mm)
Y=6B
Y=5B
Y=4B
Y=3B
Y=2B
Y=B

(c)

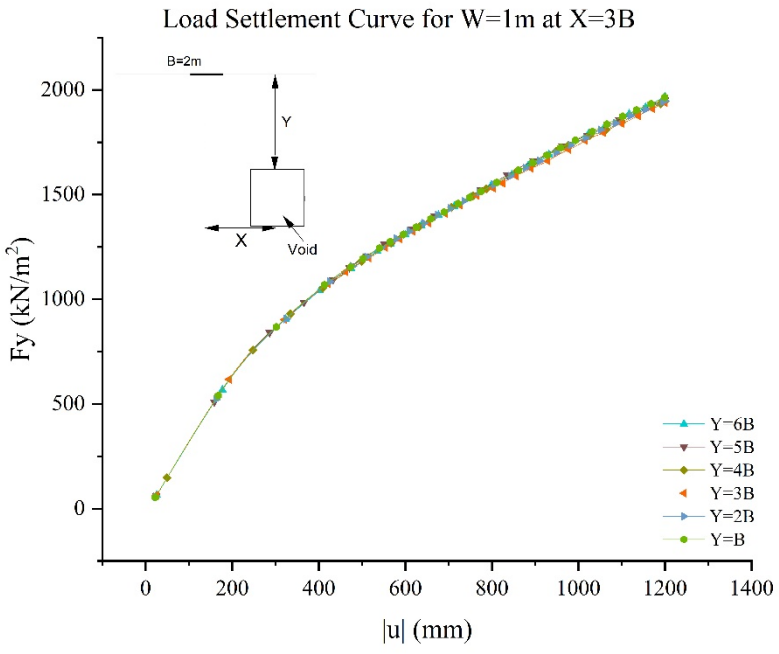
Load Settlement Curve for W=1m at X=3B
B=2m
Y
X
Void
Fy (kN/m²)
|u| (mm)
Y=6B
Y=5B
Y=4B
Y=3B
Y=2B
Y=B

(d)

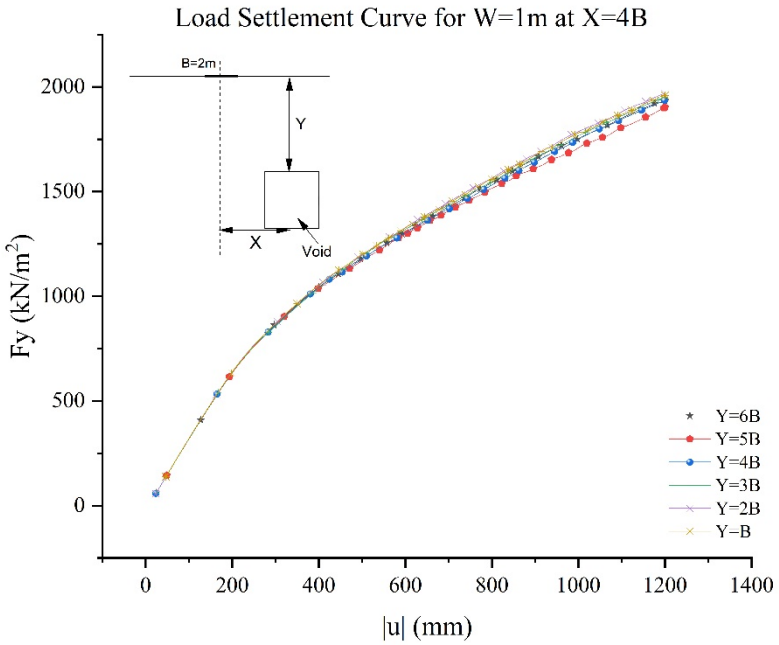

(e)

Figure A.7: Stress Load-Settlement Curve for a Square void, W=1m for variation in depth of void (y) at horizontal offset (x) as (a) x=0B, (b) x=B, (c) x=2B, (d) x=3B and (e) x=4B

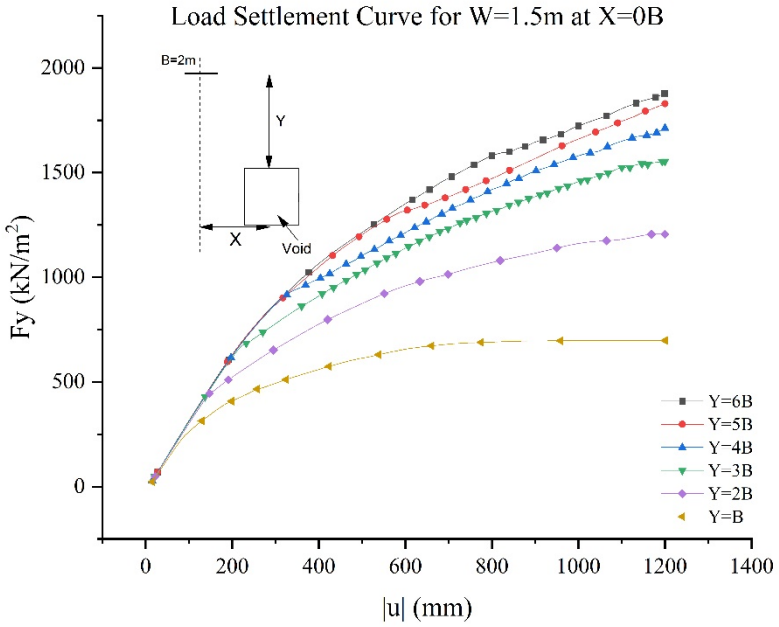

(a)

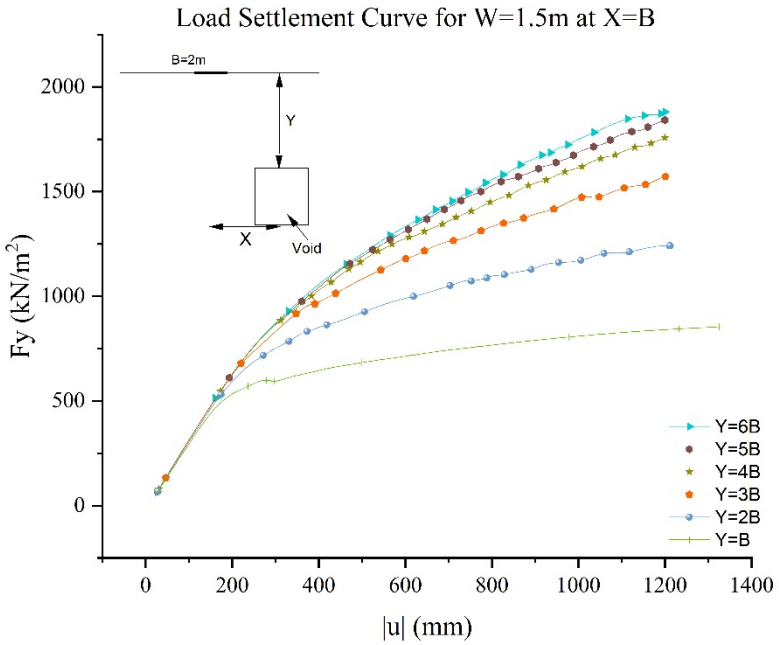
Load Settlement Curve for W=1.5m at X=B
B=2m
Y
X
Void
Fy (kN/m²)
|u| (mm)
Y=6B
Y=5B
Y=4B
Y=3B
Y=2B
Y=B

(b)

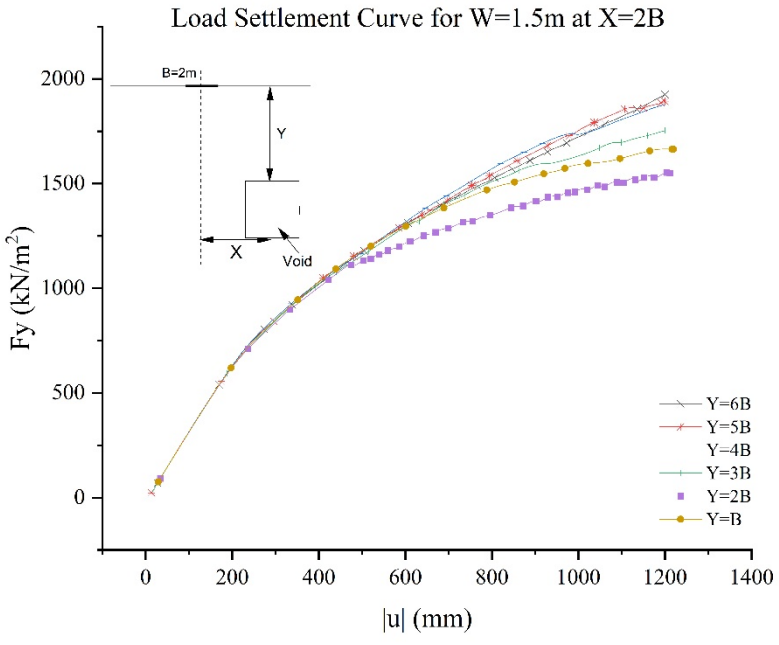
Load Settlement Curve for W=1.5m at X=2B
B=2m
Y
X
Void
Fy (kN/m²)
|u| (mm)
Y=6B
Y=5B
Y=4B
Y=3B
Y=2B
Y=B

(c)

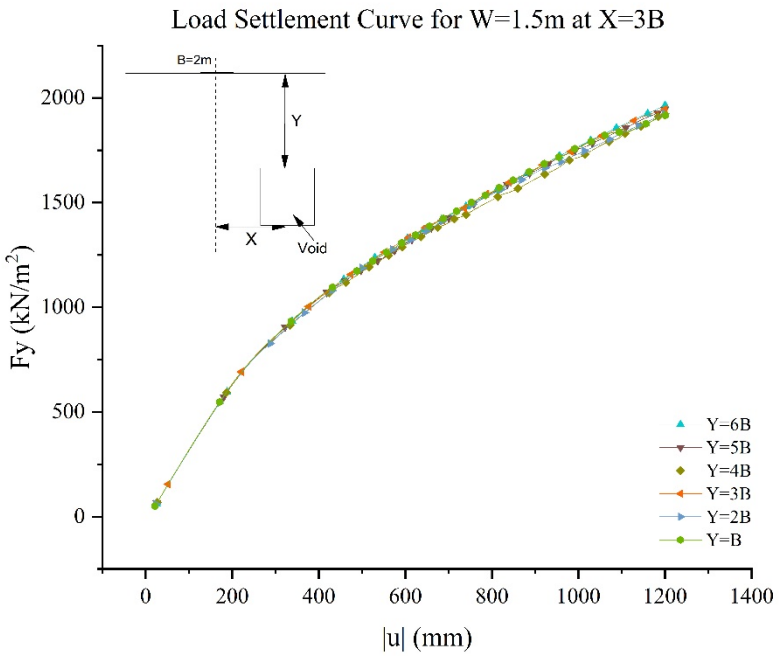

(d)

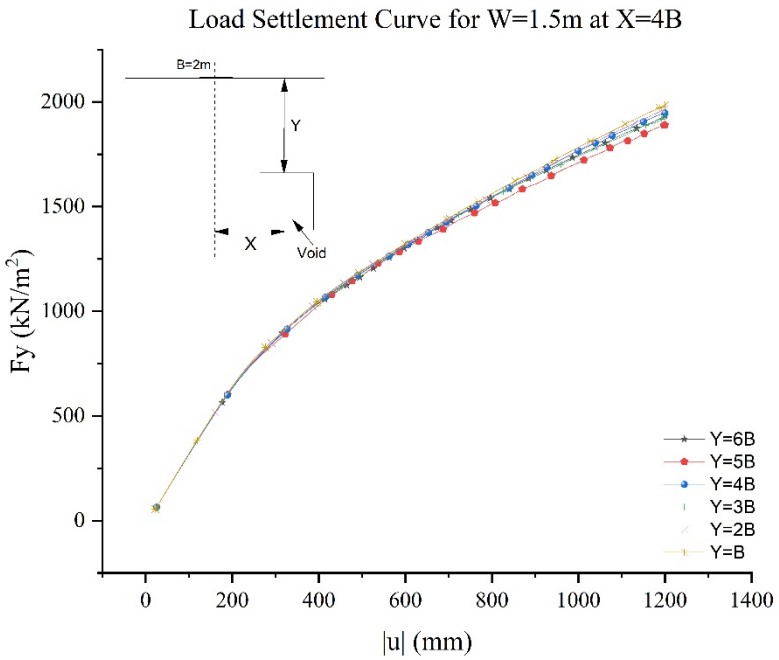

(e)

Figure A.8: Stress Load-Settlement Curve for a Square void, W=1.5m for variation in depth of void (y) at horizontal offset (x) as (a) x=0B, (b) x=B, (c) x=2B, (d) x=3B and (e) x=4B

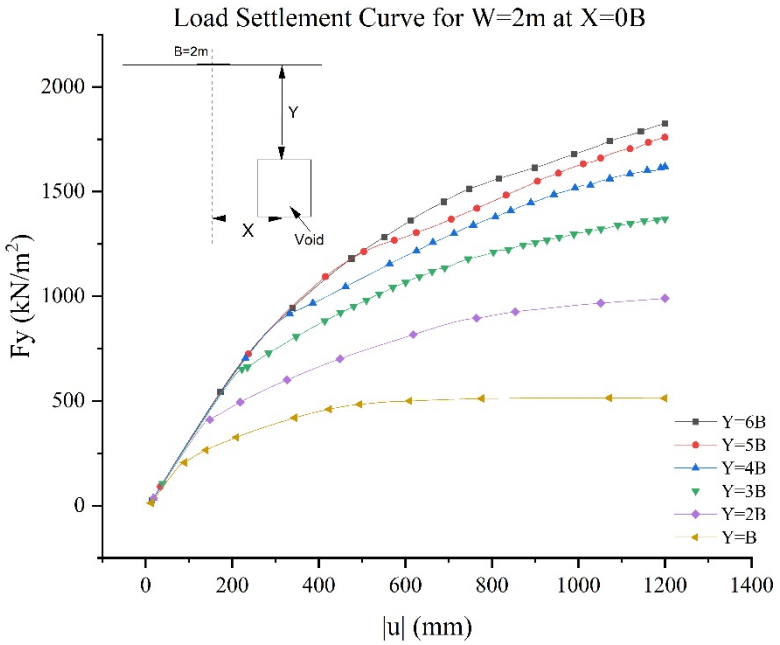
Load Settlement Curve for W=2m at X=0B
B=2m
Y
X
Void
Fy (kN/m²)
|u| (mm)
Y=6B
Y=5B
Y=4B
Y=3B
Y=2B
Y=B

(a)

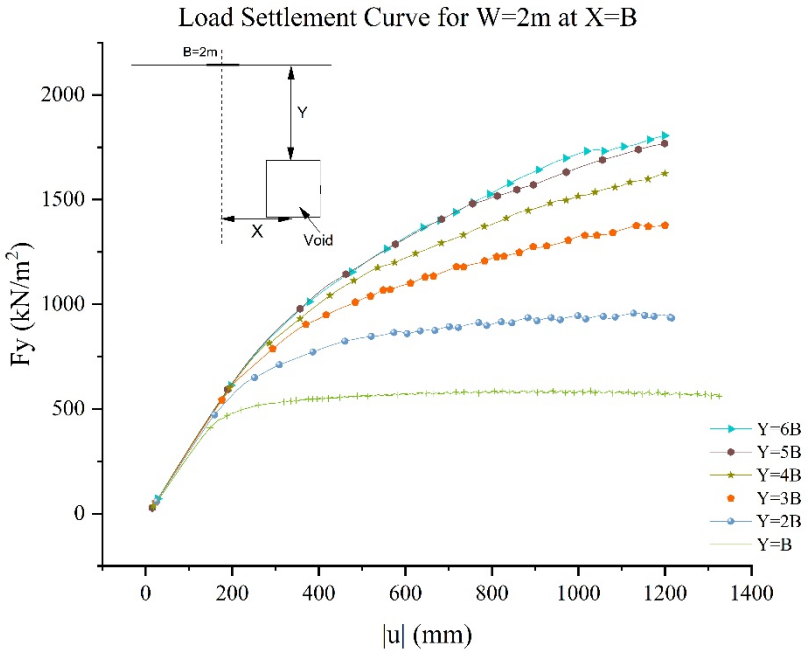
Load Settlement Curve for W=2m at X=B
B=2m
Y
X
Void
Fy (kN/m²)
|u| (mm)
Y=6B
Y=5B
Y=4B
Y=3B
Y=2B
Y=B

(b)

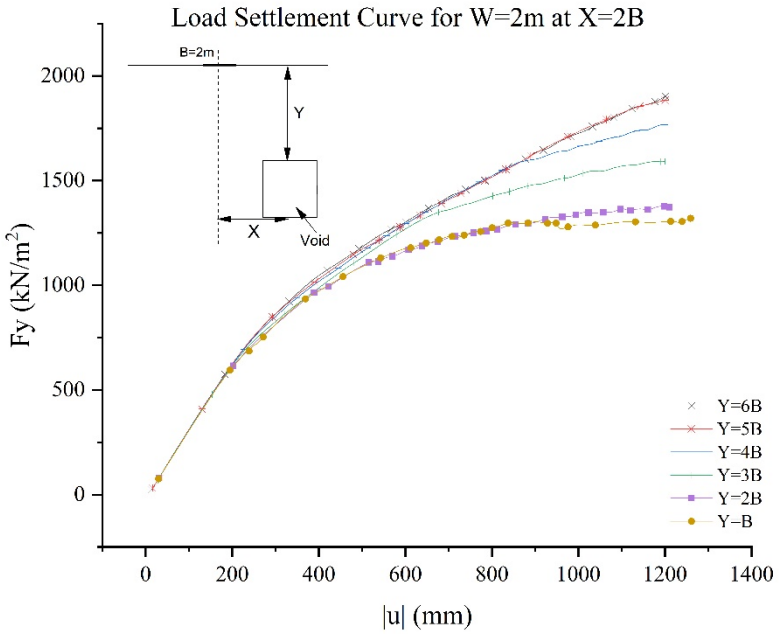
Load Settlement Curve for W=2m at X=2B
B=2m
Y
X
Void
Fy (kN/m²)
|u| (mm)
Y=6B
Y=5B
Y=4B
Y=3B
Y=2B
Y=B

(c)

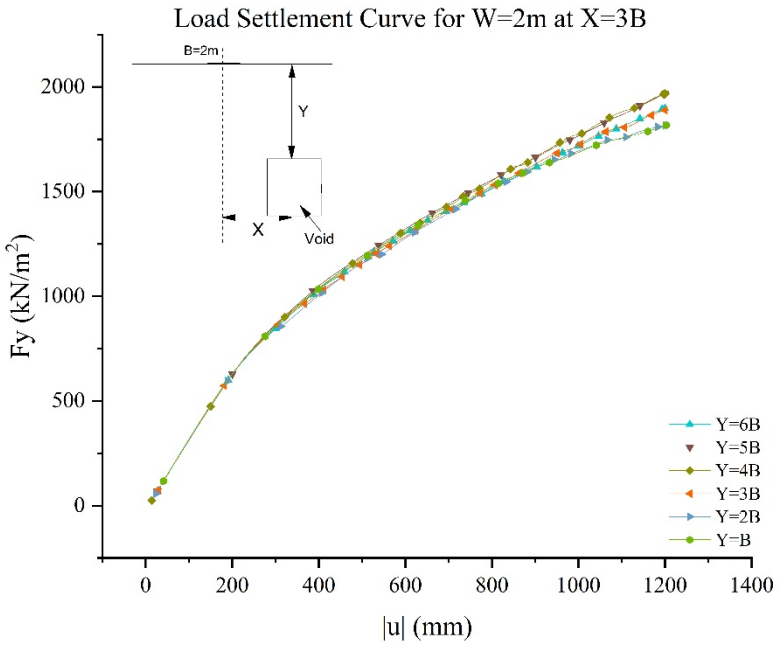
Load Settlement Curve for W=2m at X=3B
B=2m
Y
X
Void
Fy (kN/m²)
|u| (mm)
Y=6B
Y=5B
Y=4B
Y=3B
Y=2B
Y=B

(d)

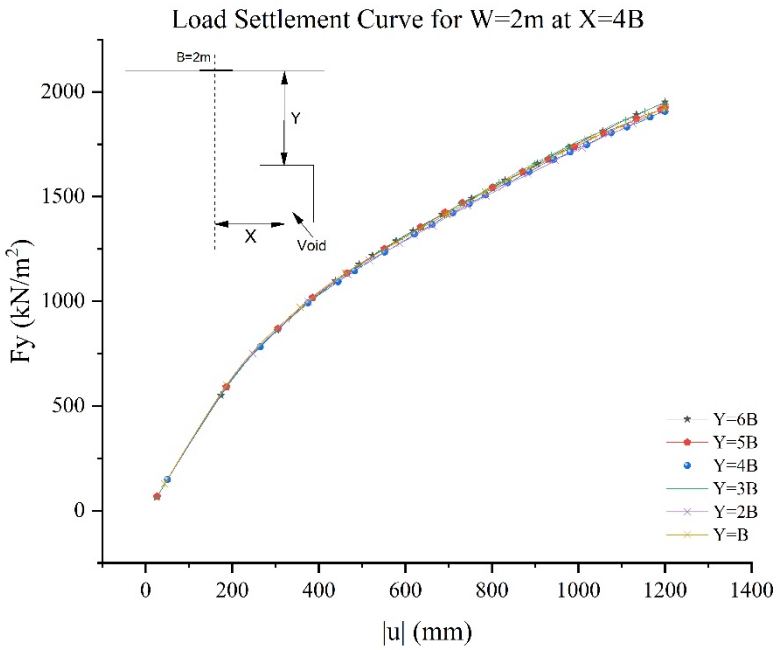

(e)

Figure A.9: Stress Load-Settlement Curve for Square void, W=2m for variation in depth of void (y) at horizontal offset (x) as (a) x=0B, (b) x=B, (c) x=2B, (d) x=3B and (e) x=4B

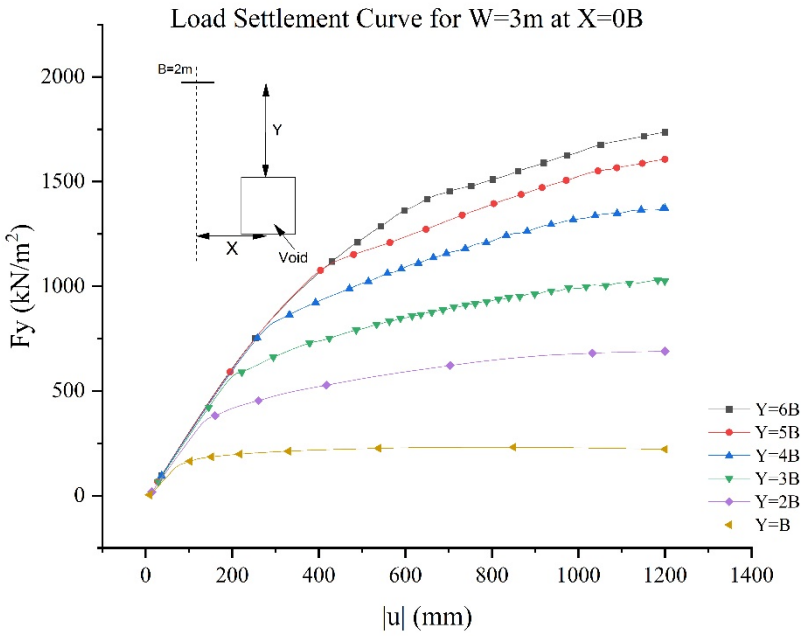

(a)

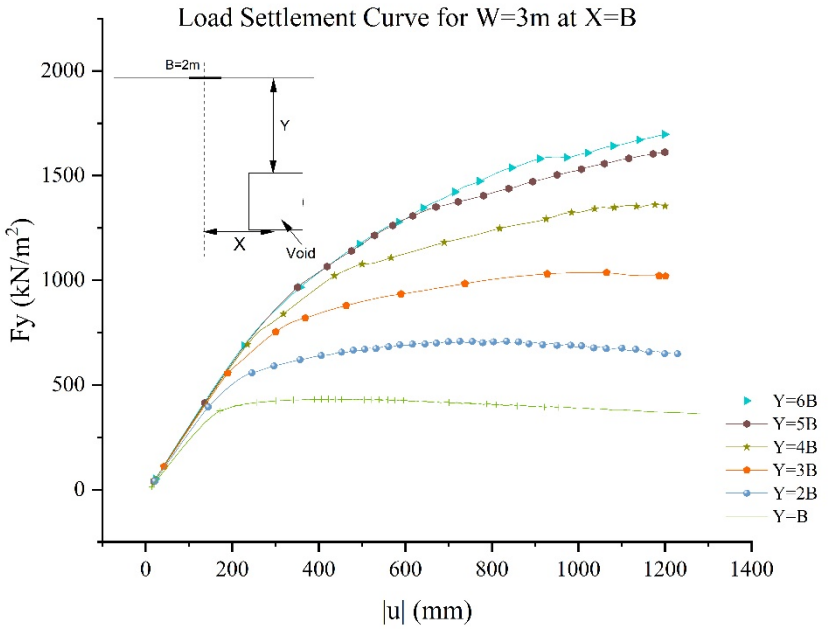
Load Settlement Curve for W=3m at X=B
B=2m
Y
X
Void
Fy (kN/m²)
|u| (mm)
Y=6B
Y=5B
Y=4B
Y=3B
Y=2B
Y=B

(b)

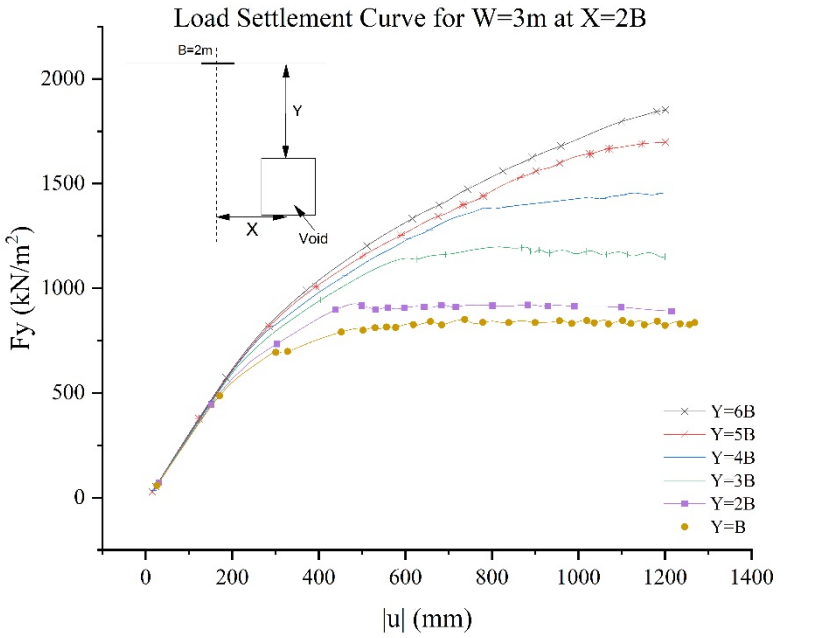
Load Settlement Curve for W=3m at X=2B
B=2m
Y
X
Void
Fy (kN/m²)
|u| (mm)
Y=6B
Y=5B
Y=4B
Y=3B
Y=2B
Y=B

(c)

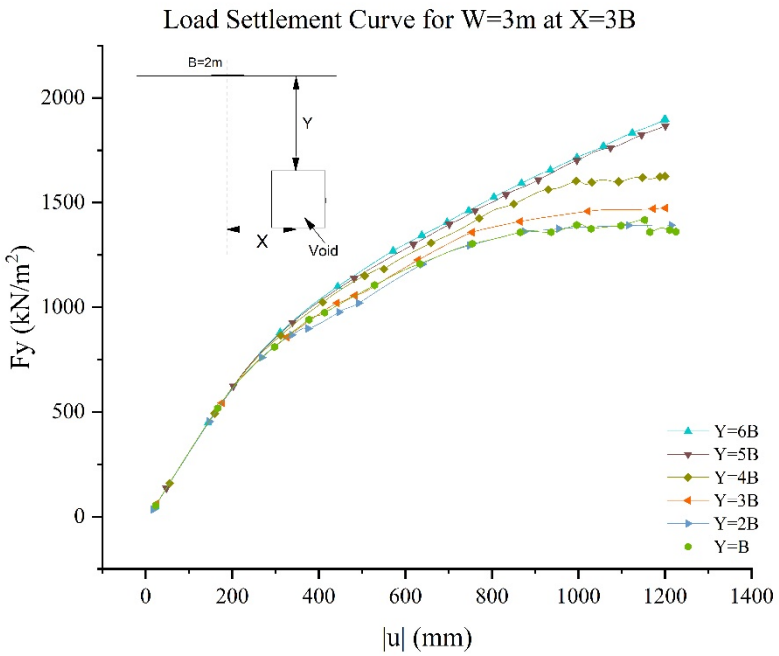

(d)

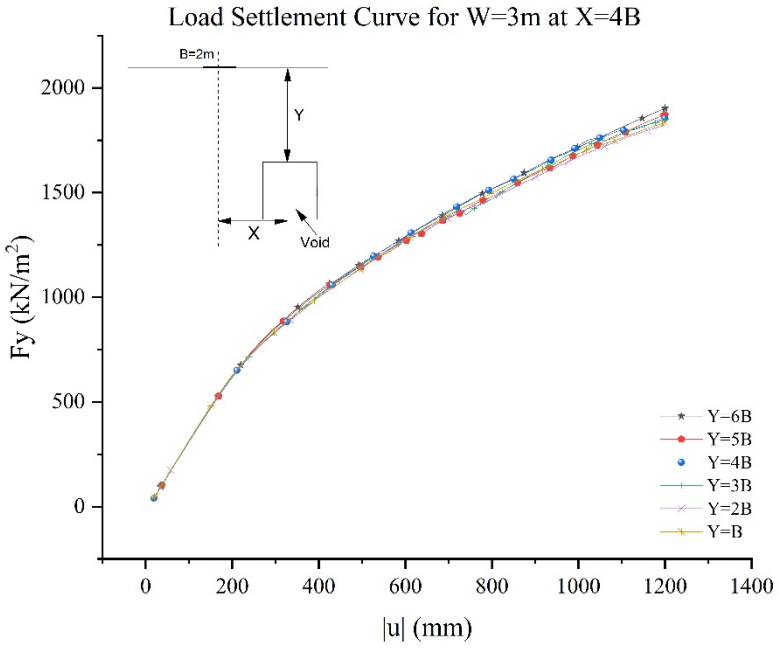

(e)

Figure A.10: Stress Load-Settlement Curve for a Square void, W=3m for variation in depth of void (y) at horizontal offset (x) as (a) x=0B, (b) x=B, (c) x=2B, (d) x=3B and (e) x=4B

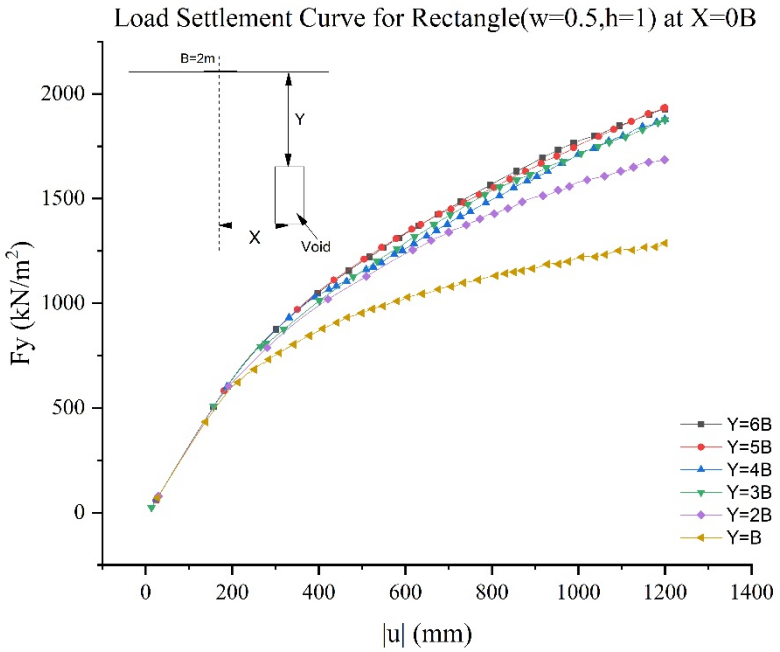
Load Settlement Curve for Rectangle(w=0.5,h=1) at X=0B
B=2m
Y
X
Void
Fy (kN/m²)
|u| (mm)
Y=6B
Y=5B
Y=4B
Y=3B
Y=2B
Y=B

(a)

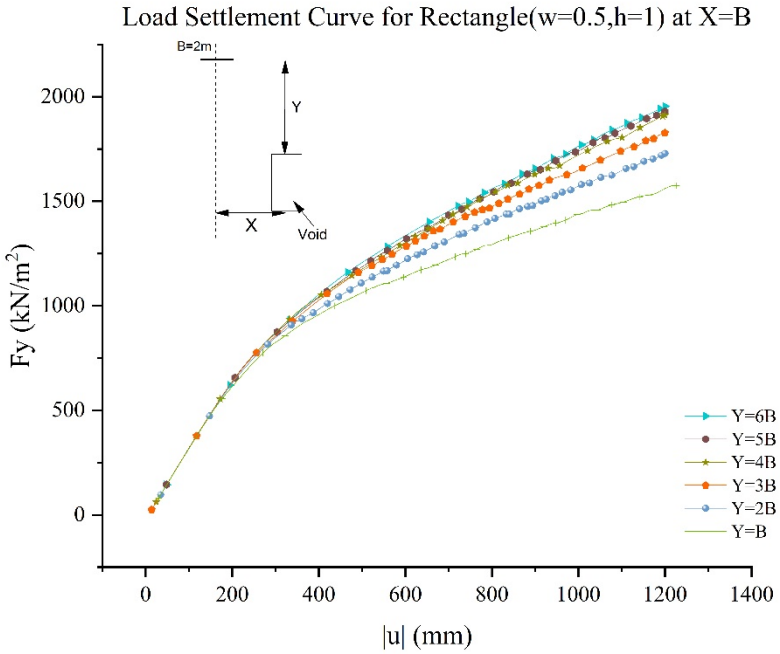
Load Settlement Curve for Rectangle(w=0.5,h=1) at X=B
B=2m
Y
X
Void
Fy (kN/m²)
|u| (mm)
Y=6B
Y=5B
Y=4B
Y=3B
Y=2B
Y=B

(b)

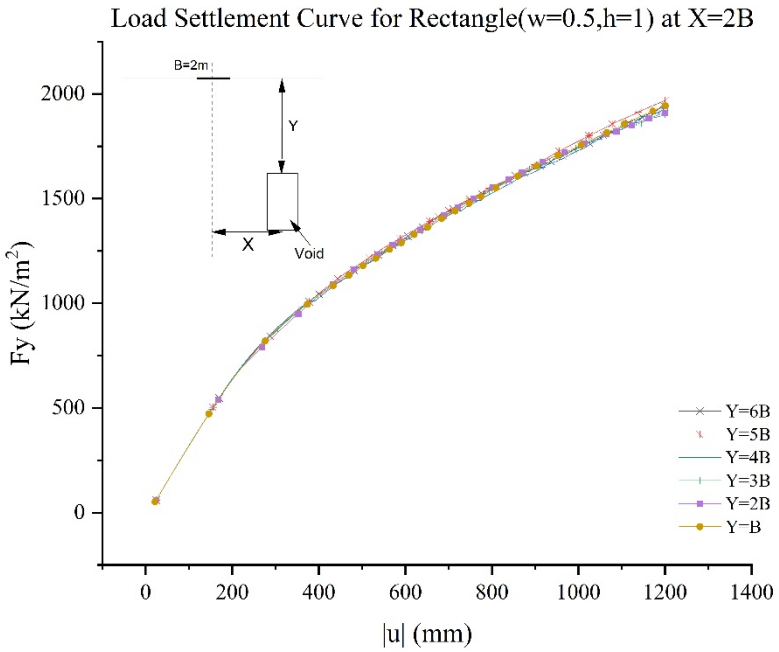
Load Settlement Curve for Rectangle(w=0.5,h=1) at X=2B
B=2m
Y
X
Void
Fy (kN/m2)
|u| (mm)
Y=6B
Y=5B
Y=4B
Y=3B
Y=2B
Y=B

(c)

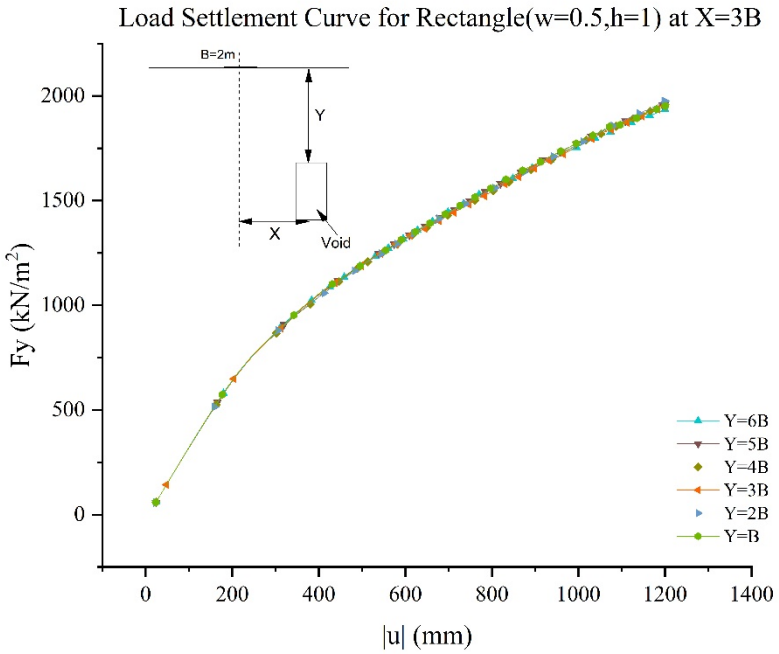
Load Settlement Curve for Rectangle(w=0.5,h=1) at X=3B
B=2m
Y
X
Void
Fy (kN/m2)
|u| (mm)
Y=6B
Y=5B
Y=4B
Y=3B
Y=2B
Y=B

(d)

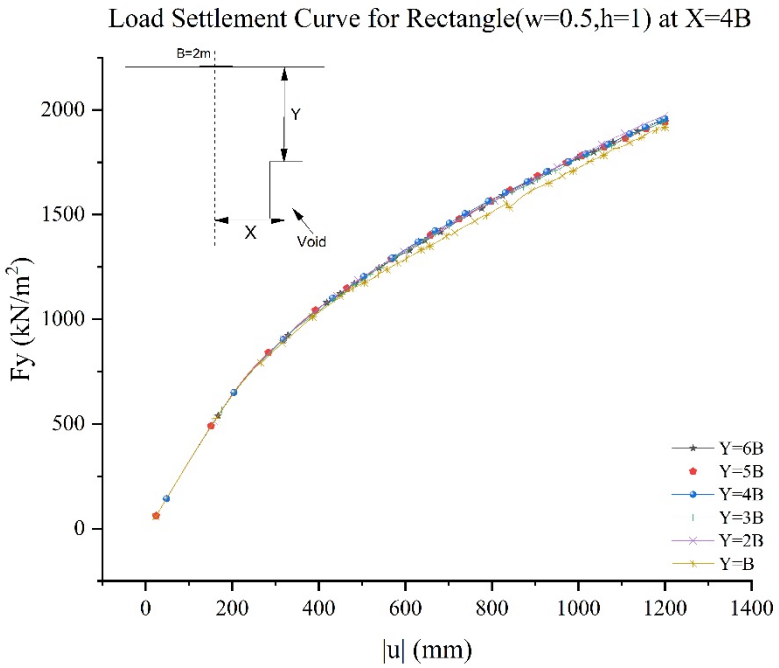

(e)

Figure A.11: Stress Load-Settlement Curve for Rectangular void(w=0.5,h=1,h/w=2), for variation in depth of void (y) at horizontal offset (x) as (a) x=0B, (b) x=B, (c) x=2B, (d) x=3B and (e) x=4B

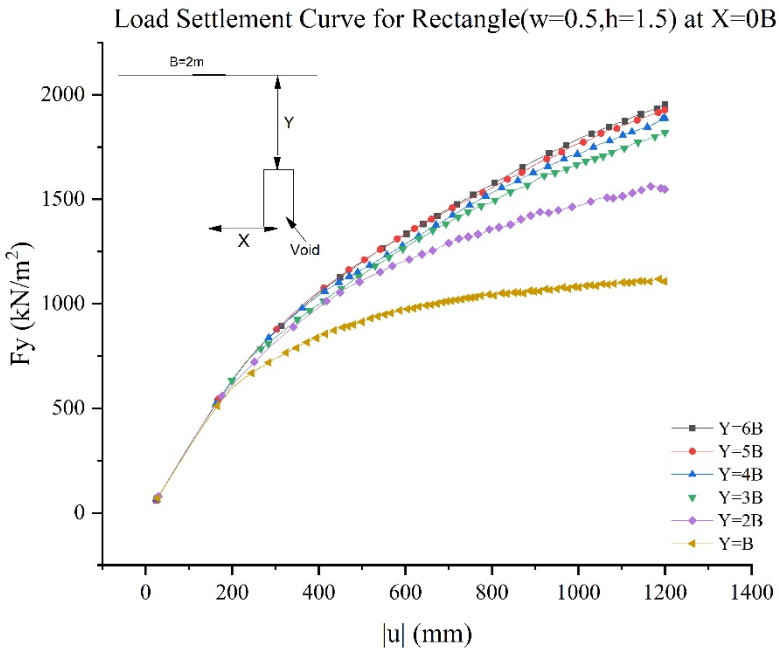

(a)

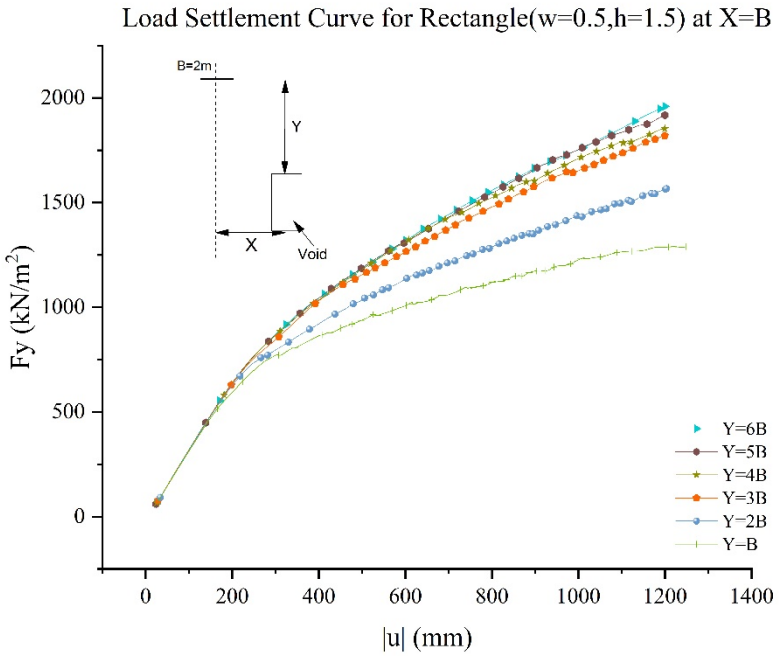
Load Settlement Curve for Rectangle(w=0.5,h=1.5) at X=B
B=2m
Y
X
Void
Fy (kN/m²)
|u| (mm)
Y=6B
Y=5B
Y=4B
Y=3B
Y=2B
Y=B

(b)

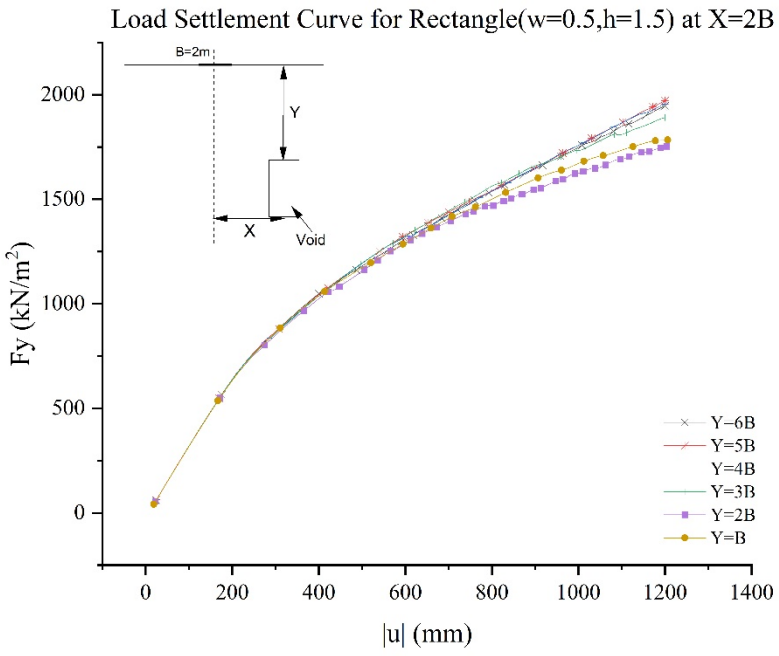
Load Settlement Curve for Rectangle(w=0.5,h=1.5) at X=2B
B=2m
Y
X
Void
Fy (kN/m²)
|u| (mm)
Y=6B
Y=5B
Y=4B
Y=3B
Y=2B
Y=B

(c)

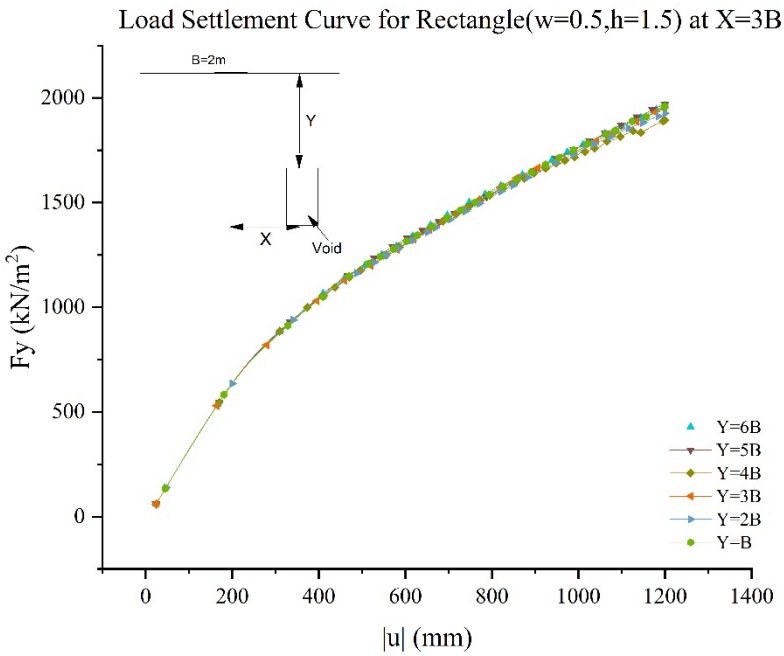

(d)

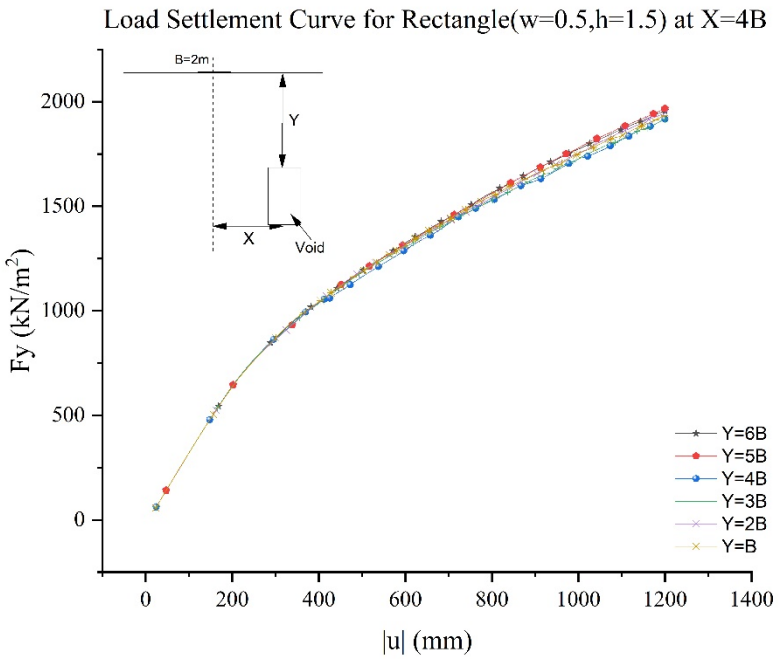

(e)

Figure A.12: Stress Load-Settlement Curve for Rectangular void(w=0.5,h=1.5,h/w=3) for variation in depth of void (y) at horizontal offset (x) as (a) x=0B, (b) x=B, (c) x=2B, (d) x=3B and (e) x=4B

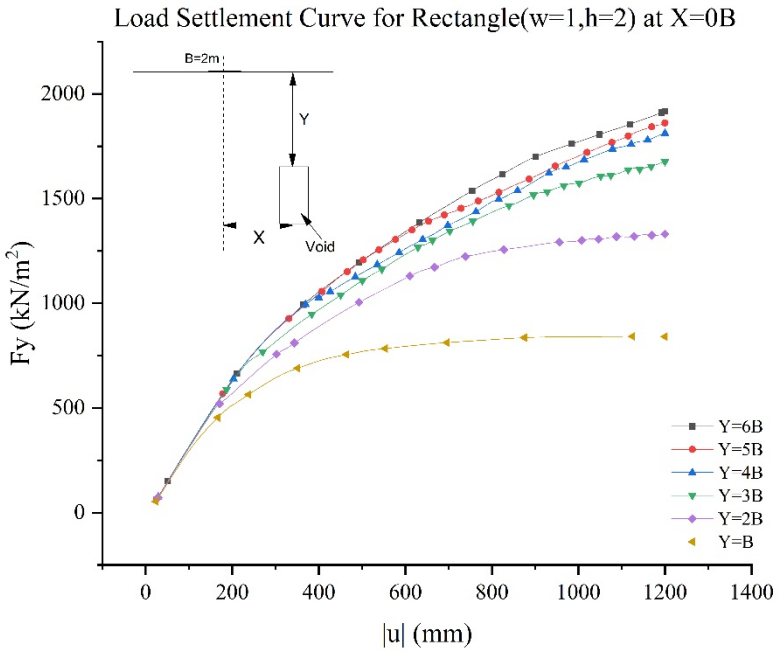
Load Settlement Curve for Rectangle(w=1,h=2) at X=0B
B=2m
Y
X
Void
Fy (kN/m²)
|u| (mm)
Y=6B
Y=5B
Y=4B
Y=3B
Y=2B
Y=B

(a)

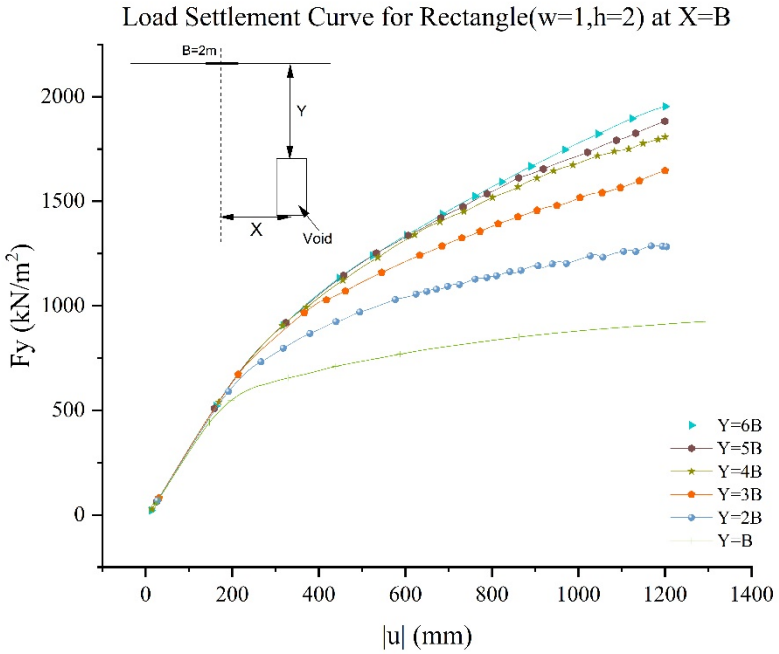
Load Settlement Curve for Rectangle(w=1,h=2) at X=B
B=2m
Y
X
Void
Fy (kN/m²)
|u| (mm)
Y=6B
Y=5B
Y=4B
Y=3B
Y=2B
Y=B

(b)

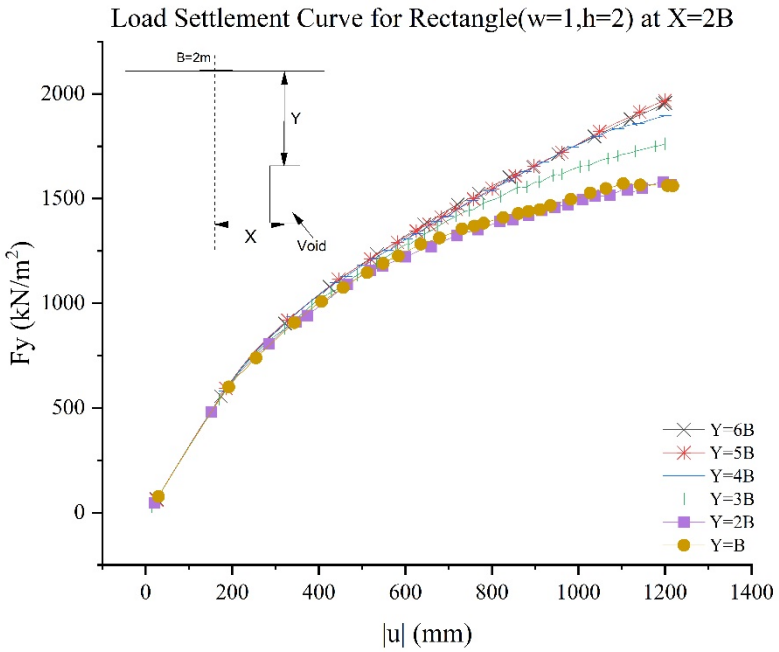
Load Settlement Curve for Rectangle(w=1,h=2) at X=2B
B=2m
Y
X
Void
Fy (kN/m²)
|u| (mm)
Y=6B
Y=5B
Y=4B
Y=3B
Y=2B
Y=B

(c)

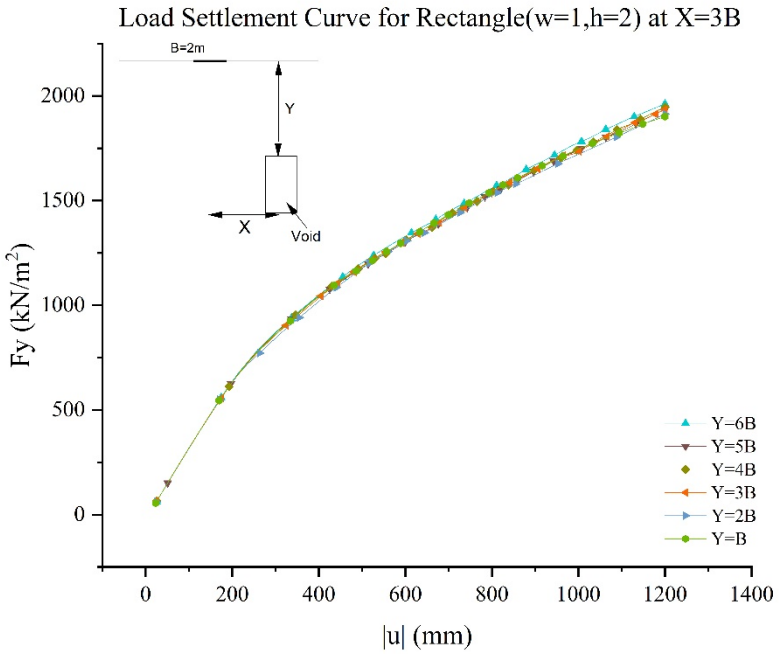
Load Settlement Curve for Rectangle(w=1,h=2) at X=3B
B=2m
Y
X
Void
Fy (kN/m²)
|u| (mm)
Y=6B
Y=5B
Y=4B
Y=3B
Y=2B
Y=B

(d)

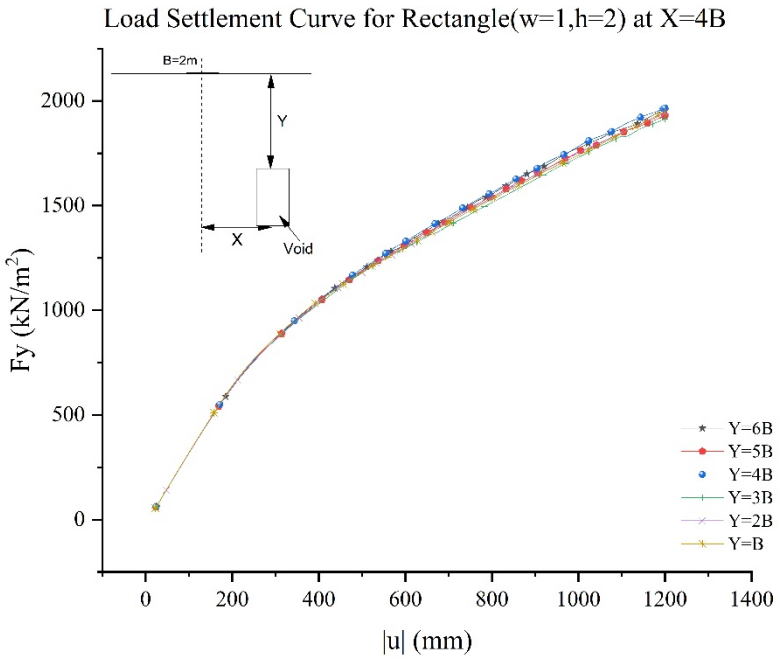

(e)

Figure A.13: Stress Load-Settlement Curve for Rectangular void(w=1,h=2,h/w=2), for variation in depth of void (y) at horizontal offset (x) as (a) x=0B, (b) x=B, (c) x=2B, (d) x=3B and (e) x=4B

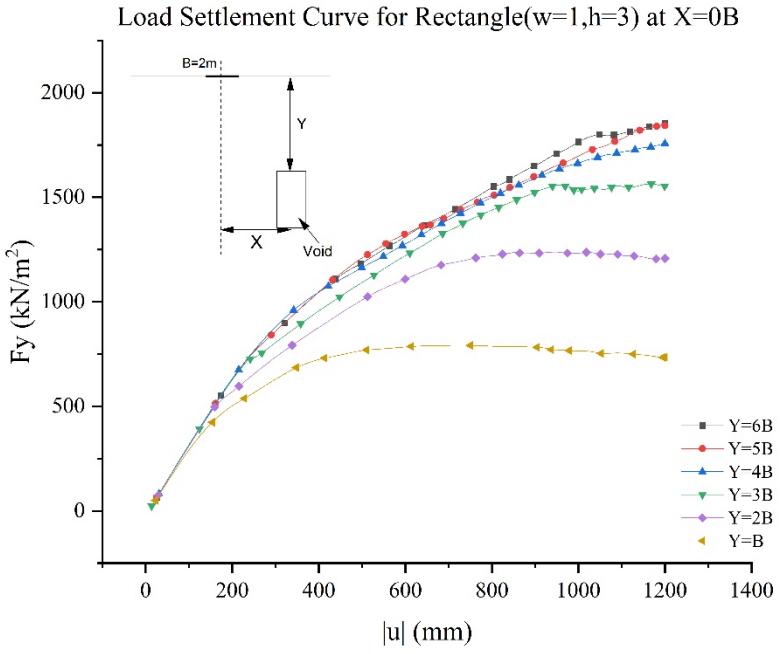

(a)

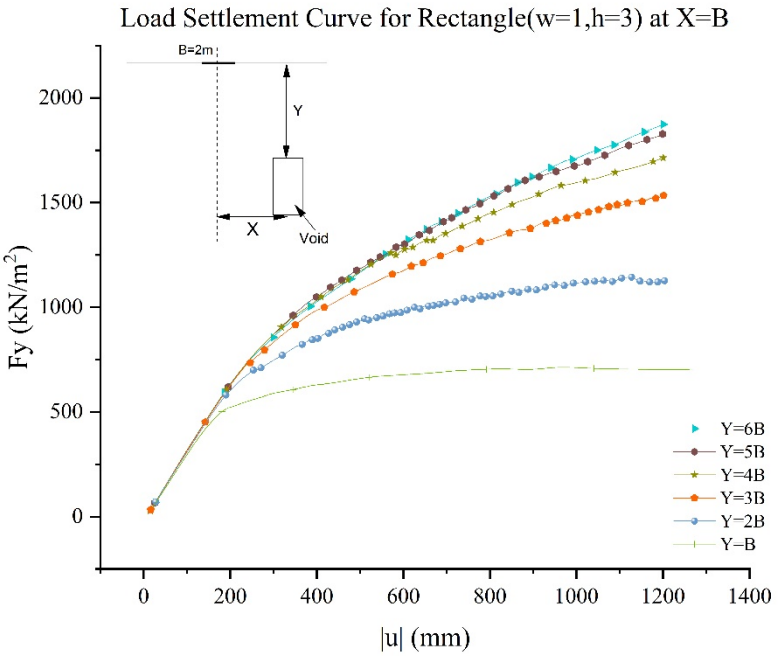
Load Settlement Curve for Rectangle(w=1,h=3) at X=B
B=2m
Y
X
Void
Fy (kN/m²)
|u| (mm)
Y=6B
Y=5B
Y=4B
Y=3B
Y=2B
Y=B

(b)

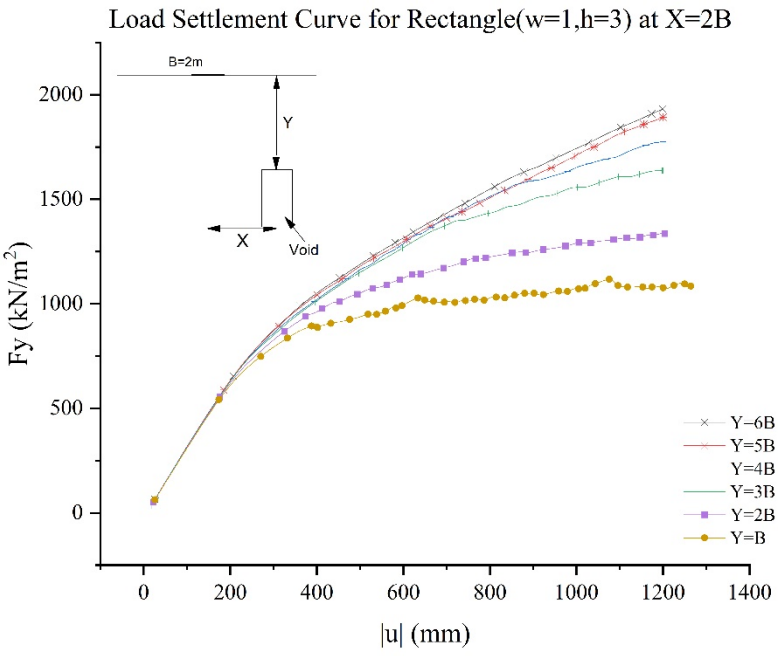
Load Settlement Curve for Rectangle(w=1,h=3) at X=2B
B=2m
Y
X
Void
Fy (kN/m²)
|u| (mm)
Y=6B
Y=5B
Y=4B
Y=3B
Y=2B
Y=B

(c)

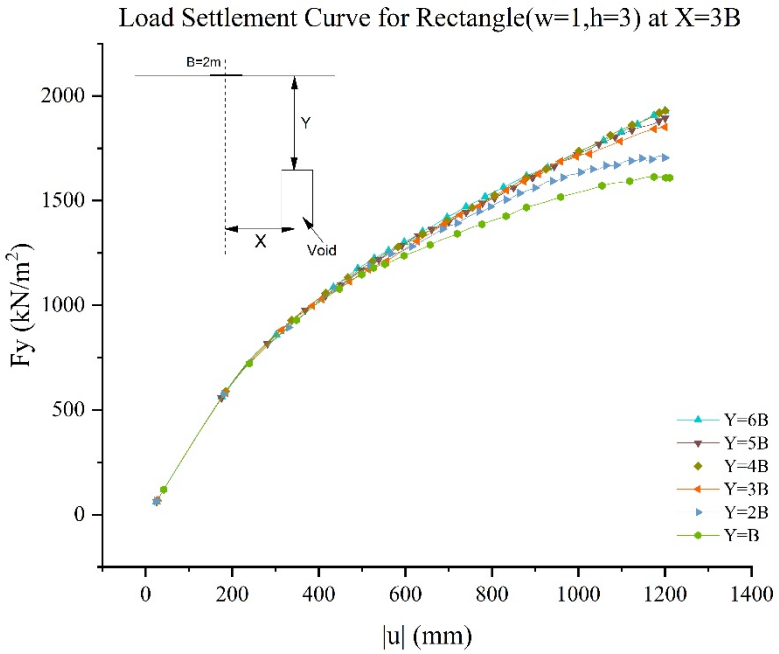

(d)

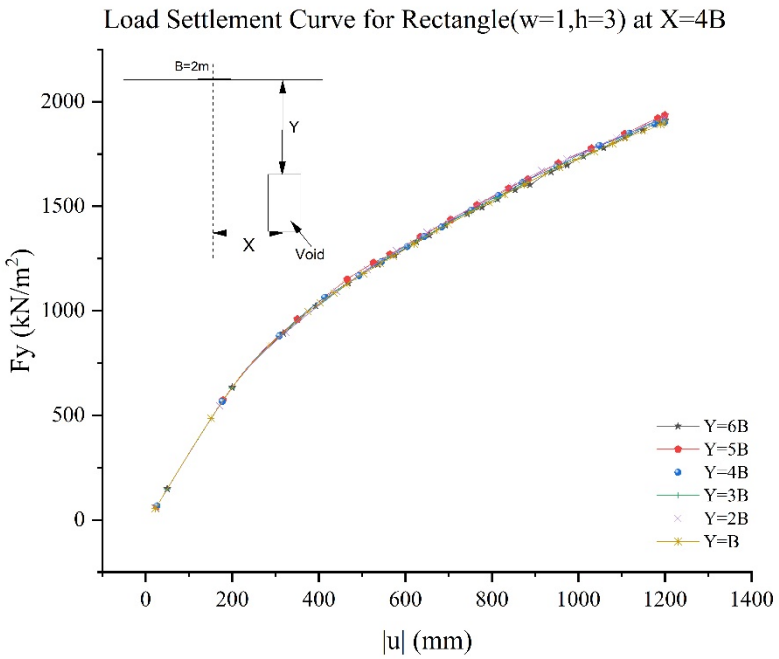

(e)

Figure A.14: Stress Load-Settlement Curve for Rectangular void(w=1,h=3,h/w=3), for variation in depth of void (y) at horizontal offset (x) as (a) x=0B, (b) x=B, (c) x=2B, (d) x=3B and (e) x=4B

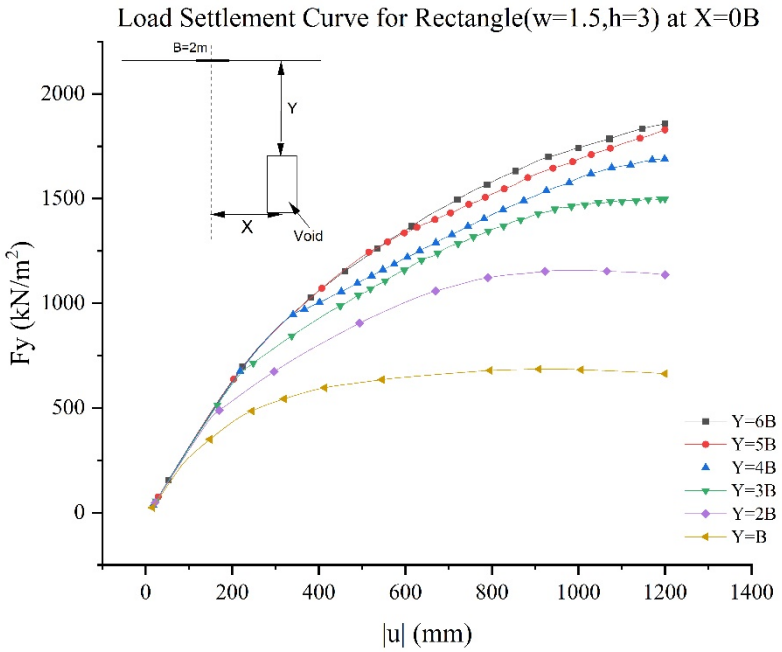
Load Settlement Curve for Rectangle(w=1.5,h=3) at X=0B
B=2m
Y
X
Void
Fy (kN/m²)
|u| (mm)
Y=6B
Y=5B
Y=4B
Y=3B
Y=2B
Y=B

(a)

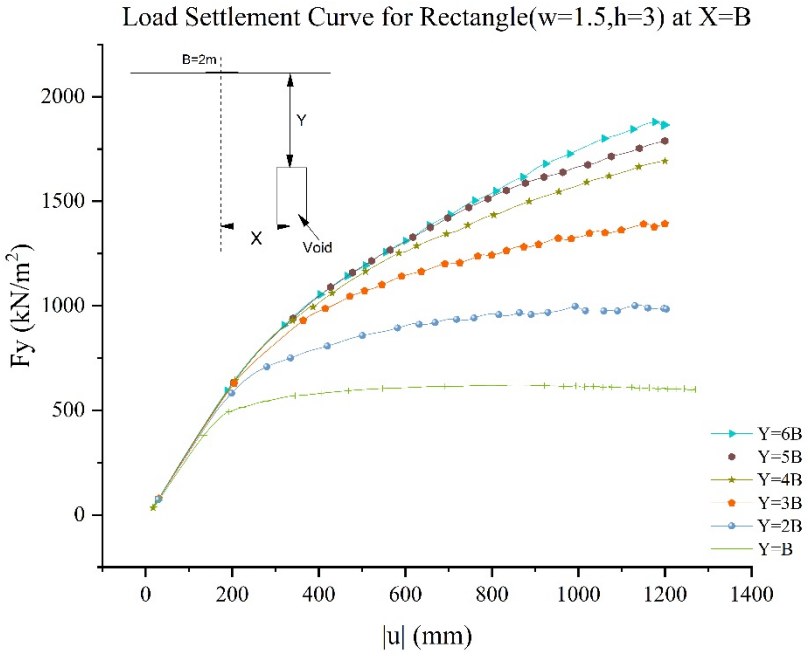
Load Settlement Curve for Rectangle(w=1.5,h=3) at X=B
B=2m
Y
X
Void
Fy (kN/m²)
|u| (mm)
Y=6B
Y=5B
Y=4B
Y=3B
Y=2B
Y=B

(b)

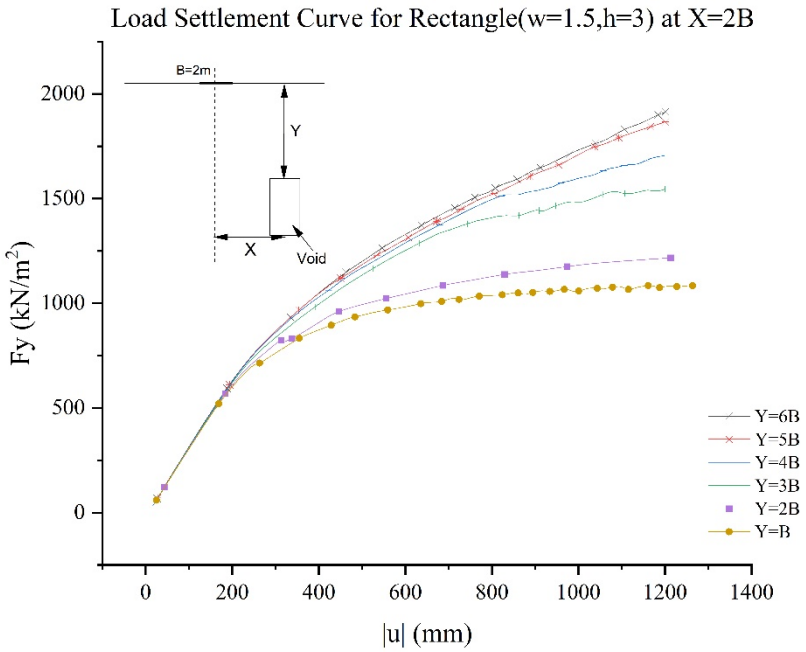
Load Settlement Curve for Rectangle(w=1.5,h=3) at X=2B
B=2m
Y
X
Void
Fy (kN/m²)
|u| (mm)
Y=6B
Y=5B
Y=4B
Y=3B
Y=2B
Y=B

(c)

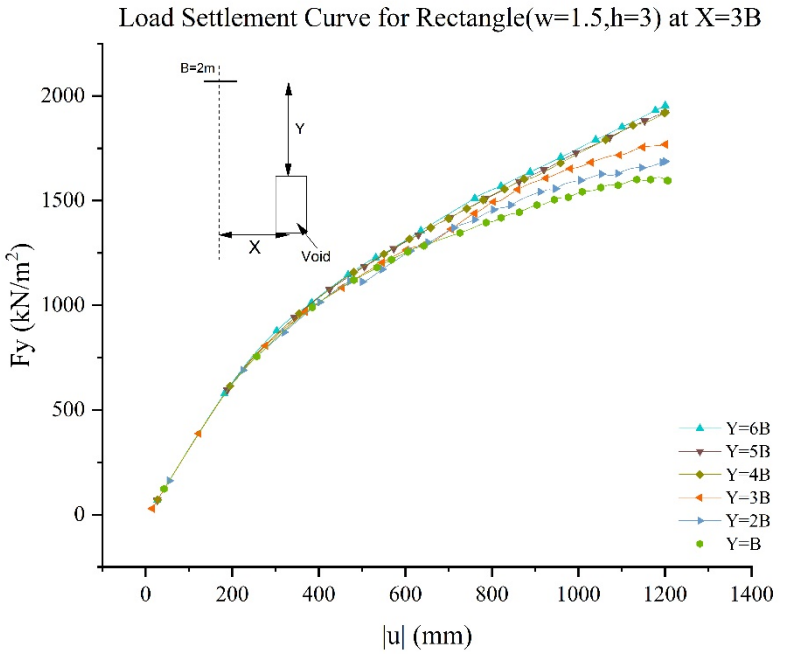
Load Settlement Curve for Rectangle(w=1.5,h=3) at X=3B
B=2m
Y
X
Void
Fy (kN/m²)
|u| (mm)
Y=6B
Y=5B
Y=4B
Y=3B
Y=2B
Y=B

(d)

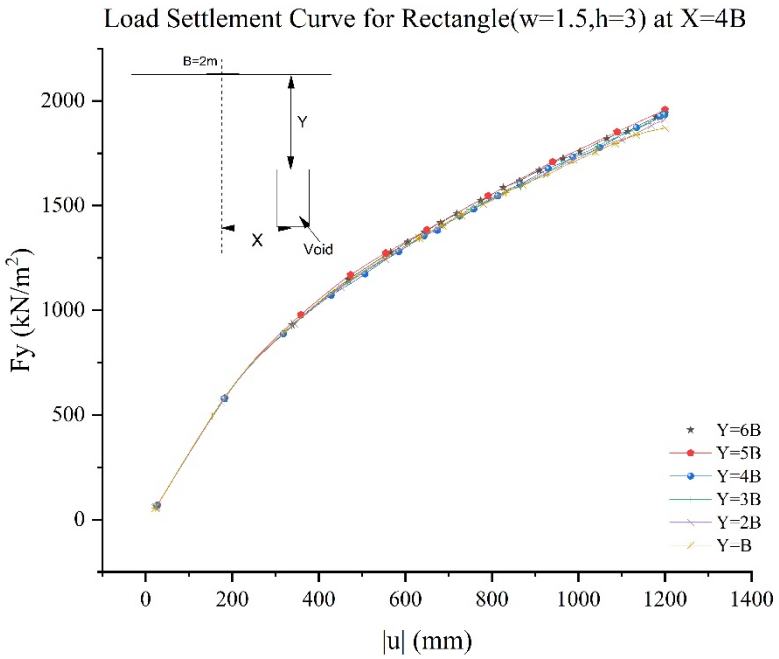

(e)

Figure A.15: Stress Load-Settlement Curve for Rectangular void(w=1.5,h=3,h/w=2), for variation in depth of void (y) at horizontal offset (x) as (a) x=0B, (b) x=B, (c) x=2B, (d) x=3B and (e) x=4B

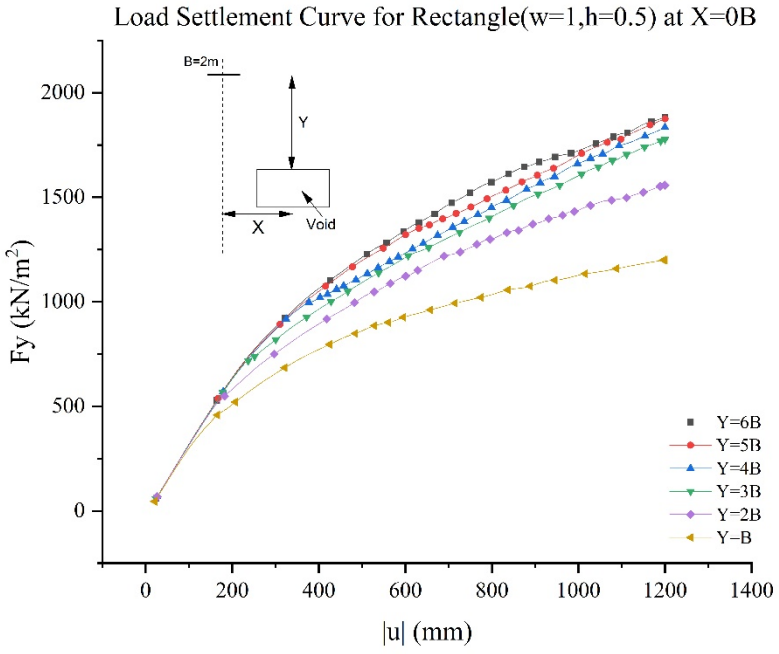

(a)

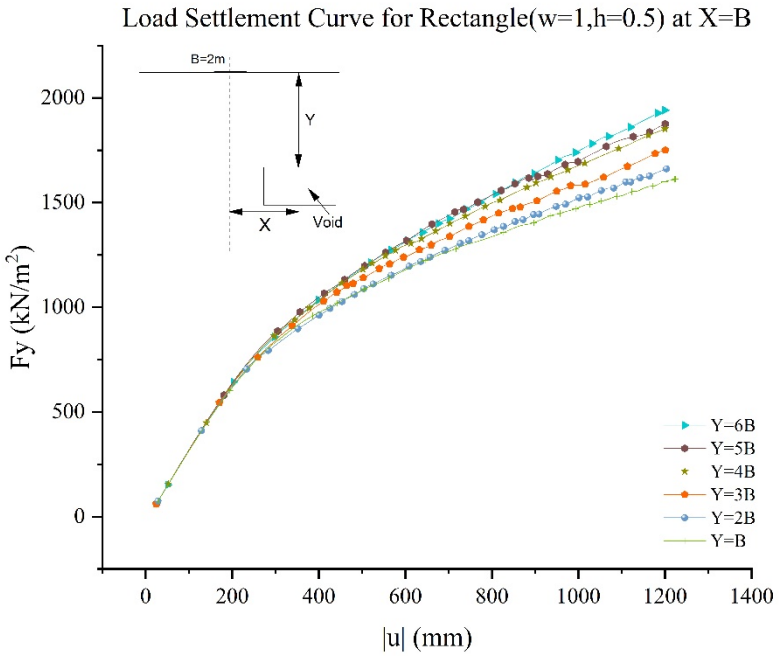
Load Settlement Curve for Rectangle(w=1,h=0.5) at X=B
B=2m
Y
X
Void
Fy (kN/m²)
|u| (mm)
Y=6B
Y=5B
Y=4B
Y=3B
Y=2B
Y=B

(b)

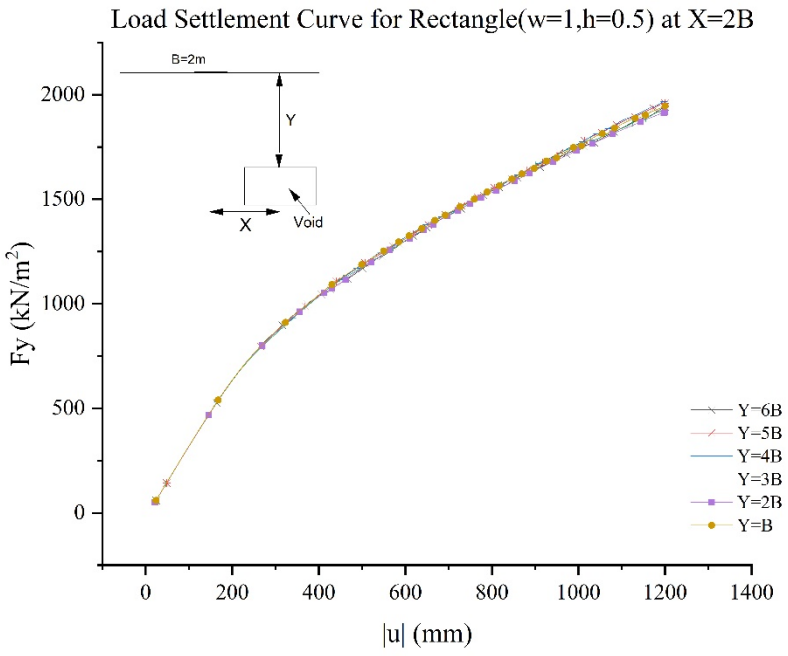
Load Settlement Curve for Rectangle(w=1,h=0.5) at X=2B
B=2m
Y
X
Void
Fy (kN/m²)
|u| (mm)
Y=6B
Y=5B
Y=4B
Y=3B
Y=2B
Y=B

(c)

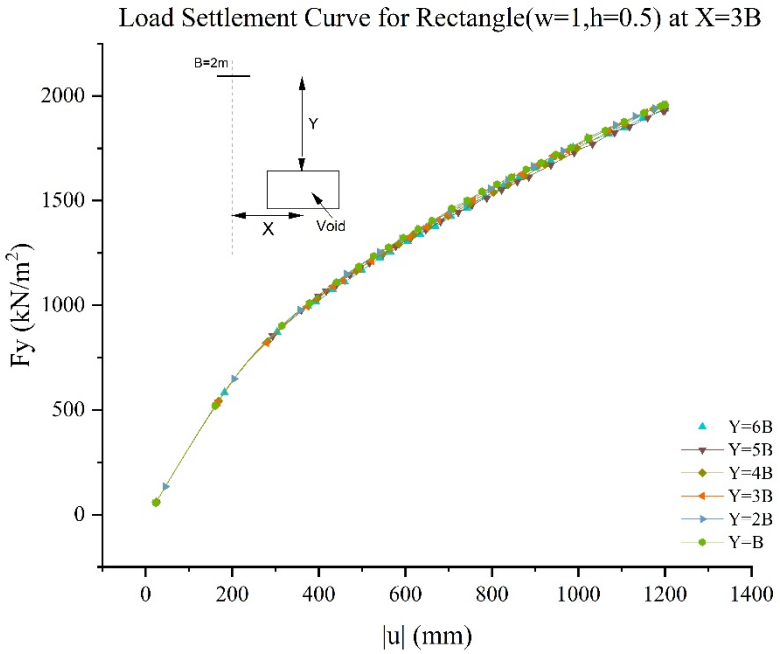

(d)

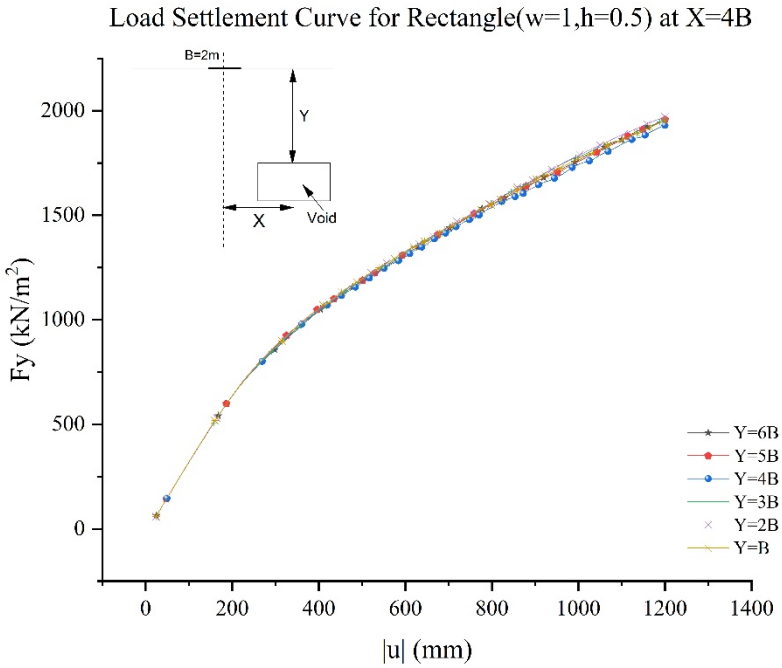

(e)

Figure A.16: Stress Load-Settlement Curve for Rectangular void(w=1,h=0.5,h/w=1/2), for variation in depth of void (y) at horizontal offset (x) as (a) x=0B, (b) x=B, (c) x=2B, (d) x=3B and (e) x=4B

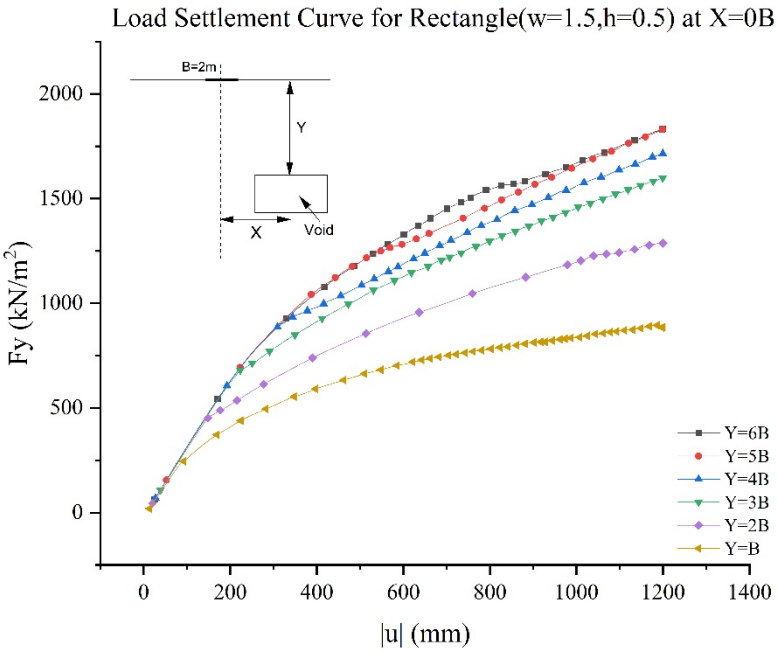
Load Settlement Curve for Rectangle(w=1.5,h=0.5) at X=0B
B=2m
Y
X
Void
Fy (kN/m²)
|u| (mm)
Y=6B
Y=5B
Y=4B
Y=3B
Y=2B
Y=B

(a)

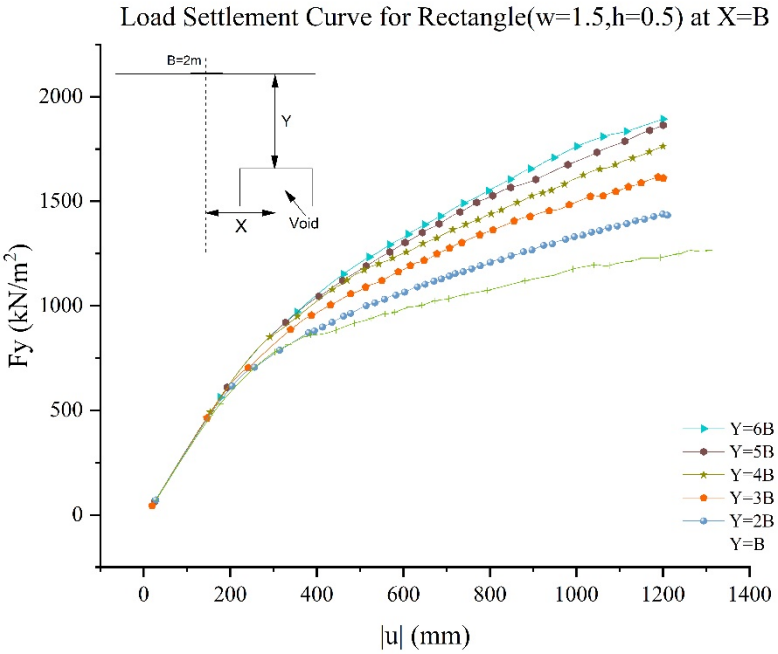
Load Settlement Curve for Rectangle(w=1.5,h=0.5) at X=B
B=2m
Y
X
Void
Fy (kN/m²)
|u| (mm)
Y=6B
Y=5B
Y=4B
Y=3B
Y=2B
Y=B

(b)

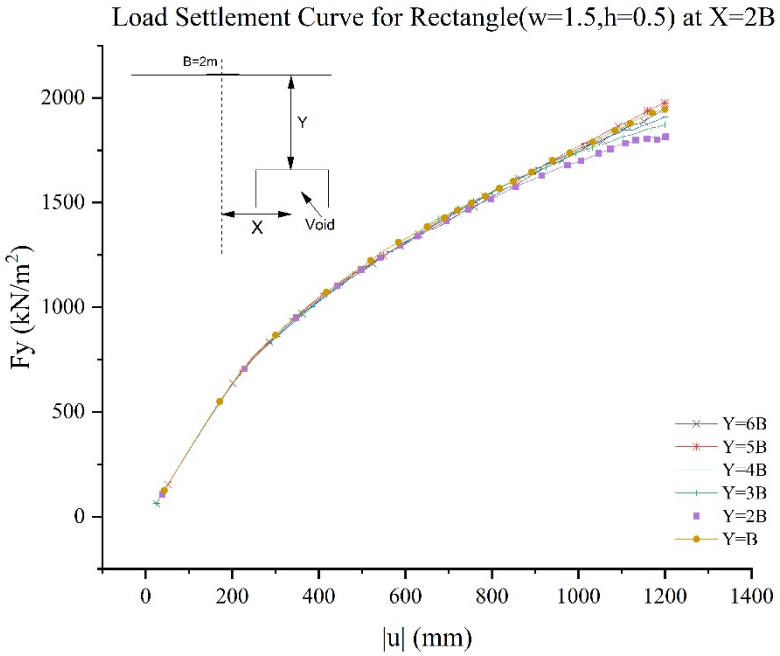
Load Settlement Curve for Rectangle(w=1.5,h=0.5) at X=2B
B=2m
Y
X
Void
Fy (kN/m2)
|u| (mm)
Y=6B
Y=5B
Y=4B
Y=3B
Y=2B
Y=B

(c)

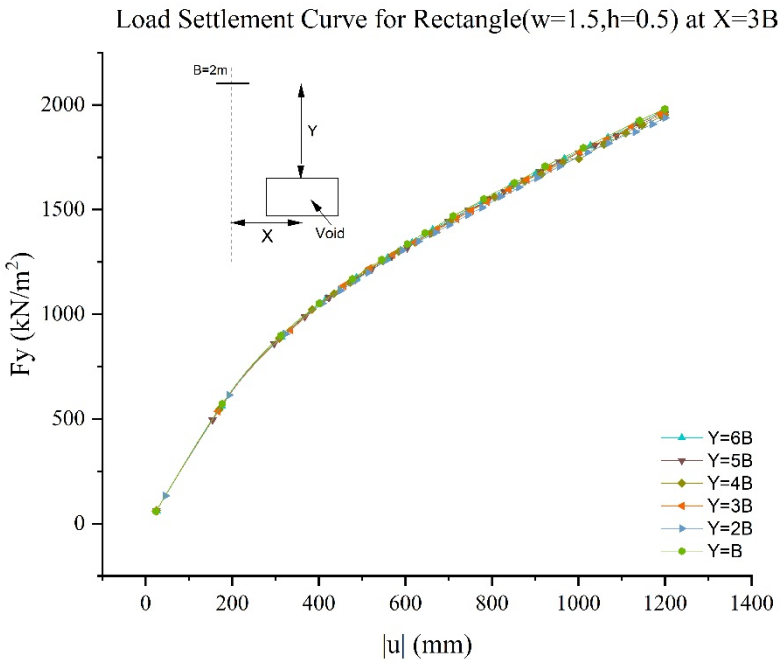
Load Settlement Curve for Rectangle(w=1.5,h=0.5) at X=3B
B=2m
Y
X
Void
Fy (kN/m2)
|u| (mm)
Y=6B
Y=5B
Y=4B
Y=3B
Y=2B
Y=B

(d)

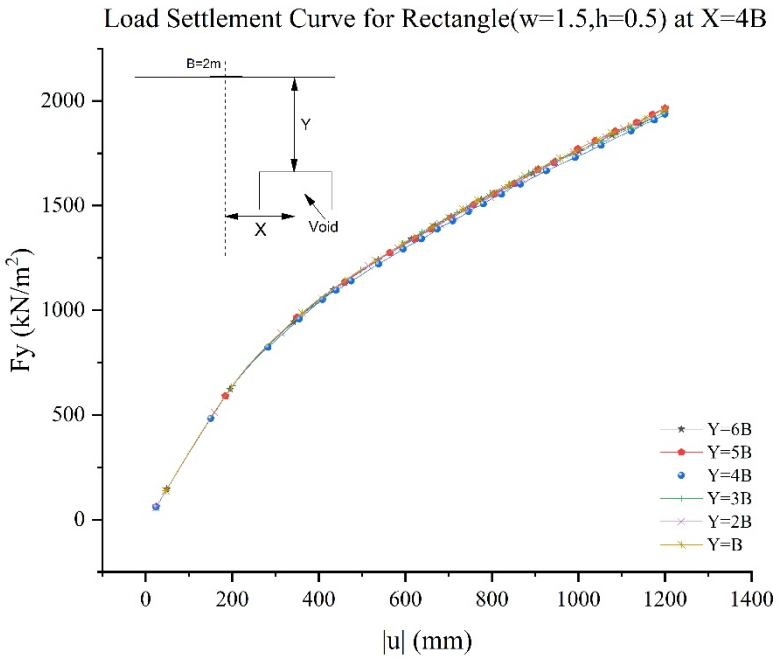

(e)

Figure A.17: Stress Load-Settlement Curve for Rectangular void(w=1.5,h=0.5,h/w=1/3), for variation in depth of void (y) at horizontal offset (x) as (a) x=0B, (b) x=B, (c) x=2B, (d) x=3B and (e) x=4B

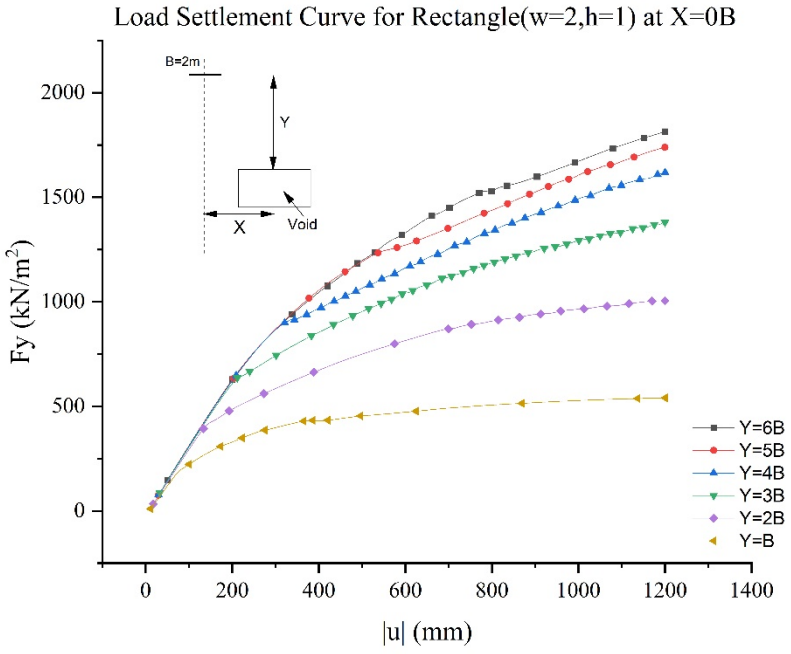

(a)

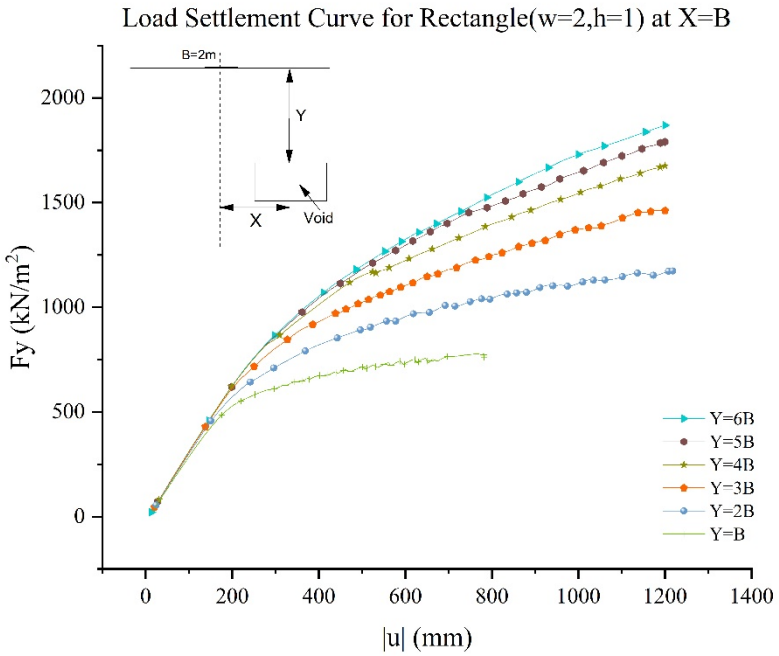
Load Settlement Curve for Rectangle(w=2,h=1) at X=B
B=2m
Y
X
Void
Fy (kN/m²)
|u| (mm)
Y=6B
Y=5B
Y=4B
Y=3B
Y=2B
Y=B

(b)

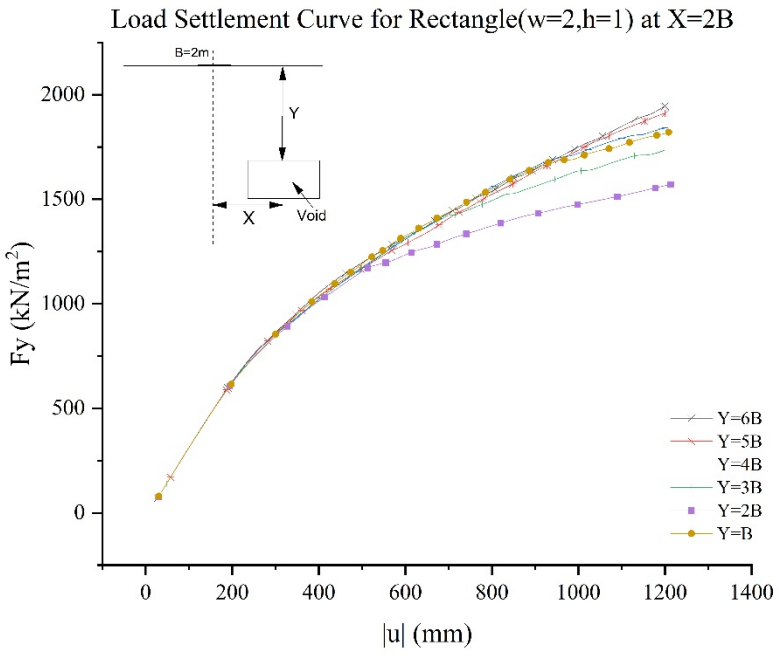
Load Settlement Curve for Rectangle(w=2,h=1) at X=2B
B=2m
Y
X
Void
Fy (kN/m²)
|u| (mm)
Y=6B
Y=5B
Y=4B
Y=3B
Y=2B
Y=B

(c)

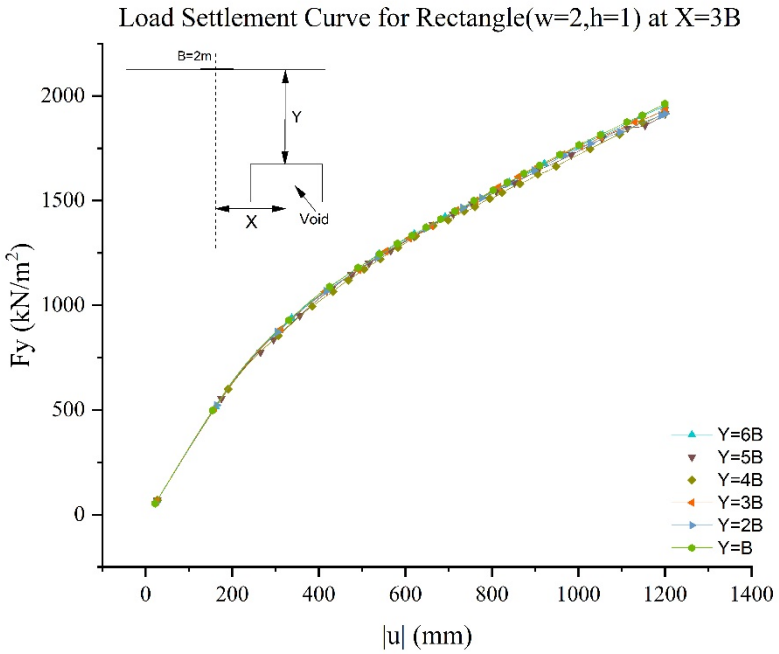

(d)

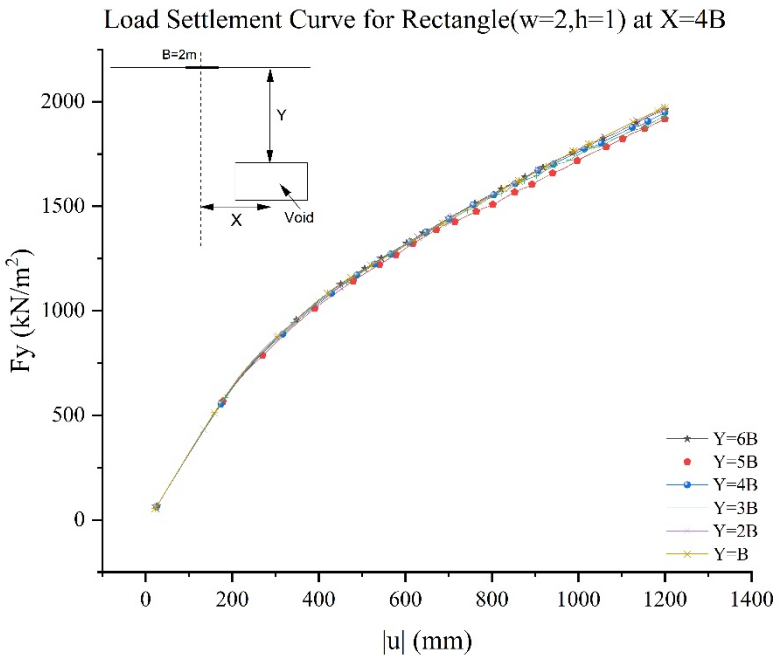

(e)

Figure A.18: Stress Load-Settlement Curve for Rectangular void(w=2,h=1,h/w=1/2), for variation in depth of void (y) at horizontal offset (x) as (a) x=0B, (b) x=B, (c) x=2B, (d) x=3B and (e) x=4B

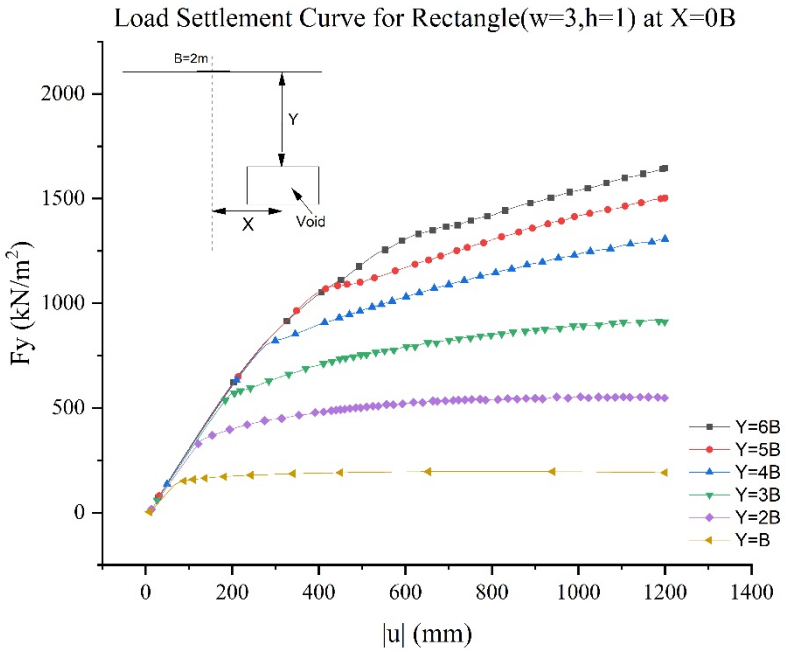
Load Settlement Curve for Rectangle(w=3,h=1) at X=0B
B=2m
Y
X
Void
Fy (kN/m²)
|u| (mm)
Y=6B
Y=5B
Y=4B
Y=3B
Y=2B
Y=B

(a)

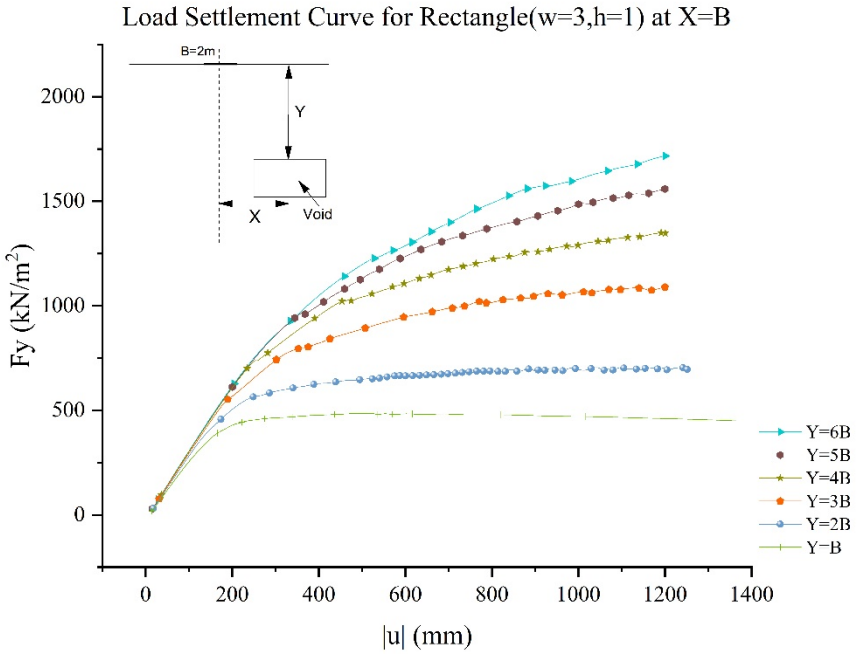
Load Settlement Curve for Rectangle(w=3,h=1) at X=B
B=2m
Y
X
Void
Fy (kN/m²)
|u| (mm)
Y=6B
Y=5B
Y=4B
Y=3B
Y=2B
Y=B

(b)

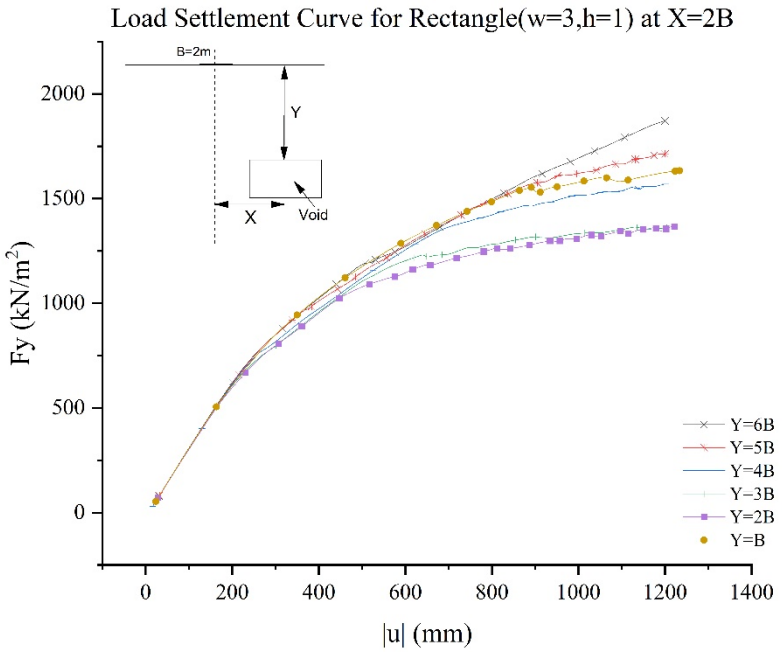
Load Settlement Curve for Rectangle(w=3,h=1) at X=2B
B=2m
Y
X
Void
Fy (kN/m²)
|u| (mm)
Y=6B
Y=5B
Y=4B
Y=3B
Y=2B
Y=B

(c)

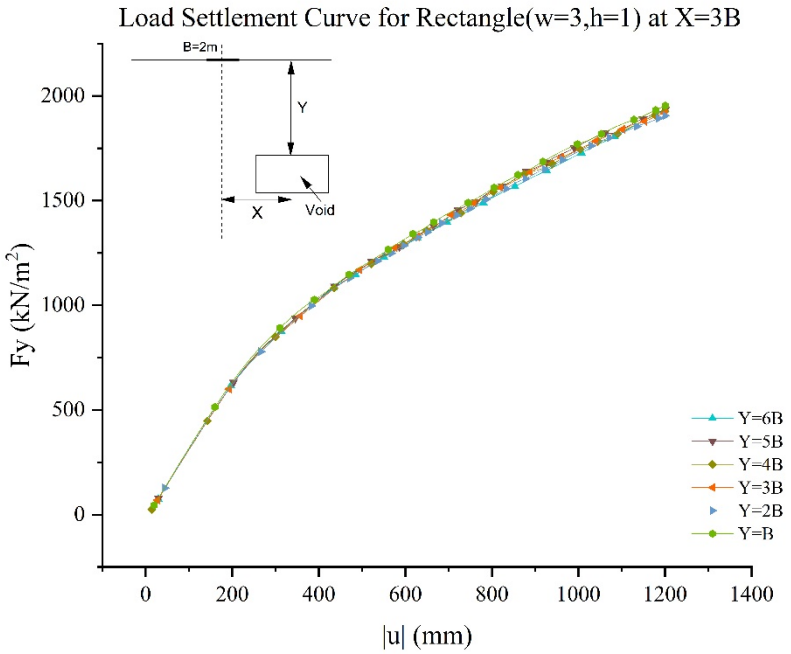
Load Settlement Curve for Rectangle(w=3,h=1) at X=3B
B=2m
Y
X
Void
Fy (kN/m²)
|u| (mm)
Y=6B
Y=5B
Y=4B
Y=3B
Y=2B
Y=B

(d)

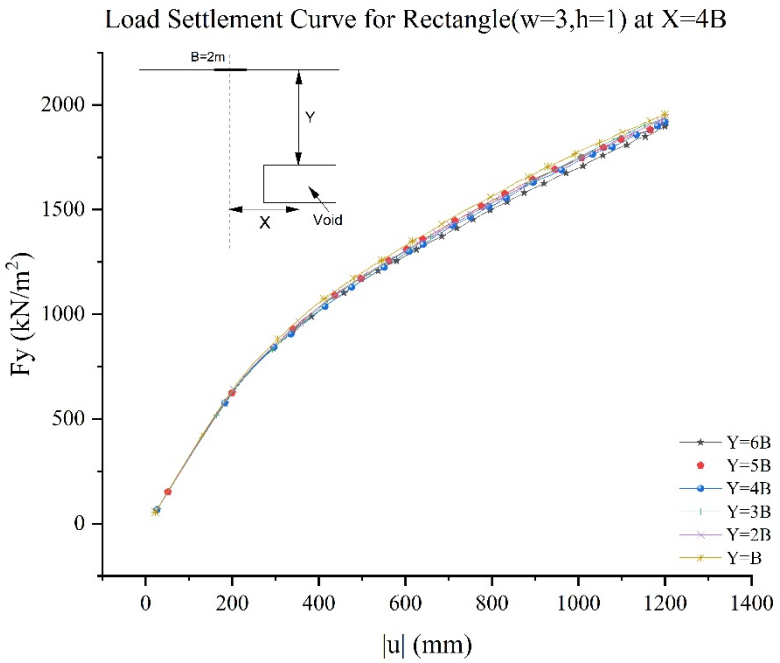

(e)

Figure A.19: Stress Load-Settlement Curve for Rectangular void(w=3,h=1,h/w=1/3), for variation in depth of void (y) at horizontal offset (x) as (a) x=0B, (b) x=B, (c) x=2B, (d) x=3B and (e) x=4B

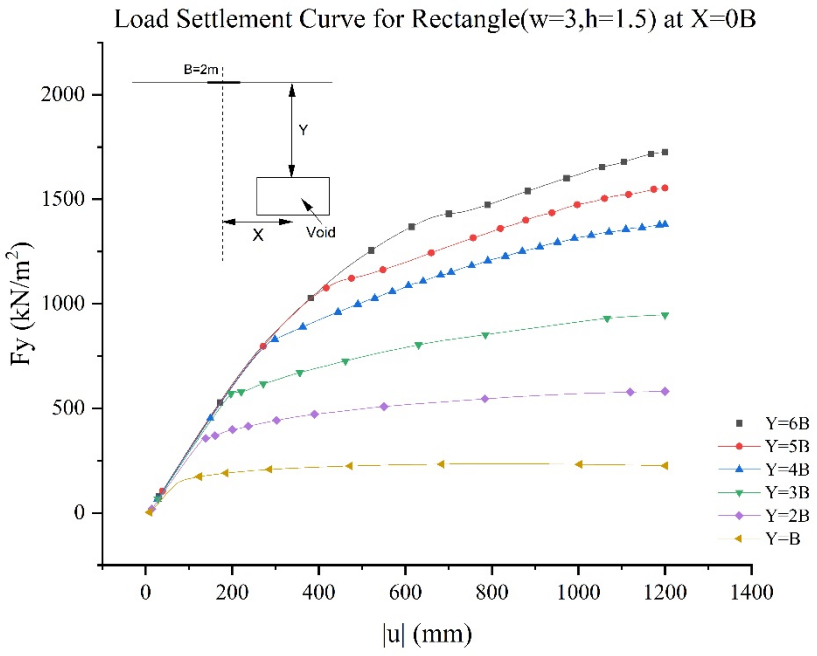

(a)

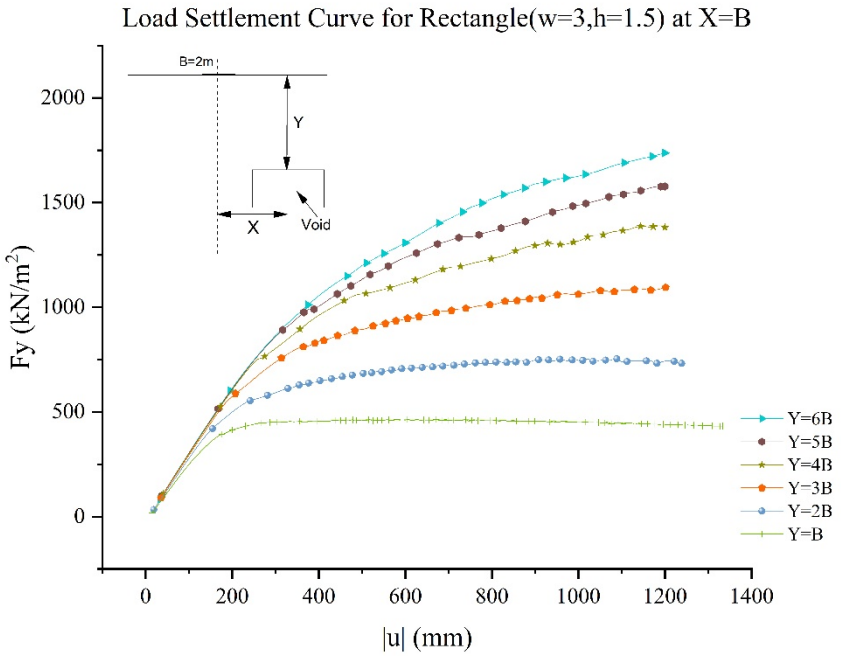
Load Settlement Curve for Rectangle(w=3,h=1.5) at X=B
B=2m
Y
X
Void
Fy (kN/m²)
|u| (mm)
Y=6B
Y=5B
Y=4B
Y=3B
Y=2B
Y=B

(b)

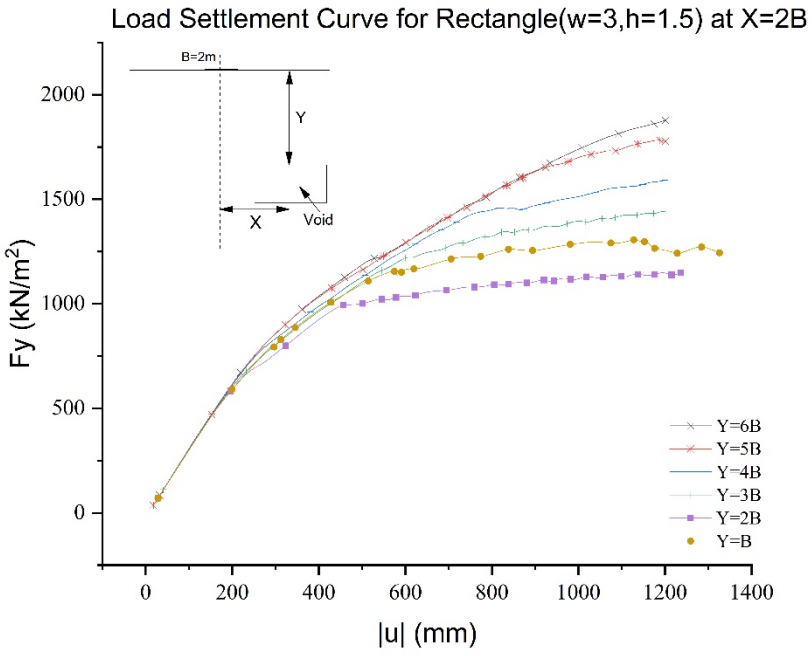
Load Settlement Curve for Rectangle(w=3,h=1.5) at X=2B
B=2m
Y
X
Void
Fy (kN/m²)
|u| (mm)
Y=6B
Y=5B
Y=4B
Y=3B
Y=2B
Y=B

(c)

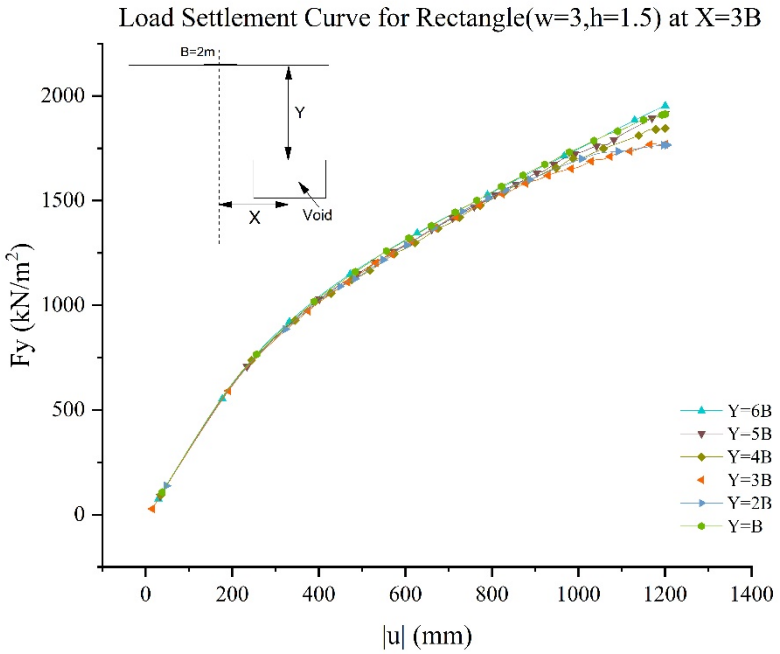

(d)

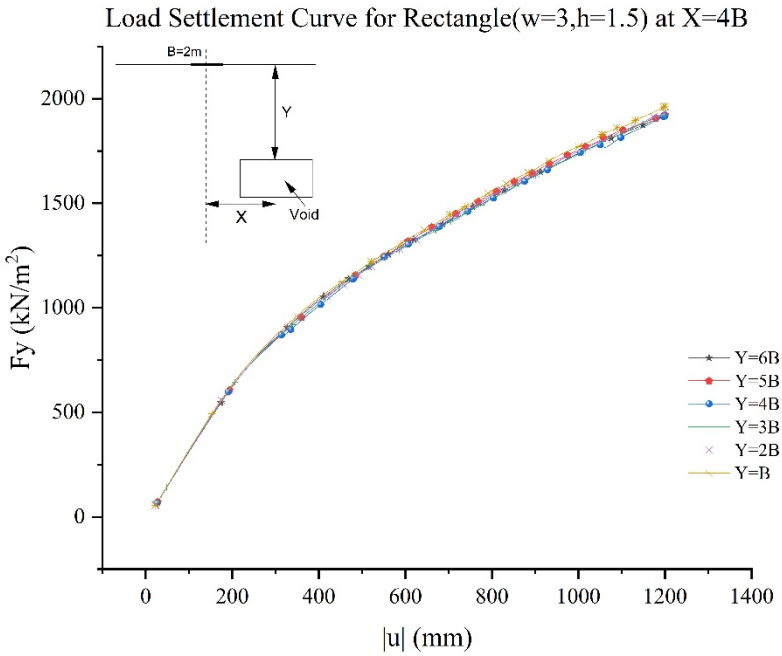

(e)

Figure A.20: Stress Load-Settlement Curve for Rectangular void(w=1.5,h=3,h/w=2), for variation in depth of void (y) at horizontal offset (x) as (a) x=0B, (b) x=B, (c) x=2B, (d) x=3B and (e) x=4B

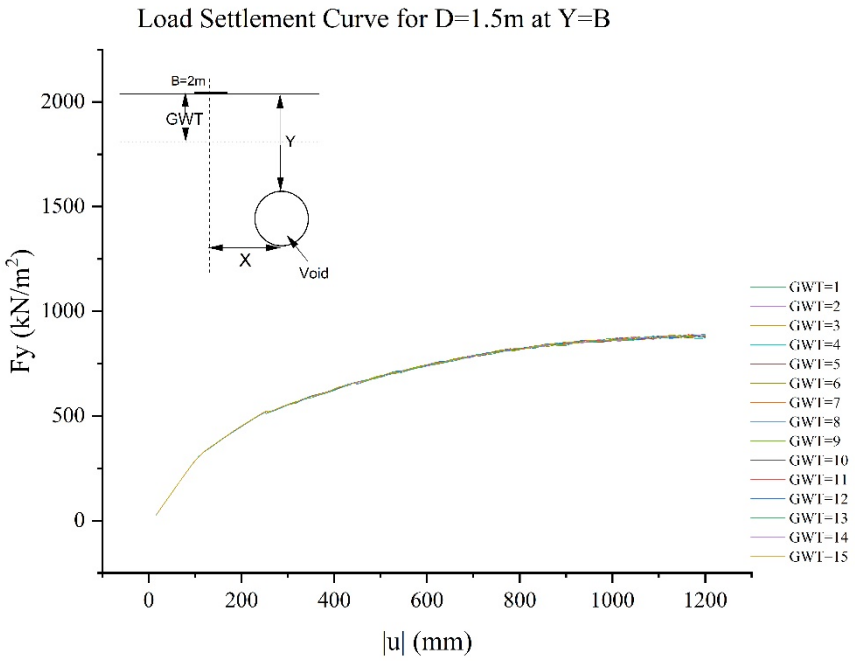
Load Settlement Curve for D=1.5m at Y=B
B=2m
GWT
Y
X
Void
Fy (kN/m²)
|u| (mm)
0
500
1000
1500
2000
0
200
400
600
800
1000
1200
GWT=1
GWT=2
GWT=3
GWT=4
GWT=5
GWT=6
GWT=7
GWT=8
GWT=9
GWT=10
GWT=11
GWT=12
GWT=13
GWT=14
GWT=15

(a)

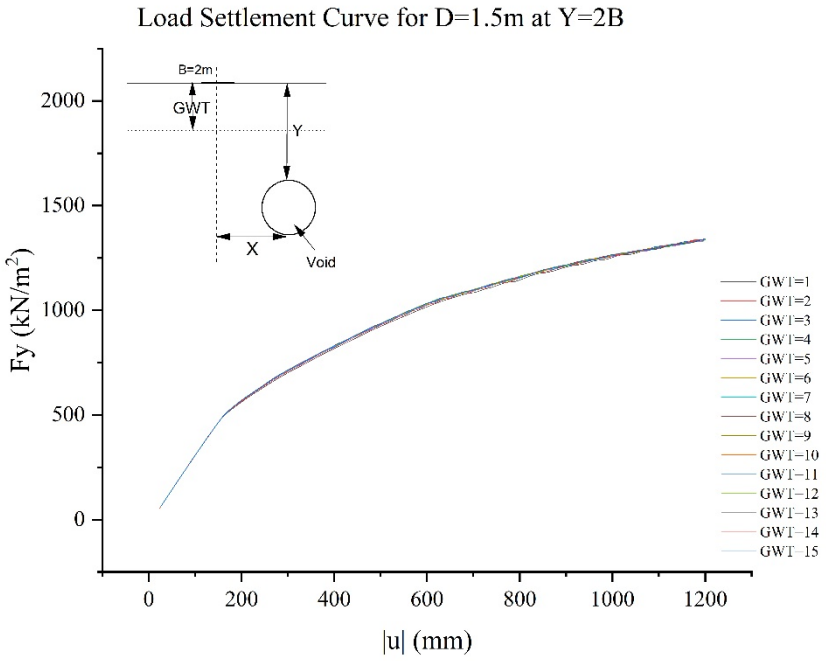
Load Settlement Curve for D=1.5m at Y=2B
B=2m
GWT
Y
X
Void
Fy (kN/m²)
|u| (mm)
0
500
1000
1500
2000
0
200
400
600
800
1000
1200
GWT=1
GWT=2
GWT=3
GWT=4
GWT=5
GWT=6
GWT=7
GWT=8
GWT=9
GWT=10
GWT=11
GWT=12
GWT=13
GWT=14
GWT=15

(b)

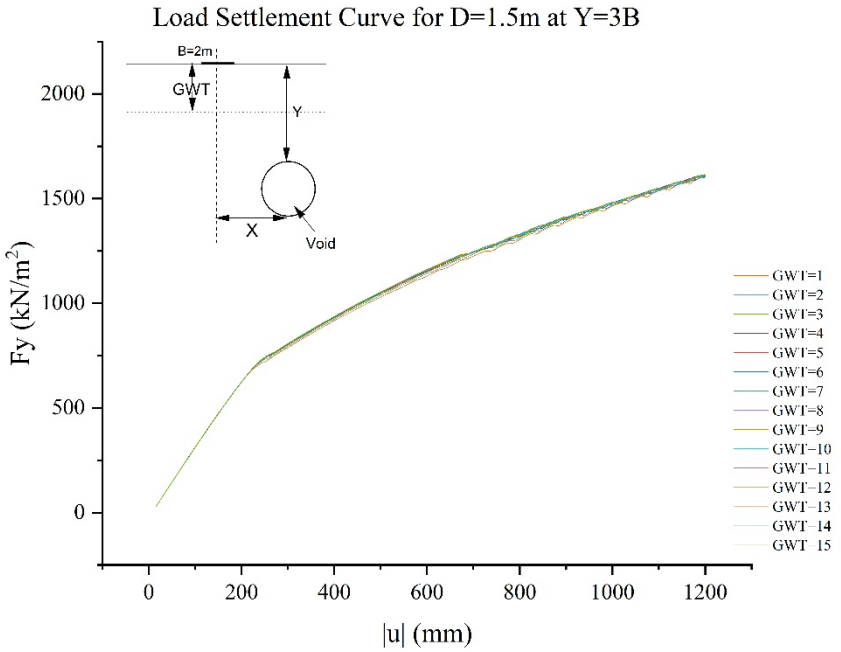
Load Settlement Curve for D=1.5m at Y=3B
B=2m
GWT
Y
X
Void
Fy (kN/m²)
|u| (mm)
GWT=1
GWT=2
GWT=3
GWT=4
GWT=5
GWT=6
GWT=7
GWT=8
GWT=9
GWT=10
GWT=11
GWT=12
GWT=13
GWT=14
GWT=15

(c)

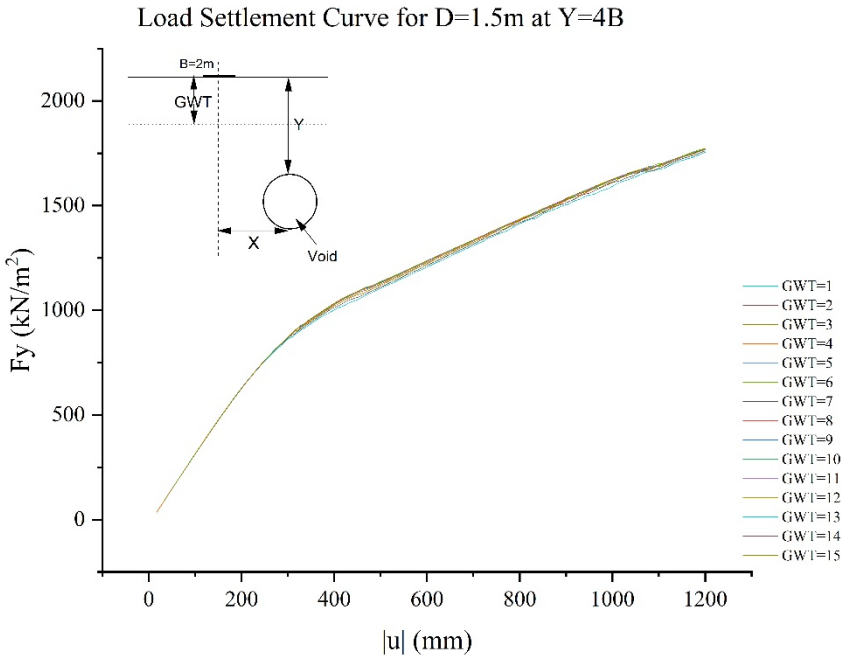
Load Settlement Curve for D=1.5m at Y=4B
B=2m
GWT
Y
X
Void
Fy (kN/m²)
|u| (mm)
GWT=1
GWT=2
GWT=3
GWT=4
GWT=5
GWT=6
GWT=7
GWT=8
GWT=9
GWT=10
GWT=11
GWT=12
GWT=13
GWT=14
GWT=15

(d)

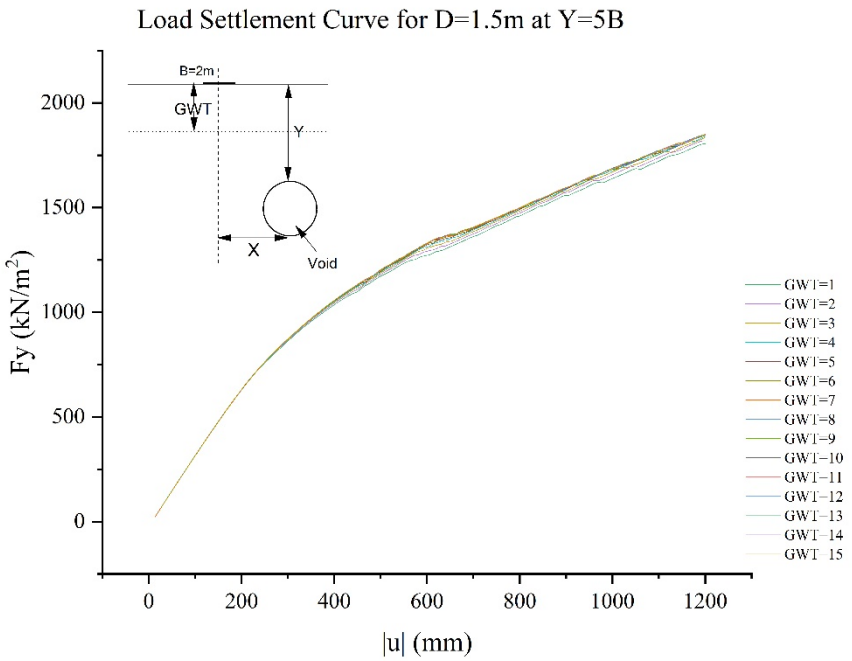

(e)

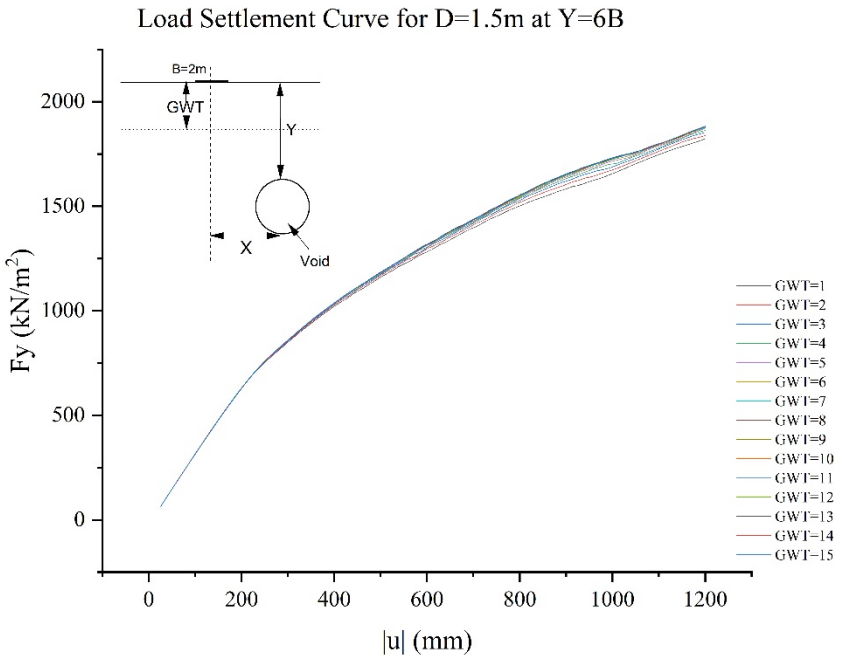

(f)

Figure A.21: Stress Load-Settlement Curve for Circular void(D=1.5m) with ground water table for variation in depth of void (y) at (a)Y=B, (b) Y=2B, (c) Y=3B, (d) Y=4B ,(e)Y=5B, and (f)Y=6B

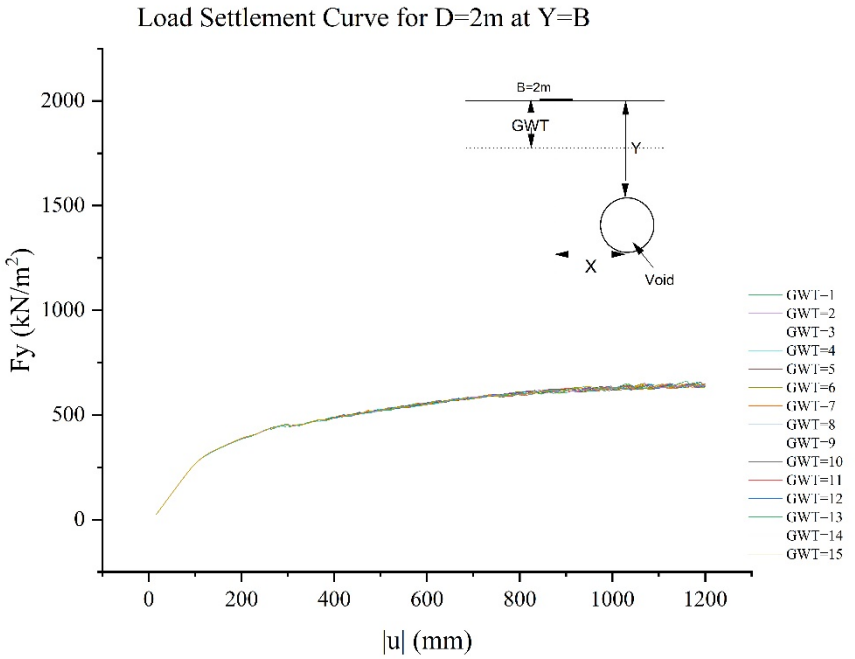
Load Settlement Curve for D=2m at Y=B
B=2m
GWT
Y
X
Void
Fy (kN/m²)
|u| (mm)
0
500
1000
1500
2000
0
200
400
600
800
1000
1200
GWT=1
GWT=2
GWT=3
GWT=4
GWT=5
GWT=6
GWT=7
GWT=8
GWT=9
GWT=10
GWT=11
GWT=12
GWT=13
GWT=14
GWT=15

(a)

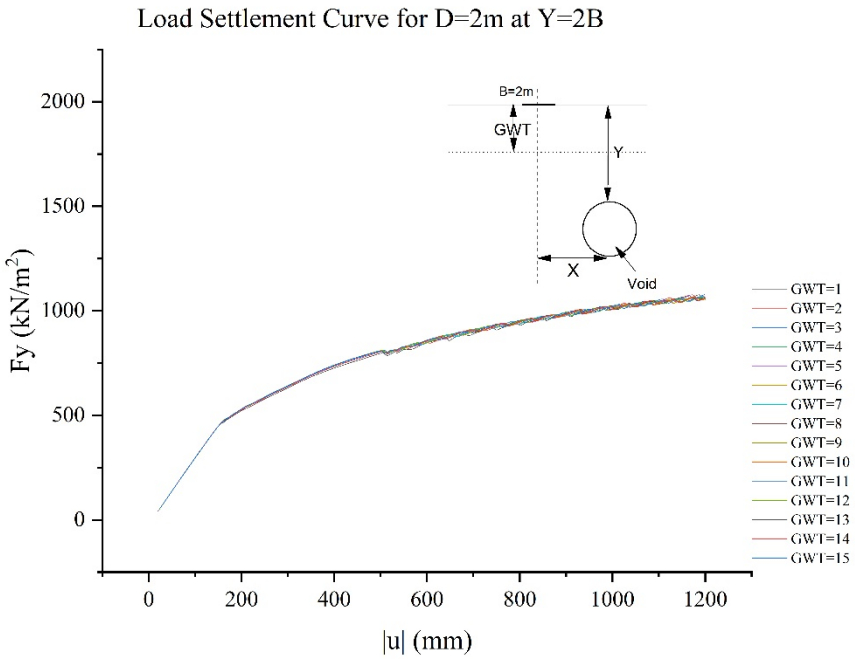
Load Settlement Curve for D=2m at Y=2B
B=2m
GWT
Y
X
Void
Fy (kN/m²)
|u| (mm)
0
500
1000
1500
2000
0
200
400
600
800
1000
1200
GWT=1
GWT=2
GWT=3
GWT=4
GWT=5
GWT=6
GWT=7
GWT=8
GWT=9
GWT=10
GWT=11
GWT=12
GWT=13
GWT=14
GWT=15

(b)

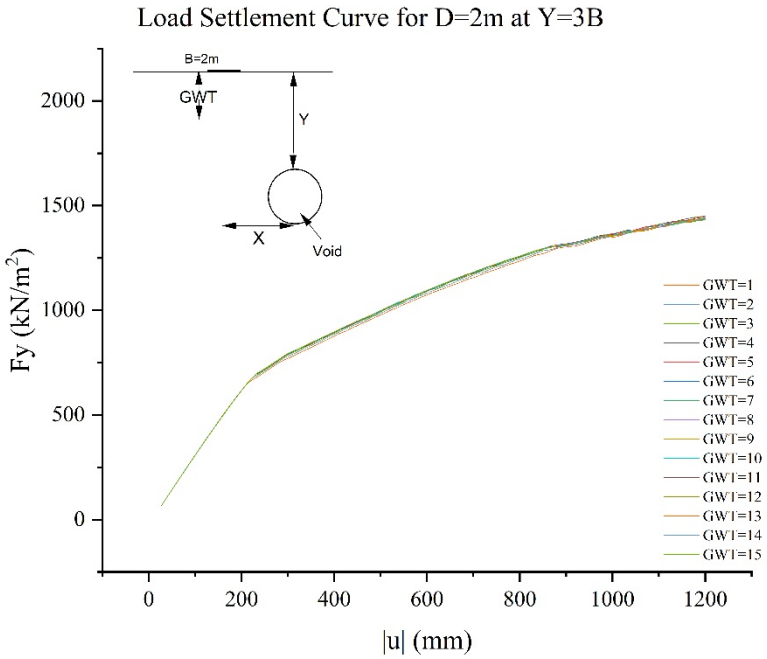
Load Settlement Curve for D=2m at Y=3B
B=2m
GWT
Y
X
Void
Fy (kN/m²)
|u| (mm)
GWT=1
GWT=2
GWT=3
GWT=4
GWT=5
GWT=6
GWT=7
GWT=8
GWT=9
GWT=10
GWT=11
GWT=12
GWT=13
GWT=14
GWT=15

(c)

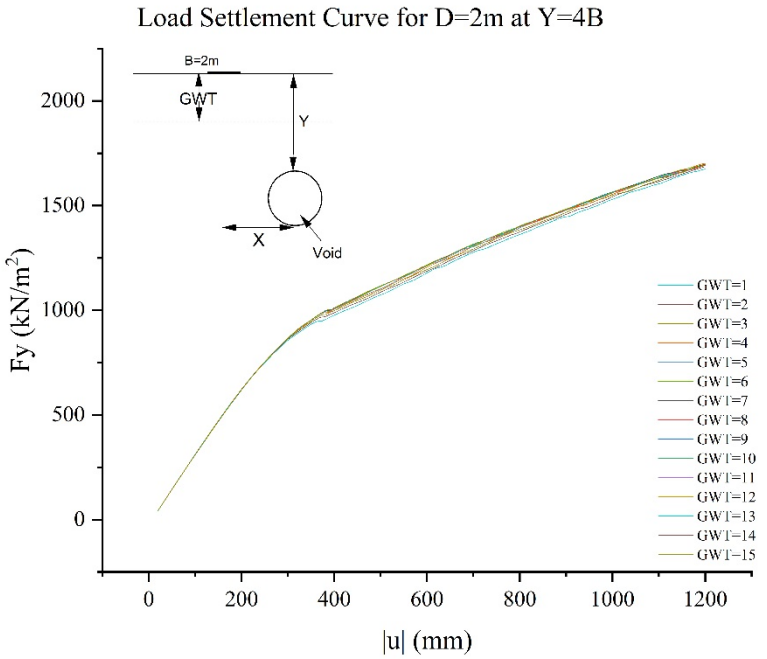
Load Settlement Curve for D=2m at Y=4B
B=2m
GWT
Y
X
Void
Fy (kN/m²)
|u| (mm)
GWT=1
GWT=2
GWT=3
GWT=4
GWT=5
GWT=6
GWT=7
GWT=8
GWT=9
GWT=10
GWT=11
GWT=12
GWT=13
GWT=14
GWT=15

(d)

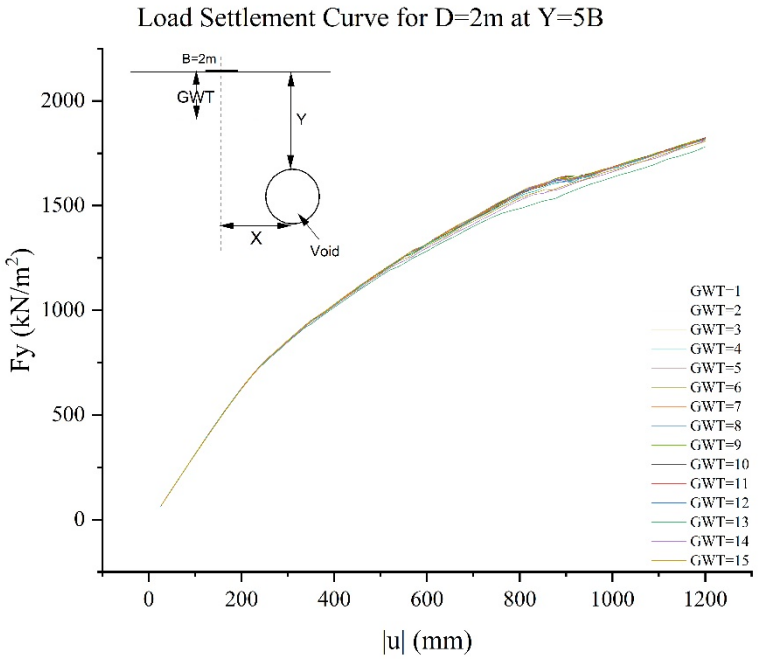

(e)

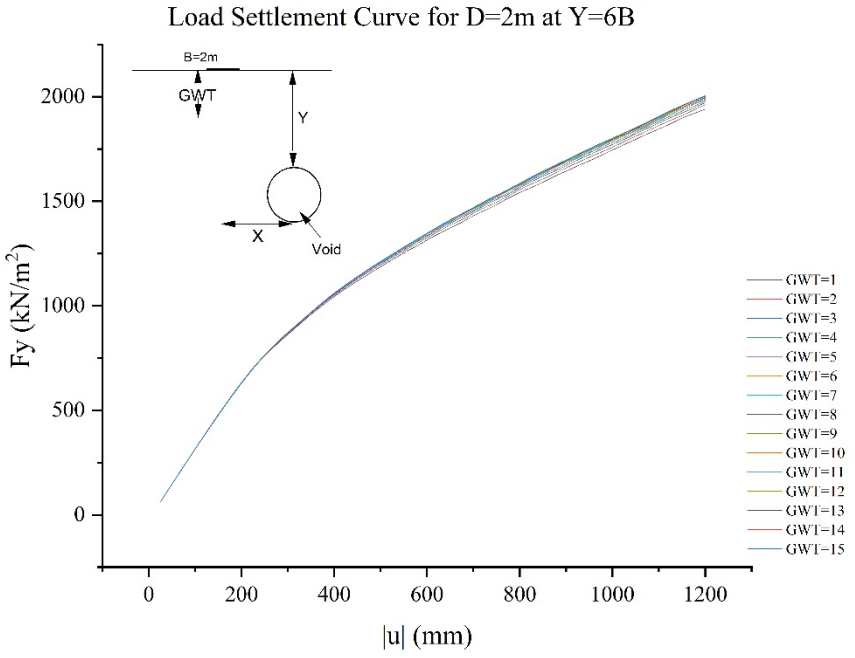

(f)

Figure A.22: Stress Load-Settlement Curve for Circular void(D=2m) with ground water table for variation in depth of void (y) at (a)Y=B, (b) Y=2B, (c) Y=3B, (d) Y=4B ,(e) Y=5B, and (f) Y=6B

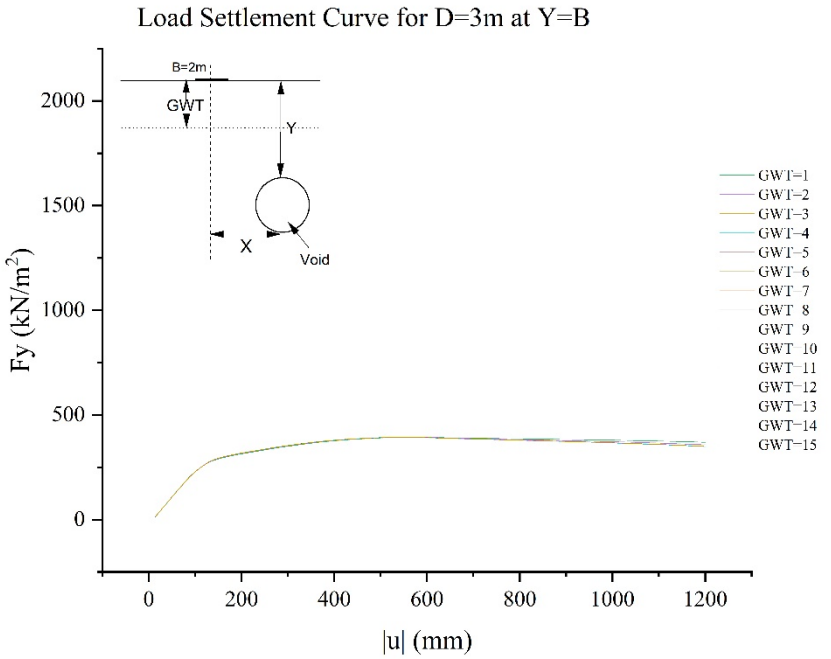
Load Settlement Curve for D=3m at Y=B
B=2m
GWT
Y
X
Void
Fy (kN/m²)
|u| (mm)
GWT=1
GWT=2
GWT=3
GWT=4
GWT=5
GWT=6
GWT=7
GWT=8
GWT=9
GWT=10
GWT=11
GWT=12
GWT=13
GWT=14
GWT=15

(a)

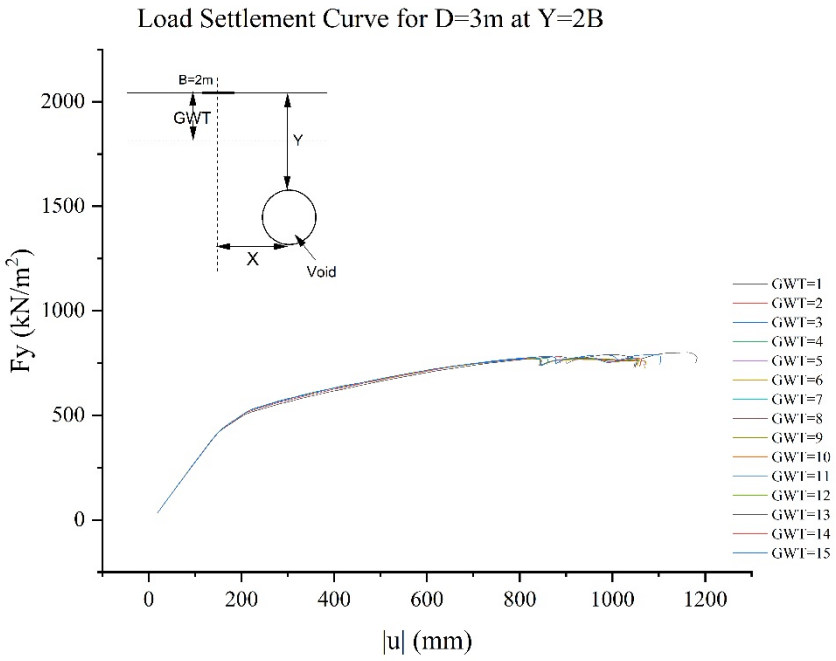
Load Settlement Curve for D=3m at Y=2B
B=2m
GWT
Y
X
Void
Fy (kN/m²)
|u| (mm)
GWT=1
GWT=2
GWT=3
GWT=4
GWT=5
GWT=6
GWT=7
GWT=8
GWT=9
GWT=10
GWT=11
GWT=12
GWT=13
GWT=14
GWT=15

(b)

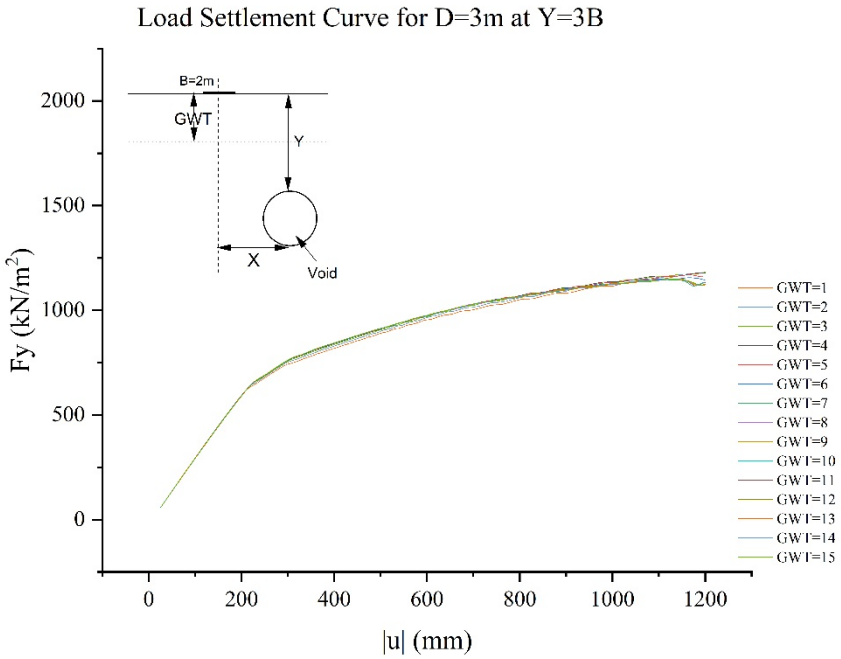
Load Settlement Curve for D=3m at Y=3B
B=2m
GWT
Y
X
Void
Fy (kN/m²)
|u| (mm)
0
500
1000
1500
2000
0
200
400
600
800
1000
1200
GWT=1
GWT=2
GWT=3
GWT=4
GWT=5
GWT=6
GWT=7
GWT=8
GWT=9
GWT=10
GWT=11
GWT=12
GWT=13
GWT=14
GWT=15

(c)

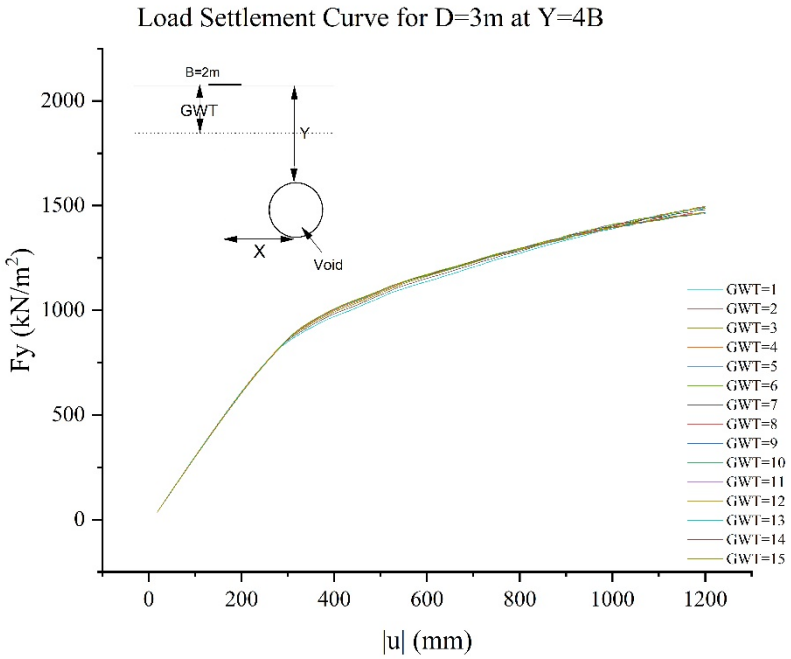
Load Settlement Curve for D=3m at Y=4B
B=2m
GWT
Y
X
Void
Fy (kN/m²)
|u| (mm)
0
500
1000
1500
2000
0
200
400
600
800
1000
1200
GWT=1
GWT=2
GWT=3
GWT=4
GWT=5
GWT=6
GWT=7
GWT=8
GWT=9
GWT=10
GWT=11
GWT=12
GWT=13
GWT=14
GWT=15

(d)

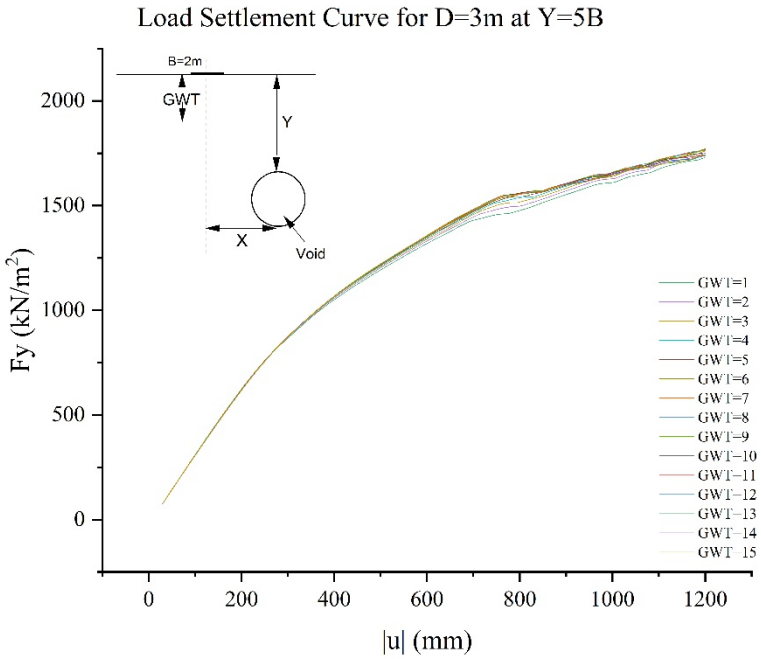

(e)

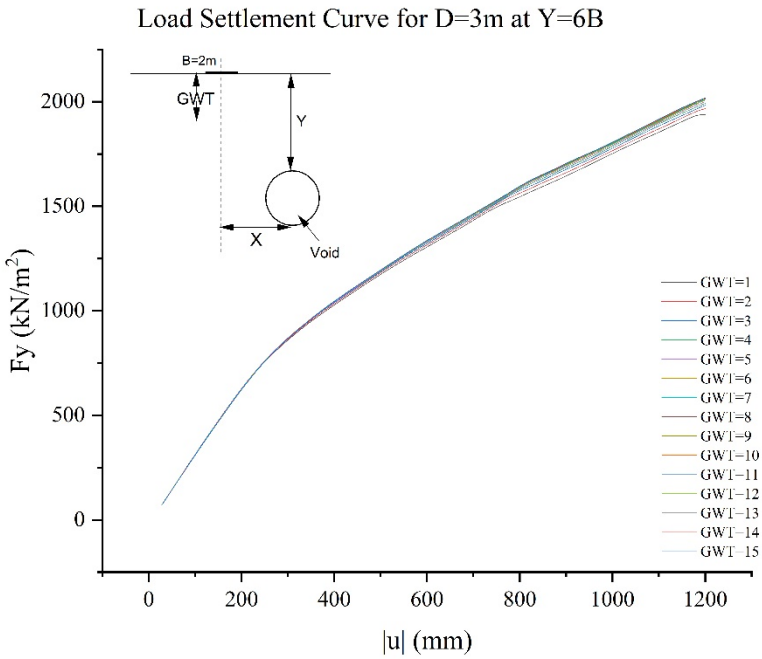

(f)

Figure A.23: Stress Load-Settlement Curve for Circular void(D=3m) with ground water table for variation in depth of void (y) at (a)Y=B, (b) Y=2B, (c) Y=3B, (d) Y=4B ,(e)Y=5B, and (f)Y=6B

ANNEX B: RESULTS IN TABULAR FORM

Table B.1: Ultimate Bearing capacity at different location of void with consideration of circular void.

S.N	Shape	Size(D)	Horizontal Offset(x)	Vertical Offset(y)					
		(m)	X/B↓	Y= B	Y=2 B	Y=3 B	Y=4 B	Y=5 B	Y=6 B
1	Circular	0.5	0	637	620	747	735	730	726
2			1	711	769	760	747	764	768
3			2	728	743	737	763	753	768
4			3	766	764	706	729	730	763
5			4	752	733	722	751	771	768
6		1	0	446	548	604	700	703	738
7			1	713	754	748	742	744	754
8			2	745	745	746	743	745	747
9			3	748	748	753	753	753	754
10			4	731	735	747	754	751	753
11		1.5	0	291	484	680	720	720	720
12			1	529	548	644	709	748	747
13			2	744	756	754	739	753	721
14			3	623	699	704	739	737	754
15			4	751	741	693	742	736	718
16		2	0	259	459	659	667	713	735
17			1	435	509	676	690	726	752
18			2	661	681	698	723	731	731
19			3	679	721	729	729	734	739
20			4	742	751	752	752	752	752
21		3	0	271	436	625	845	766	733
22			1	342	464	626	632	683	763
23			2	390	471	665	746	728	759
24			3	570	594	701	723	741	746
25			4	737	725	713	729	751	750
26	Square	0.5	0	574	636	750	681	743	762
27			1	650	719	717	707	678	716
28			2	701	684	660	717	719	736
29			3	735	749	718	736	664	723
30			4	727	699	708	745	738	760
31		1	0	434	472	674	686	753	725
32			1	650	666	739	726	756	731
33			2	693	720	719	715	758	752
34			3	738	749	691	725	728	759

S.N	Shape	Size(D)	Horizontal Offset(x)	Vertical Offset(y)					
		(m)	X/B↓	Y=B	Y=2B	Y=3B	Y=4B	Y=5B	Y=6B
35			4	739	751	759	756	757	767
36		1.5	0	237	386	587	746	748	767
37			1	412	520	620	733	738	767
38			2	678	703	679	744	750	760
39			3	596	632	721	658	703	759
40			4	684	705	759	709	756	768
41		2	0	174	367	644	660	709	739
42			1	428	462	504	697	718	784
43			2	615	612	641	690	715	747
44			3	574	642	678	612	739	768
45			4	745	728	739	768	760	759
46		3	0	131	340	565	746	759	739
47			1	365	406	565	629	717	740
48			2	393	417	562	581	629	696
49			3	590	628	623	784	731	746
50			4	660	694	725	732	730	769
51	Rectangle	w=0.5m,h=1.0m, h/w=2	0	598	596	648	708	713	769
52			1	630	709	765	772	779	778
53			2	662	681	721	765	769	770
54			3	669	679	680	682	685	689
55			4	642	686	686	758	738	693
56		w=0.5m,h=1.5m, h/w=3	0	570	566	685	690	668	760
57			1	672	647	755	738	693	738
58			2	680	711	754	690	668	709
59			3	796	784	734	719	746	746
60			4	747	758	725	736	700	695
61		w=1.0m,h=2.0m, h/w=2	0	453	513	677	713	712	754
62			1	566	694	712	765	769	763
63			2	648	625	661	717	741	734
64			3	687	738	752	784	786	760
65			4	668	731	767	779	765	766
66		w=1.0m,h=3.0m, h/w=3	0	363	453	541	589	683	732
67			1	481	621	677	642	666	768
68			2	670	691	626	665	712	737
69			3	683	666	641	638	633	744
70			4	667	686	690	697	706	724
71		w=1.5m,h=3.0m, h/w=2	0	204	401	580	632	742	751
72			1	453	614	596	590	745	733
73			2	669	738	724	729	734	747

S.N	Shape	Size(D)	Horizontal Offset(x)	Vertical Offset(y)					
		(m)	X/B↓	Y=B	Y=2B	Y=3B	Y=4B	Y=5B	Y=6B
74			3	727	742	752	769	773	730
75			4	715	734	740	744	747	748
76	Rectangle	w=1.0m,h=0.5m, h/w=1/2	0	350	506	581	737	752	762
77			1	675	690	700	726	759	782
78			2	676	686	695	710	737	742
79			3	681	694	712	746	758	771
80			4	692	700	707	752	764	776
81		w=1.5m,h=0.5m, h/w=1/3	0	219	425	635	641	661	664
82			1	479	485	532	690	740	744
83			2	660	687	702	720	747	767
84			3	640	660	663	679	681	746
85			4	602	645	704	742	744	765
86		w=2.0m,h=1.0m, h/w=1/2	0	183	288	536	637	729	768
87			1	429	495	521	624	678	684
88			2	674	708	716	724	728	742
89			3	657	681	695	701	748	752
90			4	690	714	717	741	743	757
91		w=3.0m,h=1.0m, h/w=1/3	0	134	332	484	715	757	763
92			1	388	497	534	663	686	706
93			2	624	631	689	693	722	741
94			3	640	692	708	720	736	738
95			4	677	698	729	737	745	750
96		w=3.0m,h=1.5m, h/w=1/2	0	142	340	358	521	612	649
97			1	350	384	536	604	714	741
98			2	635	650	654	689	741	742
99			3	702	757	628	710	742	702
100			4	756	762	765	711	720	726

Table B.2: Ultimate Bearing capacity at different location of void with consideration of circular void and water Table

S.N	Shape	Size(D)	Water Table Below Ground Level	Vertical Offset(y)					
		(m)	GWT↓	Y= B	Y=2 B	Y=3 B	Y=4 B	Y=5 B	Y=6 B
1	Circular	1.5	1	233	387	543	578	575	570
2			2	242	401	564	596	594	592
3			3	254	424	596	632	630	637
4			4	278	463	610	690	688	698
5			5	284	476	652	705	701	712
6			6	291	484	680	720	720	720
7			7	291	484	680	720	720	720
8			8	291	484	680	720	720	720
9			9	291	484	680	720	720	720
10			10	291	484	680	720	720	720
11			11	291	484	680	720	720	720
12			12	291	484	680	720	720	720
13			13	291	484	680	720	720	720
14			14	291	484	680	720	720	720
15			15	291	484	680	720	720	720
16		2	1	230	431	617	620	633	624
17			2	232	432	644	646	636	654
18			3	243	433	647	650	651	676.2
19			4	251	443	649	658	674	705
20			5	255	454	654	662	699	723
21			6	259	459	659	667	713	735
22			7	259	459	659	667	713	735
23			8	259	459	659	667	713	735
24			9	259	459	659	667	713	735
25			10	259	459	659	667	713	735
26			11	259	459	659	667	713	735
27			12	259	459	659	667	713	735
28			13	259	459	659	667	713	735
29			14	259	459	659	667	713	735
30			15	259	459	659	667	713	735
31		3	1	220	343	512	597	586	582
32			2	227	362	526	641	630	611
33			3	245	382	556	670	669	652
34			4	257	415	601	692	690	712

35			5	265	432	609	710	712	718
36			6	271	436	625	845	766	733
37			7	271	436	625	845	766	733
38			8	271	436	625	845	766	733
39			9	271	436	625	845	766	733
40			10	271	436	625	845	766	733
41			11	271	436	625	845	766	733
42			12	271	436	625	845	766	733
43			13	271	436	625	845	766	733
44			14	271	436	625	845	766	733
45			15	271	436	625	845	766	733

ANNEX C :BOREHOLE LOG

BOREHOLE - 3

PROJECT : Geotechnical Investigation of Proposed Building Block
CLIENT : Jaya Manakamana Saving and Credit Cooperative Society Ltd
LOCATION : Lamachaur, PMC - 19, Kaski — Total Depth, m : **15.0**
Drilling Method : Rotary — Depth to Ground Water: NA
Inclination of Hole:Vertical
Borehole Coordinates : 28°15'40.26" N, 83°58'18.03" E

Soil Description	Depth, m	Test Type	No. of blows 15 cm	15 cm	15 cm	N-Value
Very dense brownish silty sandy GRAVELS with BOULDERS	1–2	DCPT	50/9			> 50
Medium dense to dense brownish very silty fine SAND; no samples in SPT tube recovered	3	SPT	9	7	19	26
	4	SPT	8	11	23	34
	5–6	SPT	17	19	26	45
	7–8	SPT	8	11	13	24
Very loose brownish sandy SILT with gravels and clay (Direct run of SPT tube)	9	Just Press- 1 Blow penetrates 45 cm				0
	10–11	Just Press- 1 Blow penetrates 45 cm				0
Very dense brownish silty sandy GRAVELS with BOULDERS	12	DCPT	50/8			> 50
	13	DCPT	50/9			> 50
	14–15	DCPT	50/7			> 50

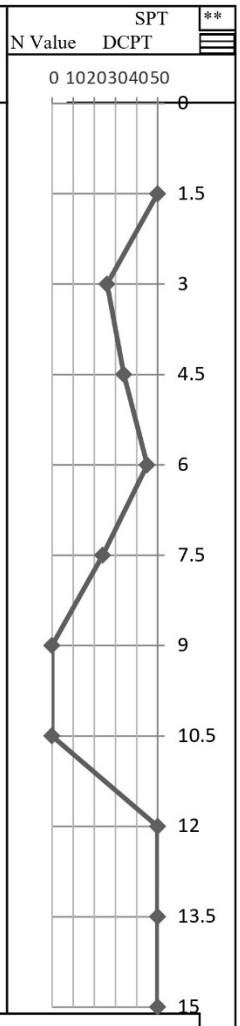

Types of Soil		N Value					
Granular Soil	Compactness	0 to 4 Very Loose	4 to 10 Loose	10 to 30 Med. Dense	30 to 50 Dense	> 50 Very Dense	
Cohesive Soil	Consistency	0 to 2 Very Soft	2 to 4 Soft	4 to 8 Med. Soft	8 to 16 Stiff	16 to 32 Very Stiff	> 32 Hard

LIST OF PUBLICATION

1. Nepal, B., &Yadav, S.K. (2023). Numerical Study of Bearing Capacity under Strip footing having underground void. In 14th IOE Graduate Conference (Accepted)